

MIXED-MODE FRACTURE ANALYSIS OF ORTHOTROPIC FGM
COATINGS UNDER MECHANICAL AND THERMAL LOADS

A THESIS SUBMITTED TO
THE GRADUATE SCHOOL OF NATURAL AND APPLIED SCIENCES
OF
MIDDLE EAST TECHNICAL UNIVERSITY

BY

KÜÇÜK AYŞE İLHAN

IN PARTIAL FULFILLMENT OF THE REQUIREMENTS
FOR
THE DEGREE OF DOCTOR OF PHILOSOPHY
IN
MECHANICAL ENGINEERING

SEPTEMBER 2007

**MIXED-MODE FRACTURE ANALYSIS OF ORTHOTROPIC FGM
COATINGS UNDER MECHANICAL AND THERMAL LOADS**

submitted by **KÜÇÜK AYŞE İLHAN** in partial fulfillment of the requirements for
the degree of **Doctor of Philosophy in Mechanical Engineering Department,**
Middle East Technical University by,

Prof. Dr. Canan ÖZGEN
Dean, Graduate School of **Natural and Applied Sciences**

Prof. Dr. S. Kemal İDER
Head of Department, **Mechanical Engineering**

Asst. Prof. Dr. Serkan DAĞ
Supervisor, **Mechanical Engineering Dept., METU**

Examining Committee Members:

Prof. Dr. Bülent DOYUM
Mechanical Engineering Dept., METU

Asst. Prof. Dr. Serkan DAĞ
Mechanical Engineering Dept., METU

Prof. Dr. Ruşen GEÇİT
Engineering Sciences Dept., METU

Prof. Dr. Suat KADIOĞLU
Mechanical Engineering Dept., METU

Prof. Dr. Müfit GÜLGEÇ
Mechanical Engineering Dept., Gazi University

Date: 4 September 2007

I hereby declare that all information in this document has been obtained and presented in accordance with academic rules and ethical conduct. I also declare that, as required by these rules and conduct, I have fully cited and referenced all material and results that are not original to this work.

Name, Last name: Küçük Ayşe İLHAN

Signature:

ABSTRACT

MIXED-MODE FRACTURE ANALYSIS OF ORTHOTROPIC FGM COATINGS UNDER MECHANICAL AND THERMAL LOADS

İLHAN, Küçük Ayşe

Ph.D., Department of Mechanical Engineering

Supervisor: Asst. Prof. Dr. Serkan DAĞ

September 2007, 164 pages

In this study, it is aimed to investigate the mixed-mode fracture behavior of orthotropic functionally graded material (FGM) coatings bonded to a homogeneous substrate through a homogeneous bond-coat. Analytical and computational methods are used to solve the embedded cracking problems under mechanical or thermal loading conditions. It is assumed that the material property gradation of the FGM coating is in the thickness direction and cracks are parallel to the boundaries. The principal axes of orthotropy are parallel and perpendicular to the boundaries. A single embedded crack in the orthotropic FGM coating is investigated analytically assuming that crack surfaces are subjected to either uniform normal or uniform shear stresses. Using Fourier transformations, the problem is reduced to a couple of singular integral equations that are solved numerically to obtain the mixed-mode stress intensity factors, energy release rate and crack opening displacements. To investigate the analytically untractable problems without restrictive assumptions, a computational approach is employed. The adopted computational approach is based on finite element method and displacement correlation technique. Using the computational approach, fracture parameters are obtained considering single and

periodic embedded cracking conditions in the orthotropic FGM coatings under mechanical or thermal loads. The results obtained in this study show the effects of material nonhomogeneity, material orthotropy and geometric variables on the fracture behavior of the structure.

Keywords: Orthotropic functionally graded coating, embedded crack, periodic cracks, singular integral equations, displacement correlation technique.

ÖZ

ORTOTROP FDM KAPLAMALARIN MEKANİK VE ISIL YÜKLER ALTINDA KARIŞIK MOD KIRILMA ANALİZİ

İLHAN, Küçük Ayşe

Doktora, Makine Mühendisliği Bölümü

Tez Yöneticisi: Yrd. Doç. Dr. Serkan DAĞ

Eylül 2007, 164 sayfa

Bu çalışmada, homojen bir birleşme tabakası ile homojen bir taban tabakaya bağlanmış ortotrop fonksiyonel derecelendirilmiş malzeme (FDM) kaplamaların karışık mod kırılma davranışının araştırılması amaçlanmıştır. Gömülü çatlak problemlerini mekanik veya ısıl yükleme koşulları altında çözmek için analitik ve hesaplamalı yöntemler kullanılmıştır. FDM kaplama malzeme özellik değişiminin kalınlık yönünde ve çatlakların sınırlara paralel olduğu varsayılmıştır. Ortotropi ana eksenleri sınırlara paralel ve diktir. Ortotrop FDM kaplama içindeki tek gömülü çatlak, çatlak yüzeylerinin ya düzgün yayılı normal veya düzgün yayılı kayma gerilmelerine uğratıldığı varsayılarak analitik olarak incelenmiştir. Problem, Fourier dönüşümleri kullanılarak karışık mod gerilme şiddeti faktörleri, enerji bırakma oranı ve çatlak açılma yer değiştirmelerini elde etmek için sayısal olarak çözülen bir çift tekil integral denkleminde indirgenmiştir. Analitik olarak kontrol edilemeyen sınırlayıcı varsayımlar içermeyen problemleri incelemek için bir hesaplamalı yaklaşım kullanılmıştır. Benimsenen hesaplamalı yaklaşım sonlu elemanlar yöntemine ve yer değiştirme korelasyon tekniğine dayanır. Mekanik veya ısıl yükler altındaki ortotrop FDM kaplamalarda tek ve periyodik gömülü

çatlak durumları göz önüne alınarak kırılma parametreleri hesaplamalı yaklaşım kullanılarak elde edilmiştir. Bu çalışmada elde edilen sonuçlar malzeme homojenliğinin olmamasının, malzeme ortotropisinin ve geometrik değişkenlerin yapının kırılma davranışı üzerindeki etkilerini göstermektedir.

Anahtar kelimeler: Ortotrop fonksiyonel derecelendirilmiş kaplama, gömülü çatlak, periyodik çatlaklar, tekil integral denklemleri, yer değiştirme korelasyon tekniği.

To My Family

ACKNOWLEDGMENTS

I would like to thank to my supervisor Asst. Prof. Dr. Serkan DAĞ for his help and guidance during this study.

I would like to thank to Prof. Dr. Ruşen GEÇİT, Prof. Dr. Suat KADIOĞLU and Prof. Dr. Müfit GÜLGEÇ for their valuable suggestions and comments during this study.

I express my appreciation to my parents who supported and encouraged me during this study.

TABLE OF CONTENTS

ABSTRACT	iv
ÖZ	vi
DEDICATION	viii
ACKNOWLEDGMENTS	ix
TABLE OF CONTENTS	x
LIST OF TABLES	xiii
LIST OF FIGURES	xiv
CHAPTER	
1. INTRODUCTION	1
1.1 Functionally Graded Materials	1
1.2 Literature Survey	2
1.3 Objective of the Study.....	8
2. ANALYTICAL SOLUTION FOR THE SINGLE EMBEDDED CRACK PROBLEM IN AN ORTHOTROPIC FGM COATING UNDER CRACK SURFACE TRACTIONS	10
2.1 Description of the Problem	10
2.2 Formulation of the Problem	11
3. COMPUTATIONAL SOLUTION FOR THE CRACK PROBLEMS IN AN ORTHOTROPIC FGM COATING	44
3.1 Computational Solution	44

3.2 Review of Displacement Correlation Technique	44
4. NUMERICAL RESULTS	50
4.1 Verification of the Analytical Study	50
4.2 Numerical Results Based on Analytical and Computational Approaches	52
4.2.1 Single Embedded Crack Problem Considering Uniform Normal Stress on Crack Surfaces	55
4.2.2 Single Embedded Crack Problem Considering Uniform Shear Stress on Crack Surfaces	71
4.2.3 Periodic Embedded Cracking Problem Considering Uniform Normal Stress on Crack Surfaces	80
5. COMPUTATIONAL SOLUTION FOR THE EMBEDDED CRACK PROBLEMS IN AN ORTHOTROPIC FGM COATING UNDER THERMAL LOADING	85
5.1 Description of the Problem	85
5.2 Numerical Results	87
5.2.1 Single Embedded Crack Problem under Thermal Loading	88
5.2.2 Periodic Embedded Cracking Problem under Thermal Loading	92
6. CONCLUSIONS AND FUTURE STUDIES	99
6.1 Conclusions	99
6.2 Future Studies	107
REFERENCES	109
APPENDICES	
A. DETERMINATION OF UNKNOWN FUNCTIONS	134
B. ASYMPTOTIC BEHAVIORS OF THE INTEGRANDS	140

C. DEFINITIONS OF FUNCTIONS APPEARING IN THE INTEGRAL EQUATIONS	156
D. CHEBYSHEV POLYNOMIALS	161
E. INTEGRALS EVALUATED IN CLOSED FORM	162
CURRICULUM VITAE	163

LIST OF TABLES

TABLES

- 4.1.1 Comparison of the stress intensity factors, $2h_1/(h_1 + h_2) = 1.0$,
 $\delta(h_1 + h_2)/(2c) = 0.35$, $\sigma_{22}(x_1, 0) = -\sigma_0$ for $|x_1| < c$ 51
- 4.1.2 Comparison of the stress intensity factors, $2h_1/(h_1 + h_2) = 0.4$,
 $\delta(h_1 + h_2)/(2c) = 0.35$, $\sigma_{22}(x_1, 0) = -\sigma_0$ for $|x_1| < c$ 51
- 4.1.3 Comparison of the stress intensity factors, $2h_1/(h_1 + h_2) = 1.0$,
 $\delta(h_1 + h_2)/(2c) = 0.35$, $\sigma_{12}(x_1, 0) = -\tau_0$ for $|x_1| < c$ 51
- 4.1.4 Comparison of the stress intensity factors, $2h_1/(h_1 + h_2) = 0.4$,
 $\delta(h_1 + h_2)/(2c) = 0.35$, $\sigma_{12}(x_1, 0) = -\tau_0$ for $|x_1| < c$ 52

LIST OF FIGURES

FIGURES

2.1.1	Illustration of the problem	10
3.2.1	Quarter-point singular elements located at the crack tip	45
4.1.1	Illustration of the crack problem solved by Cinar and Erdogan [134]	50
4.2.1.1	Finite element model of the single embedded crack problem under uniform normal crack surface tractions	56
4.2.1.2	Normalized mode I stress intensity factor versus h_1/c and nonhomogeneity constant βc , $E_0 \exp(-\beta h_2) = E_3 = E_4/1.5$, $\nu_0 = \nu_3 = 0.25$, $\nu_4 = 0.3$, $\kappa_0 = \kappa_3 = 2$, $\kappa_4 = 1$, $\delta_0^4 = \delta_3^4 = 2$, $\delta_4^4 = 1$, $2h_2 = 2h_3 = h_4/2 = c$, $p(x_1) = \sigma_0$, $q(x_1) = 0$	58
4.2.1.3	Normalized mode II stress intensity factor versus h_1/c and nonhomogeneity constant βc , $E_0 \exp(-\beta h_2) = E_3 = E_4/1.5$, $\nu_0 = \nu_3 = 0.25$, $\nu_4 = 0.3$, $\kappa_0 = \kappa_3 = 2$, $\kappa_4 = 1$, $\delta_0^4 = \delta_3^4 = 2$, $\delta_4^4 = 1$, $2h_2 = 2h_3 = h_4/2 = c$, $p(x_1) = \sigma_0$, $q(x_1) = 0$	58
4.2.1.4	Normalized energy release rate versus h_1/c and nonhomogeneity constant βc , $E_0 \exp(-\beta h_2) = E_3 = E_4/1.5$, $\nu_0 = \nu_3 = 0.25$, $\nu_4 = 0.3$, $\kappa_0 = \kappa_3 = 2$, $\kappa_4 = 1$, $\delta_0^4 = \delta_3^4 = 2$, $\delta_4^4 = 1$, $2h_2 = 2h_3 = h_4/2 = c$, $p(x_1) = \sigma_0$, $q(x_1) = 0$	59
4.2.1.5	Normalized mode I stress intensity factor versus shear parameter κ_0 and nonhomogeneity constant βc , $E_0 \exp(-\beta h_2) = E_3 = E_4/1.5$, $\nu_0 = \nu_3 = 0.25$, $\nu_4 = 0.3$, $\kappa_0 = \kappa_3$, $\kappa_4 = 1$, $\delta_0^4 = \delta_3^4 = 2$, $\delta_4^4 = 1$, $2h_1 = 2h_2 = 2h_3 = h_4/2 = c$, $p(x_1) = \sigma_0$, $q(x_1) = 0$	59

- 4.2.1.6 Normalized mode II stress intensity factor versus shear parameter κ_0 and nonhomogeneity constant βc , $E_0 \exp(-\beta h_2) = E_3 = E_4/1.5$,
 $\nu_0 = \nu_3 = 0.25$, $\nu_4 = 0.3$, $\kappa_0 = \kappa_3$, $\kappa_4 = 1$, $\delta_0^4 = \delta_3^4 = 2$, $\delta_4^4 = 1$,
 $2h_1 = 2h_2 = 2h_3 = h_4/2 = c$, $p(x_1) = \sigma_0$, $q(x_1) = 0$ 60
- 4.2.1.7 Normalized energy release rate versus shear parameter κ_0 and nonhomogeneity constant βc , $E_0 \exp(-\beta h_2) = E_3 = E_4/1.5$,
 $\nu_0 = \nu_3 = 0.25$, $\nu_4 = 0.3$, $\kappa_0 = \kappa_3$, $\kappa_4 = 1$, $\delta_0^4 = \delta_3^4 = 2$, $\delta_4^4 = 1$,
 $2h_1 = 2h_2 = 2h_3 = h_4/2 = c$, $p(x_1) = \sigma_0$, $q(x_1) = 0$ 60
- 4.2.1.8 Normalized mode I stress intensity factor versus stiffness ratio δ_0^4 and nonhomogeneity constant βc , $E_0 \exp(-\beta h_2) = E_3 = E_4/1.5$,
 $\nu_0 = \nu_3 = 0.25$, $\nu_4 = 0.3$, $\kappa_0 = \kappa_3 = 2$, $\kappa_4 = 1$, $\delta_0^4 = \delta_3^4$, $\delta_4^4 = 1$,
 $2h_1 = 2h_2 = 2h_3 = h_4/2 = c$, $p(x_1) = \sigma_0$, $q(x_1) = 0$ 61
- 4.2.1.9 Normalized mode II stress intensity factor versus stiffness ratio δ_0^4 and nonhomogeneity constant βc , $E_0 \exp(-\beta h_2) = E_3 = E_4/1.5$,
 $\nu_0 = \nu_3 = 0.25$, $\nu_4 = 0.3$, $\kappa_0 = \kappa_3 = 2$, $\kappa_4 = 1$, $\delta_0^4 = \delta_3^4$, $\delta_4^4 = 1$,
 $2h_1 = 2h_2 = 2h_3 = h_4/2 = c$, $p(x_1) = \sigma_0$, $q(x_1) = 0$ 61
- 4.2.1.10 Normalized energy release rate versus stiffness ratio δ_0^4 and nonhomogeneity constant βc , $E_0 \exp(-\beta h_2) = E_3 = E_4/1.5$,
 $\nu_0 = \nu_3 = 0.25$, $\nu_4 = 0.3$, $\kappa_0 = \kappa_3 = 2$, $\kappa_4 = 1$, $\delta_0^4 = \delta_3^4$, $\delta_4^4 = 1$,
 $2h_1 = 2h_2 = 2h_3 = h_4/2 = c$, $p(x_1) = \sigma_0$, $q(x_1) = 0$ 62
- 4.2.1.11 Normalized mode I stress intensity factor versus effective Poisson's ratio ν_0 and nonhomogeneity constant βc , $E_0 \exp(-\beta h_2) = E_3 = E_4/1.5$,
 $\nu_0 = \nu_3$, $\nu_4 = 0.3$, $\kappa_0 = \kappa_3 = 2$, $\kappa_4 = 1$, $\delta_0^4 = \delta_3^4 = 2$, $\delta_4^4 = 1$,
 $2h_1 = 2h_2 = 2h_3 = h_4/2 = c$, $p(x_1) = \sigma_0$, $q(x_1) = 0$ 62
- 4.2.1.12 Normalized mode II stress intensity factor versus effective Poisson's ratio ν_0 and nonhomogeneity constant βc , $E_0 \exp(-\beta h_2) = E_3 = E_4/1.5$,
 $\nu_0 = \nu_3$, $\nu_4 = 0.3$, $\kappa_0 = \kappa_3 = 2$, $\kappa_4 = 1$, $\delta_0^4 = \delta_3^4 = 2$, $\delta_4^4 = 1$,
 $2h_1 = 2h_2 = 2h_3 = h_4/2 = c$, $p(x_1) = \sigma_0$, $q(x_1) = 0$ 63

- 4.2.1.13 Normalized energy release rate versus effective Poisson's ratio ν_0 and nonhomogeneity constant βc , $E_0 \exp(-\beta h_2) = E_3 = E_4/1.5$, $\nu_0 = \nu_3$, $\nu_4 = 0.3$, $\kappa_0 = \kappa_3 = 2$, $\kappa_4 = 1$, $\delta_0^4 = \delta_3^4 = 2$, $\delta_4^4 = 1$, $2h_1 = 2h_2 = 2h_3 = h_4/2 = c$, $p(x_1) = \sigma_0$, $q(x_1) = 0$ 63
- 4.2.1.14 Normalized normal crack opening displacement for various values of shear parameter κ_0 and nonhomogeneity constant βc , $E_0 \exp(-\beta h_2) = E_3 = E_4/1.5$, $\nu_0 = \nu_3 = 0.25$, $\nu_4 = 0.3$, $\kappa_0 = \kappa_3$, $\kappa_4 = 1$, $\delta_0^4 = \delta_3^4 = 2$, $\delta_4^4 = 1$, $2h_1 = 2h_2 = 2h_3 = h_4/2 = c$, $p(x_1) = \sigma_0$, $q(x_1) = 0$ 64
- 4.2.1.15 Normalized tangential crack opening displacement for various values of shear parameter κ_0 and nonhomogeneity constant βc , $E_0 \exp(-\beta h_2) = E_3 = E_4/1.5$, $\nu_0 = \nu_3 = 0.25$, $\nu_4 = 0.3$, $\kappa_0 = \kappa_3$, $\kappa_4 = 1$, $\delta_0^4 = \delta_3^4 = 2$, $\delta_4^4 = 1$, $2h_1 = 2h_2 = 2h_3 = h_4/2 = c$, $p(x_1) = \sigma_0$, $q(x_1) = 0$ 64
- 4.2.1.16 Normalized normal crack opening displacement for various values of stiffness ratio δ_0^4 and nonhomogeneity constant βc , $E_0 \exp(-\beta h_2) = E_3 = E_4/1.5$, $\nu_0 = \nu_3 = 0.25$, $\nu_4 = 0.3$, $\kappa_0 = \kappa_3 = 2$, $\kappa_4 = 1$, $\delta_0^4 = \delta_3^4$, $\delta_4^4 = 1$, $2h_1 = 2h_2 = 2h_3 = h_4/2 = c$, $p(x_1) = \sigma_0$, $q(x_1) = 0$ 65
- 4.2.1.17 Normalized tangential crack opening displacement for various values of stiffness ratio δ_0^4 and nonhomogeneity constant βc , $E_0 \exp(-\beta h_2) = E_3 = E_4/1.5$, $\nu_0 = \nu_3 = 0.25$, $\nu_4 = 0.3$, $\kappa_0 = \kappa_3 = 2$, $\kappa_4 = 1$, $\delta_0^4 = \delta_3^4$, $\delta_4^4 = 1$, $2h_1 = 2h_2 = 2h_3 = h_4/2 = c$, $p(x_1) = \sigma_0$, $q(x_1) = 0$ 65
- 4.2.1.18 Normalized normal crack opening displacement for various values of effective Poisson's ratio ν_0 and nonhomogeneity constant βc , $E_0 \exp(-\beta h_2) = E_3 = E_4/1.5$, $\nu_0 = \nu_3$, $\nu_4 = 0.3$, $\kappa_0 = \kappa_3 = 2$, $\kappa_4 = 1$, $\delta_0^4 = \delta_3^4 = 2$, $\delta_4^4 = 1$, $2h_1 = 2h_2 = 2h_3 = h_4/2 = c$, $p(x_1) = \sigma_0$, $q(x_1) = 0$ 66
- 4.2.1.19 Normalized tangential crack opening displacement for various values of effective Poisson's ratio ν_0 and nonhomogeneity constant βc ,

$E_0 \exp(-\beta h_2) = E_3 = E_4/1.5$, $\nu_0 = \nu_3$, $\nu_4 = 0.3$, $\kappa_0 = \kappa_3 = 2$, $\kappa_4 = 1$,
 $\delta_0^4 = \delta_3^4 = 2$, $\delta_4^4 = 1$, $2h_1 = 2h_2 = 2h_3 = h_4/2 = c$, $p(x_1) = \sigma_0$, $q(x_1) = 0$
 66

4.2.1.20 Normalized mode I stress intensity factor versus h_3/c and
 nonhomogeneity constant βc , $E_0 \exp(-\beta h_2) = E_3 = E_4/3.0$,
 $\nu_0 = \nu_3 = 0.25$, $\nu_4 = 0.3$, $\kappa_0 = \kappa_3 = 2$, $\kappa_4 = 1$, $\delta_0^4 = \delta_3^4 = 2$, $\delta_4^4 = 1$,
 $h_1 = 0.95c$, $h_2 = 0.05c$, $h_4 = 2c$, $p(x_1) = \sigma_0$, $q(x_1) = 0$ 67

4.2.1.21 Normalized mode II stress intensity factor versus h_3/c and
 nonhomogeneity constant βc , $E_0 \exp(-\beta h_2) = E_3 = E_4/3.0$,
 $\nu_0 = \nu_3 = 0.25$, $\nu_4 = 0.3$, $\kappa_0 = \kappa_3 = 2$, $\kappa_4 = 1$, $\delta_0^4 = \delta_3^4 = 2$, $\delta_4^4 = 1$,
 $h_1 = 0.95c$, $h_2 = 0.05c$, $h_4 = 2c$, $p(x_1) = \sigma_0$, $q(x_1) = 0$ 67

4.2.1.22 Normalized energy release rate versus h_3/c and nonhomogeneity
 constant βc , $E_0 \exp(-\beta h_2) = E_3 = E_4/3.0$, $\nu_0 = \nu_3 = 0.25$, $\nu_4 = 0.3$,
 $\kappa_0 = \kappa_3 = 2$, $\kappa_4 = 1$, $\delta_0^4 = \delta_3^4 = 2$, $\delta_4^4 = 1$, $h_1 = 0.95c$, $h_2 = 0.05c$,
 $h_4 = 2c$, $p(x_1) = \sigma_0$, $q(x_1) = 0$ 68

4.2.2.1 Normalized mode I stress intensity factor versus shear parameter κ_0 and
 nonhomogeneity constant βc , $E_0 \exp(-\beta h_2) = E_3 = E_4/1.5$,
 $\nu_0 = \nu_3 = 0.25$, $\nu_4 = 0.3$, $\kappa_0 = \kappa_3$, $\kappa_4 = 1$, $\delta_0^4 = \delta_3^4 = 2$, $\delta_4^4 = 1$,
 $2h_1 = 2h_2 = 2h_3 = h_4/2 = c$, $p(x_1) = 0$, $q(x_1) = \tau_0$ 72

4.2.2.2 Normalized mode II stress intensity factor versus shear parameter κ_0 and
 nonhomogeneity constant βc , $E_0 \exp(-\beta h_2) = E_3 = E_4/1.5$,
 $\nu_0 = \nu_3 = 0.25$, $\nu_4 = 0.3$, $\kappa_0 = \kappa_3$, $\kappa_4 = 1$, $\delta_0^4 = \delta_3^4 = 2$, $\delta_4^4 = 1$,
 $2h_1 = 2h_2 = 2h_3 = h_4/2 = c$, $p(x_1) = 0$, $q(x_1) = \tau_0$ 73

4.2.2.3 Normalized mode I stress intensity factor versus stiffness ratio δ_0^4 and
 nonhomogeneity constant βc , $E_0 \exp(-\beta h_2) = E_3 = E_4/1.5$,
 $\nu_0 = \nu_3 = 0.25$, $\nu_4 = 0.3$, $\kappa_0 = \kappa_3 = 2$, $\kappa_4 = 1$, $\delta_0^4 = \delta_3^4$, $\delta_4^4 = 1$,
 $2h_1 = 2h_2 = 2h_3 = h_4/2 = c$, $p(x_1) = 0$, $q(x_1) = \tau_0$ 73

- 4.2.2.4 Normalized mode II stress intensity factor versus stiffness ratio δ_0^4 and nonhomogeneity constant βc , $E_0 \exp(-\beta h_2) = E_3 = E_4/1.5$,
 $\nu_0 = \nu_3 = 0.25$, $\nu_4 = 0.3$, $\kappa_0 = \kappa_3 = 2$, $\kappa_4 = 1$, $\delta_0^4 = \delta_3^4$, $\delta_4^4 = 1$,
 $2h_1 = 2h_2 = 2h_3 = h_4/2 = c$, $p(x_1) = 0$, $q(x_1) = \tau_0$ 74
- 4.2.2.5 Normalized mode I stress intensity factor versus effective Poisson's ratio ν_0 and nonhomogeneity constant βc , $E_0 \exp(-\beta h_2) = E_3 = E_4/1.5$,
 $\nu_0 = \nu_3$, $\nu_4 = 0.3$, $\kappa_0 = \kappa_3 = 2$, $\kappa_4 = 1$, $\delta_0^4 = \delta_3^4 = 2$, $\delta_4^4 = 1$,
 $2h_1 = 2h_2 = 2h_3 = h_4/2 = c$, $p(x_1) = 0$, $q(x_1) = \tau_0$ 74
- 4.2.2.6 Normalized mode II stress intensity factor versus effective Poisson's ratio ν_0 and nonhomogeneity constant βc , $E_0 \exp(-\beta h_2) = E_3 = E_4/1.5$,
 $\nu_0 = \nu_3$, $\nu_4 = 0.3$, $\kappa_0 = \kappa_3 = 2$, $\kappa_4 = 1$, $\delta_0^4 = \delta_3^4 = 2$, $\delta_4^4 = 1$,
 $2h_1 = 2h_2 = 2h_3 = h_4/2 = c$, $p(x_1) = 0$, $q(x_1) = \tau_0$ 75
- 4.2.2.7 Normalized normal crack opening displacement for various values of shear parameter κ_0 and nonhomogeneity constant βc ,
 $E_0 \exp(-\beta h_2) = E_3 = E_4/1.5$, $\nu_0 = \nu_3 = 0.25$, $\nu_4 = 0.3$, $\kappa_0 = \kappa_3$, $\kappa_4 = 1$,
 $\delta_0^4 = \delta_3^4 = 2$, $\delta_4^4 = 1$, $2h_1 = 2h_2 = 2h_3 = h_4/2 = c$, $p(x_1) = 0$, $q(x_1) = \tau_0$
..... 75
- 4.2.2.8 Normalized tangential crack opening displacement for various values of shear parameter κ_0 and nonhomogeneity constant βc ,
 $E_0 \exp(-\beta h_2) = E_3 = E_4/1.5$, $\nu_0 = \nu_3 = 0.25$, $\nu_4 = 0.3$, $\kappa_0 = \kappa_3$, $\kappa_4 = 1$,
 $\delta_0^4 = \delta_3^4 = 2$, $\delta_4^4 = 1$, $2h_1 = 2h_2 = 2h_3 = h_4/2 = c$, $p(x_1) = 0$, $q(x_1) = \tau_0$
..... 76
- 4.2.2.9 Normalized normal crack opening displacement for various values of stiffness ratio δ_0^4 and nonhomogeneity constant βc ,
 $E_0 \exp(-\beta h_2) = E_3 = E_4/1.5$, $\nu_0 = \nu_3 = 0.25$, $\nu_4 = 0.3$, $\kappa_0 = \kappa_3 = 2$,
 $\kappa_4 = 1$, $\delta_0^4 = \delta_3^4$, $\delta_4^4 = 1$, $2h_1 = 2h_2 = 2h_3 = h_4/2 = c$, $p(x_1) = 0$,
 $q(x_1) = \tau_0$ 76
- 4.2.2.10 Normalized tangential crack opening displacement for various values of stiffness ratio δ_0^4 and nonhomogeneity constant βc ,
 $E_0 \exp(-\beta h_2) = E_3 = E_4/1.5$, $\nu_0 = \nu_3 = 0.25$, $\nu_4 = 0.3$, $\kappa_0 = \kappa_3 = 2$,

	$\kappa_4 = 1, \delta_0^4 = \delta_3^4, \delta_4^4 = 1, 2h_1 = 2h_2 = 2h_3 = h_4/2 = c, p(x_1) = 0,$ $q(x_1) = \tau_0$	77
4.2.2.11	Normalized normal crack opening displacement for various values of effective Poisson's ratio ν_0 and nonhomogeneity constant βc , $E_0 \exp(-\beta h_2) = E_3 = E_4/1.5, \nu_0 = \nu_3, \nu_4 = 0.3, \kappa_0 = \kappa_3 = 2, \kappa_4 = 1,$ $\delta_0^4 = \delta_3^4 = 2, \delta_4^4 = 1, 2h_1 = 2h_2 = 2h_3 = h_4/2 = c, p(x_1) = 0, q(x_1) = \tau_0$	77
4.2.2.12	Normalized tangential crack opening displacement for various values of effective Poisson's ratio ν_0 and nonhomogeneity constant βc , $E_0 \exp(-\beta h_2) = E_3 = E_4/1.5, \nu_0 = \nu_3, \nu_4 = 0.3, \kappa_0 = \kappa_3 = 2, \kappa_4 = 1,$ $\delta_0^4 = \delta_3^4 = 2, \delta_4^4 = 1, 2h_1 = 2h_2 = 2h_3 = h_4/2 = c, p(x_1) = 0, q(x_1) = \tau_0$	78
4.2.3.1	Illustration of the periodic embedded cracking problem	80
4.2.3.2	Applied symmetry and periodicity conditions on the unit cell	81
4.2.3.3	Normalized mode I stress intensity factor versus c/W and nonhomogeneity constant $\beta c, E_0 \exp(-\beta h_2) = E_3 = E_4/1.5,$ $\nu_0 = \nu_3 = 0.25, \nu_4 = 0.3, \kappa_0 = \kappa_3 = 2, \kappa_4 = 1, \delta_0^4 = \delta_3^4 = 2, \delta_4^4 = 1,$ $2h_2 = 2h_3 = h_4/2 = c, p(x_1) = \sigma_0$	82
4.2.3.4	Normalized mode II stress intensity factor versus c/W and nonhomogeneity constant $\beta c, E_0 \exp(-\beta h_2) = E_3 = E_4/1.5,$ $\nu_0 = \nu_3 = 0.25, \nu_4 = 0.3, \kappa_0 = \kappa_3 = 2, \kappa_4 = 1, \delta_0^4 = \delta_3^4 = 2, \delta_4^4 = 1,$ $2h_2 = 2h_3 = h_4/2 = c, p(x_1) = \sigma_0$	83
4.2.3.5	Normalized energy release rate versus c/W and nonhomogeneity constant $\beta c, E_0 \exp(-\beta h_2) = E_3 = E_4/1.5, \nu_0 = \nu_3 = 0.25, \nu_4 = 0.3,$ $\kappa_0 = \kappa_3 = 2, \kappa_4 = 1, \delta_0^4 = \delta_3^4 = 2, \delta_4^4 = 1, 2h_2 = 2h_3 = h_4/2 = c,$ $p(x_1) = \sigma_0$	83
4.2.3.6	Deformed shape of the unit cell for $c/W = 0.3$ and $\beta c = 1.0$	84
5.1.1	Illustration of the problem for the single embedded crack	86

5.1.2	Illustration of the problem for the periodic embedded cracks	86
5.2.1.1	Applied symmetry conditions	89
5.2.1.2	Normalized mode I stress intensity factor versus nonhomogeneity parameters p and q under steady state thermal loading, $r = 1.0$, $2h_1 = 2h_2 = 2h_3 = h_4/2 = c$, $T_1 = 10T_0$ and $T_2 = T_0$	90
5.2.1.3	Normalized mode II stress intensity factor versus nonhomogeneity parameters p and q under steady state thermal loading, $r = 1.0$, $2h_1 = 2h_2 = 2h_3 = h_4/2 = c$, $T_1 = 10T_0$ and $T_2 = T_0$	90
5.2.1.4	Normalized mode I stress intensity factor versus nonhomogeneity parameters p and r under steady state thermal loading, $q = 1.0$, $2h_1 = 2h_2 = 2h_3 = h_4/2 = c$, $T_1 = 10T_0$ and $T_2 = T_0$	91
5.2.1.5	Normalized mode II stress intensity factor versus nonhomogeneity parameters p and r under steady state thermal loading, $q = 1.0$, $2h_1 = 2h_2 = 2h_3 = h_4/2 = c$, $T_1 = 10T_0$ and $T_2 = T_0$	91
5.2.1.6	Deformed shape of the structure for $p = q = r = 1.0$	92
5.2.2.1	Applied symmetry and periodicity conditions on the unit cell	93
5.2.2.2	Normalized mode I stress intensity factor versus c/W and the nonhomogeneity parameter p under steady state thermal loading, $q = 1.0$, $r = 1.0$ $2h_1 = 2h_2 = 2h_3 = h_4/2 = c$, $T_1 = 10T_0$ and $T_2 = T_0$...	94
5.2.2.3	Normalized mode II stress intensity factor versus c/W and the nonhomogeneity parameter p under steady state thermal loading, $q = 1.0$, $r = 1.0$ $2h_1 = 2h_2 = 2h_3 = h_4/2 = c$, $T_1 = 10T_0$ and $T_2 = T_0$...	95
5.2.2.4	Normalized mode I stress intensity factor versus c/W and the nonhomogeneity parameter q under steady state thermal loading, $p = 1.0$, $r = 1.0$ $2h_1 = 2h_2 = 2h_3 = h_4/2 = c$, $T_1 = 10T_0$ and $T_2 = T_0$...	95
5.2.2.5	Normalized mode II stress intensity factor versus c/W and the nonhomogeneity parameter q under steady state thermal loading, $p = 1.0$, $r = 1.0$ $2h_1 = 2h_2 = 2h_3 = h_4/2 = c$, $T_1 = 10T_0$ and $T_2 = T_0$...	96

5.2.2.6	Normalized mode I stress intensity factor versus c/W and the nonhomogeneity parameter r under steady state thermal loading, $p = 1.0$, $q = 1.0$ $2h_1 = 2h_2 = 2h_3 = h_4/2 = c$, $T_1 = 10T_0$ and $T_2 = T_0$...	96
5.2.2.7	Normalized mode II stress intensity factor versus c/W and the nonhomogeneity parameter r under steady state thermal loading, $p = 1.0$, $q = 1.0$ $2h_1 = 2h_2 = 2h_3 = h_4/2 = c$, $T_1 = 10T_0$ and $T_2 = T_0$...	97
5.2.2.8	Deformed shape of the unit cell for $c/W = 0.3$ and $p = q = r = 1.0$	98
B.1	Illustration of the two orthotropic FGM half planes	140

CHAPTER 1

INTRODUCTION

1.1 Functionally Graded Materials

Functionally graded materials (FGMs) are nonhomogeneous material systems with two constituents. Compositions of the constituent materials change gradually with position to satisfy the desired properties. They were originally developed for high thermal gradient applications in Japan [1] and their constituent materials are generally ceramics and metal alloys. In the coating applications, the gradual change in material properties makes the FGMs superior to ceramics by increasing adhesion and decreasing thermal stresses resulting from mismatch of thermal expansion coefficients.

Today, they are used mainly in the thermal coating applications for high performance engines [2], gas turbines, space shuttles [3] and fusion reactors [4], interfacial zone applications for increasing the bonding strength and reducing the residual stresses [5], wear and corrosion barrier applications [6], contact damage resistant material applications [7-8], sensor and energy applications [9], biomedical applications [10].

The FGM manufacturing techniques usually include gradation and consolidation steps [11]. Gradation can be prepared via constitutive, homogenizing and segregating processes [11]. In constitutive process, graded structure is built up step by step from precursor materials or powders [11]. Homogenizing process converts a sharp interface between two materials into a gradient by material transport [11].

In segregating process, a macroscopically homogeneous material is graded by material transport due to an external field such as a gravitational or an electric field [11]. Plasma spraying [12-14], chemical vapor deposition [15], powder metallurgy [16-17], centrifugal casting [18], three dimensional printing [19] can be given as the examples of FGM processing techniques.

1.2 Literature Survey

In recent years, many researchers studied on the investigation of fracture behavior of FGMs under thermal and/or mechanical loading using theoretical or experimental approaches.

Delale and Erdogan [20] showed that the stresses around the crack tips in an elastic isotropic exponentially graded medium have the square-root singularity. Then, Konda and Erdogan [21] investigated the effects of the material nonhomogeneity constant, the crack orientation, the loading conditions and the Poisson's ratio on the stress intensity factors of a crack in an elastic exponentially graded medium. Erdogan [22] showed that the square-root singularity of the crack-tip stress field is unaffected by the discontinuity in the derivative of the shear modulus of a nonhomogeneous medium. Erdogan and Wu [23] considered the plane elasticity problem for a bounded nonhomogeneous layer containing an internal or an edge crack perpendicular to the boundaries. Ozturk and Erdogan [24] investigated an axisymmetric crack problem in a nonhomogeneous medium. Marur and Tippur [25] analyzed the nature of the singular field around the crack in FGM using finite element method by assuming linear variation of material property. Choi [26] analyzed the periodic array of parallel cracks in a functionally graded medium. Ergüven and Gross [27] considered a penny shaped crack in an infinite nonhomogeneous elastic medium. Gu, Dao and Asaro [28] proposed a finite element based method for obtaining stress intensity factors in FGMs in which the energy release rate is calculated through an area integral. Dag and Erdogan [29]

solved the problem of a surface crack in a semi-infinite elastic graded medium under general loading conditions. Wang, Mai and Sun [30] investigated the stress intensity factors for a FGM layer under anti-plane deformation. A number of authors concentrated on circumferential cracks in FGM cylinders [31-34]. Choi [35] analyzed the effects of graded layering on the tip behavior of a vertical crack in a substrate under frictional Hertzian contact. Dag and Erdogan [36] considered a coupled problem of crack contact mechanics in a semi-infinite nonhomogeneous medium to determine contact stresses and stress intensity factors. Several theoretical and experimental studies considered the crack growth behavior [37-46] and fracture toughness [47-49] of FGMs. Gu and Asaro [50], Ueda and Shindo [51] dealt with crack kinking in FGMs. T-stress effect was also incorporated into formulations to predict the crack initiation angle in FGMs [52]. Afsar and Sekine [53-54] studied on inverse problem of calculating material distribution intending to realize prescribed apparent fracture toughness in FGM circular pipes and in FGM coatings around a circular hole. Chen, Wu and Du [55] defined a modified J-integral that is path independent even in FGMs.

Delale and Erdoğan [56] obtained a solution for an interface crack between bonded homogeneous and nonhomogeneous half planes and found that the singular behavior of stresses in the nonhomogeneous medium is identical to that in a homogeneous medium if the spatial distribution of material properties is continuous near and at the crack tip. They also investigated the case of two homogeneous elastic half planes bonded through a nonhomogeneous layer with collinear cracks [57]. Erdogan and Ozturk [58] considered a mixed boundary value problem for a nonhomogeneous medium bonded to a rigid half space having a crack along the interface under antiplane shear loading. They also investigated the interface crack problem for two elastic half spaces bonded through a nonhomogeneous interfacial zone under antiplane shear loading [59]. Erdogan and Öztürk [60] also studied the antiplane elasticity problem for a functionally graded coating bonded to a homogeneous half space and containing periodic cracks

perpendicular to the surface. In another study [61], the same authors investigated the axisymmetric problem of a penny-shaped interface crack in homogeneous dissimilar materials bonded through a functionally graded interfacial region. Chen and Erdogan [62] studied the mixed-mode interface cracking in a homogeneous substrate and nonhomogeneous coating system considering continuous material properties with discontinuous derivatives at the interface and arbitrary crack surface tractions. In another paper, an interface crack between FGM coating and finite thickness homogeneous substrate was analyzed under a concentrated load [63]. Jin and Batra [64] investigated the interface cracking between ceramic and/or FGM coatings and a substrate under antiplane shear. Choi, Lee and Jin [65] analyzed a medium consisting of a surface layer and a semi-infinite substrate bonded through an interfacial zone with graded properties under the existence of three collinear cracks that are perpendicular to the interfaces and located in each one of the constituent materials. Shbeeb and Binienda [66] calculated the mixed-mode stress intensity factors and strain energy release rates of an interface crack for a FGM strip sandwiched between two homogeneous layers of finite thickness. Huang, Wang and their co-workers [67-69] modeled FGMs as a multilayered medium with the shear modulus varying linearly in each sub-layer and continuous at the sub-interfaces to investigate the crack problems. In another study, crack problems in a FGM whose upper and bottom surfaces are bonded with dissimilar homogeneous materials were analyzed using boundary element method [70]. Choi [71] provided an elasticity solution for an inclined crack in bonded media with a graded nonhomogeneous interlayer. Chi and Chung [72] dealt with the cracking in coating-substrate systems with multilayered and FGM coatings using finite element method. Chiu and Erdogan [73] formulated a plane strain interface crack problem for a graded coating bonded to homogeneous substrate by using a kinematically nonlinear continuum theory considering both instability and post-buckling.

FGM coatings and interfacial zones seem to be quite effective in reducing residual stresses and this subject was examined in many studies [74-80]. Noda and Jin [81]

analyzed a completely insulated crack in a strip of FGM with prescribed surface temperature by reducing the thermal and mechanical problems to two systems of singular integral equations employing the Fourier transform technique. They also solved a crack problem for a semi-infinite nonhomogeneous thermoelastic solid subjected to steady heat flux over the boundary using the same method [82]. In another paper [83], they analyzed the effect of nonhomogeneity on stress intensity factors considering the crack problem for an infinite nonhomogeneous elastic solid subjected to steady heat flux over the crack surfaces. Bao and Wang [84] made finite element calculations for the energy release rate of the cracks in FGM coating bonded to metal substrate considering both mechanical and thermal loads. In their study it was found that the effect of different gradations on the crack driving force is relatively small under mechanical loading but can be significant under thermal loading. Nemat-Alla and Noda [85] investigated an edge crack problem in a semi-infinite FGM plate with a bi-directional coefficient of thermal expansion under two-dimensional thermal loading. Bao and Cai [86] studied a delamination crack problem for FGM coating-metal substrate systems performing a steady state heat transfer analysis. Lee and Erdogan [87] analyzed partially insulated and symmetrically located edge cracks along the interface between homogeneous substrate and graded coating under the steady state heat conduction with convective boundary conditions. Yang [88] made a stress analysis in a joint with a functionally graded material under thermal loading. Noda [89] dealt with optimal composition profile problems of FGMs to decrease the thermal stress intensity factors. Wang and Noda [90] examined the fracture behavior of a cracked smart FGM actuator on a substrate under thermal load by using integral transform method and solving singular integral equations numerically. They also investigated thermally loaded functionally graded materials containing penny shaped cracks by modeling the FGM with a large number of layers having different material properties [91]. El-Borgi, Erdogan and Hidri [92] examined an infinite functionally graded medium with a partially insulated crack subjected to a steady state heat flux away from the crack region as well as mechanical crack surface stresses by converting heat

conduction and elasticity equations into singular integral equations. El-Borgi, Erdogan and Hatira [93] investigated the problem of a FGM coating bonded to an infinite homogeneous substrate with a partially insulated interface crack under thermal and mechanical loading by using analytical method and finite element method. Itou [94] determined the thermal stresses around a crack in a nonhomogeneous interfacial layer between two dissimilar elastic half planes under uniform heat flow by using insulated crack surface assumption. Yildirim and Erdogan [95] investigated an axisymmetric crack problem for FGM thermal barrier coatings under a uniform temperature change. Dag [96] investigated the mixed-mode fracture in FGMs under thermal stresses via a new approach using Jk-integral. Besides the aforementioned studies, there are also a large number of investigations considering transient thermal loading or thermal cycling in FGMs [97-114].

Manufacturing techniques of FGMs generally do not lead to the material isotropy [115]. In the literature, there are a number of studies about the fracture analysis of orthotropic FGMs. Gu and Asaro [116] analyzed a semi-infinite crack in a strip of an isotropic functionally graded material under edge loading and inplane deformation conditions. Then, the solution was extended to the case of an orthotropic FGM strip. Ozturk and Erdogan [115, 117] investigated mixed-mode and mode I crack problems in an orthotropic graded medium using integral equations. Kim and Paulino presented isoparametric graded finite elements for nonhomogeneous isotropic and orthotropic materials [118] and mixed-mode J-integral formulation and implementation using graded elements for fracture analysis of nonhomogeneous orthotropic materials [119]. They evaluated stress intensity factors for two dimensional crack problems in orthotropic FGMs by using the displacement correlation technique, modified crack closure method [120] and the interaction integral [121]. Dag et al. [122] analyzed the problem of an interface crack between a graded orthotropic coating and a homogeneous orthotropic substrate using analytical and computational approaches. Yildirim and his

coworkers [123] analyzed the steady state heat conduction in orthotropic FGMs containing cracks using analytical and computational techniques. Chen [124] studied on the determination of thermal stress intensity factors for an interface crack in an orthotropic graded coating-substrate structure. Dag [125] performed a thermal fracture analysis of orthotropic functionally graded materials using an equivalent domain integral approach. Dag et al. [126] analyzed the mixed-mode fracture behavior of an orthotropic FGM layer considering embedded cracking for various boundary conditions.

In computational studies, one of the methods used in determining stress intensity factors is the displacement correlation technique (DCT). In this technique, finite element model of the problem is created using singular elements around the crack tip. Then, displacements at specific nodal locations of the singular elements are correlated with the known analytical solutions to extract the stress intensity factors. Barsoum [127] stated that quadratic isoparametric elements satisfy the square root singularity by placing the mid-side node on any side at the quarter point. The method for extracting the stress intensity factors from nodal displacements of these elements was given for two-dimensional isotropic problems by Shih et al. [128]. Ingraffea and Manu [129] employed the DCT for three-dimensional isotropic problems. Saouma and Sikiotis [130] used this method for three-dimensional anisotropic problems. Boone et al. [131] showed that isoparametric quarter-point elements could be used to obtain accurate stress intensity factors for the fracture propagation analysis in the two dimensional orthotropic materials. As mentioned previously, Kim and Paulino [120] used the DCT to evaluate the mixed-mode stress intensity factors for two dimensional crack problems in the orthotropic FGMs.

1.3 Objective of the Study

The objective of this study is to investigate the mixed-mode fracture behavior of an orthotropic FGM coating bonded to a homogeneous substrate through a homogeneous bond-coat layer under thermal or mechanical loading conditions. Both analytical and computational methods are used to show the effects of material nonhomogeneity, material orthotropy and geometric variables on the fracture related parameters.

In Chapter 2, analytical mixed-mode fracture analysis of the structure is performed. The orthotropic FGM coating is assumed to contain a single embedded crack that is subjected to either uniform normal or uniform shear surface tractions. The material property gradation in the FGM coating is represented in moduli of elasticity and shear modulus along the thickness direction in an exponential form and the crack lies parallel to the boundaries. Principal directions of orthotropy are parallel and perpendicular to the crack line. Averaged constants of plane orthotropic elasticity [132] are employed to express the constitutive relations. Using Fourier transformations, the problem is reduced to a couple of singular integral equations that are solved by means of an expansion-collocation technique. Then, the expressions for the mixed-mode stress intensity factors, energy release rate and crack opening displacements are obtained.

In Chapter 3, details of the computational approach used to perform the mixed-mode fracture analysis of the structure are presented. The adopted computational approach employs the finite element method in conjunction with the displacement correlation technique (DCT). The reason of investigating the problem using the computational approach is to examine the analytically untractable conditions without the restrictive assumptions.

In Chapter 4, some numerical results obtained by analytical and/or computational approaches are presented for mechanical loading conditions. First, validation of the analytical study presented in Chapter 2 is performed referring to the literature. Then, some numerical results showing the effects of material orthotropy, material nonhomogeneity and geometric parameters on the fracture behavior of the orthotropic FGM coating are given considering the pure uniform normal stress on crack surfaces for the single embedded crack problem. Both analytical and computational results are given for this problem to assess the computational approach. Later, some numerical results based on analytical method are presented for the single embedded crack problem to show the effects of material orthotropy and material nonhomogeneity on fracture parameters when crack surfaces are subjected to a pure uniform shear stress. Finally, the periodic embedded cracking in the orthotropic FGM coating is investigated computationally and numerical results showing the effects of crack periodicity and material nonhomogeneity on the fracture parameters are given considering the pure uniform normal stress on the crack surfaces.

In Chapter 5, single and periodic embedded cracking problems are examined computationally under steady state thermal loading assuming plane stress state. It is assumed that upper and lower boundaries of the structure are subjected to uniform constant temperatures. The material property gradation of the FGM coating is represented by elastic properties, heat conductivities and thermal expansion coefficients along the thickness direction in the power function form. The obtained results show the effects of material nonhomogeneity parameters and crack periodicity on the fracture behavior of the orthotropic FGM coating.

Both of the developed analytical method and the computational method can be used to provide the useful information for the design optimization of the structure consisting of an orthotropic FGM coating, a homogeneous bond-coat and a homogeneous substrate.

CHAPTER 2

ANALYTICAL SOLUTION FOR THE SINGLE EMBEDDED CRACK PROBLEM IN AN ORTHOTROPIC FGM COATING UNDER CRACK SURFACE TRACTIONS

2.1 Description of the Problem

Fracture behavior of an orthotropic FGM coating is examined by considering an embedded crack. The coating is perfectly bonded to a homogeneous orthotropic substrate through a layer of homogeneous orthotropic bond-coat. Illustration of the problem is shown in Figure-2.1.1. Principal axes of orthotropy are along x_1 - and x_2 - directions in each medium. Material property gradation of the coating is in x_2 - direction. The crack of length $2c$ lies along $x_2 = 0$ line. Distance from the crack line to the upper and lower surfaces of the coating is h_1 and h_2 , respectively. Thickness of the bond-coat is h_3 and thickness of the substrate is h_4 . The length of the structure in x_1 - direction is infinitely long.

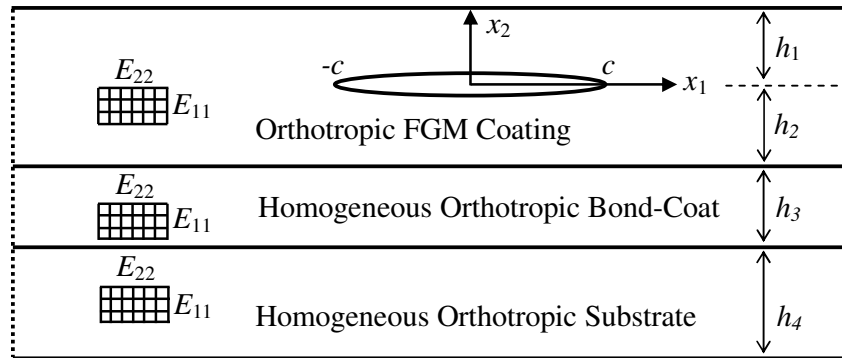


Figure-2.1.1 Illustration of the problem.

Material properties are taken to be continuous in each medium but can be discontinuous at the interfaces. The problem is formulated by applying either uniform normal or uniform shear stresses to the crack surfaces.

2.2 Formulation of the Problem

Using the principal axes of the material, Hooke's law for plane orthotropic elasticity can be written in the following form [132]:

$$\begin{bmatrix} \varepsilon_{11} \\ \varepsilon_{22} \\ \varepsilon_{12} \end{bmatrix} = \frac{1}{E} \begin{bmatrix} \delta^{-2} & -\nu & 0 \\ -\nu & \delta^2 & 0 \\ 0 & 0 & (\kappa + \nu) \end{bmatrix} \begin{bmatrix} \sigma_{11} \\ \sigma_{22} \\ \sigma_{12} \end{bmatrix} \quad (2.2.1)$$

where ε_{11} , ε_{22} , ε_{12} are the strain components and σ_{11} , σ_{22} , σ_{12} are the stress components with respect to the principal axes of the material. E is the effective stiffness, ν is the effective Poisson's ratio, δ^4 is the stiffness ratio and κ is the shear parameter. Definitions of these material parameters are such that [132]:

$$E = \begin{cases} \sqrt{E_{11}E_{22}}, & \text{generalized plane stress} \\ \sqrt{\frac{E_{11}E_{22}}{(1-\nu_{13}\nu_{31})(1-\nu_{23}\nu_{32})}}, & \text{plane strain} \end{cases} \quad (2.2.2a)$$

$$\nu = \begin{cases} \sqrt{\nu_{12}\nu_{21}}, & \text{generalized plane stress} \\ \sqrt{\frac{(\nu_{12} + \nu_{13}\nu_{32})(\nu_{21} + \nu_{23}\nu_{31})}{(1-\nu_{13}\nu_{31})(1-\nu_{23}\nu_{32})}}, & \text{plane strain} \end{cases} \quad (2.2.2b)$$

$$\delta^4 = \begin{cases} \frac{E_{11}}{E_{22}} = \frac{\nu_{12}}{\nu_{21}}, \text{ generalized plane stress} \\ \frac{E_{11}}{E_{22}} \frac{1 - \nu_{23}\nu_{32}}{1 - \nu_{13}\nu_{31}}, \text{ plane strain} \end{cases} \quad (2.2.2c)$$

$$\kappa = \frac{E}{2G_{12}} - \nu, \text{ for generalized plane stress and plane strain} \quad (2.2.2d)$$

where E_{11} and E_{22} are the moduli of elasticity, G_{12} is the shear modulus and ν_{ij} , ($i, j = 1, 2, 3$), is the Poisson's ratio with respect to the principal axes of the material.

For the orthotropic FGM coating, it is assumed that E_{11} , E_{22} and G_{12} varies proportionately in x_2 - direction in an exponential form. ν_{ij} , ($i, j = 1, 2, 3$), is assumed to be constant throughout the coating. Hence, ν , δ^4 and κ are constant throughout the coating and the nonhomogeneity in the medium is represented by the effective stiffness term. They are written as follows:

$$E_1(x_1, x_2) = E_0 \exp(\beta x_2), \quad \kappa_1(x_1, x_2) = \kappa_0, \quad \delta_1(x_1, x_2) = \delta_0, \quad \nu_1(x_1, x_2) = \nu_0 \quad (2.2.3)$$

where subscript 1 refers to the coating, β is the material nonhomogeneity parameter and E_0 is the effective stiffness at the crack line.

For the homogeneous orthotropic bond-coat, the material parameters are defined by the following expressions where subscript 3 refers to the bond-coat.

$$E_3(x_1, x_2) = E_3, \quad \kappa_3(x_1, x_2) = \kappa_3, \quad \delta_3(x_1, x_2) = \delta_3, \quad \nu_3(x_1, x_2) = \nu_3 \quad (2.2.4)$$

For the homogeneous orthotropic substrate, the material parameters are defined by the following expressions where subscript 4 refers to the substrate.

$$E_4(x_1, x_2) = E_4, \kappa_4(x_1, x_2) = \kappa_4, \delta_4(x_1, x_2) = \delta_4, \nu_4(x_1, x_2) = \nu_4 \quad (2.2.5)$$

Then, suitable transformations are introduced for the coordinates, displacements and stresses as follows [132]:

$$x = \frac{x_1}{\sqrt{\delta_0}}, \quad y = x_2 \sqrt{\delta_0} \quad (2.2.6a)$$

$$u(x, y) = u_1(x_1, x_2) \sqrt{\delta_0}, \quad v(x, y) = \frac{u_2(x_1, x_2)}{\sqrt{\delta_0}} \quad (2.2.6b)$$

$$\sigma_{xx}(x, y) = \frac{\sigma_{11}(x_1, x_2)}{\delta_0}, \quad \sigma_{yy}(x, y) = \sigma_{22}(x_1, x_2) \delta_0, \quad \sigma_{xy}(x, y) = \sigma_{12}(x_1, x_2) \quad (2.2.6c)$$

where x and y are the transformed coordinates. u and v are the displacement components along x - and y - directions, respectively. u_1 and u_2 are the displacement components along x_1 - and x_2 - directions, respectively. σ_{xx} , σ_{yy} and σ_{xy} are the stress components in the transformed coordinates.

Strain-displacement equations in x_1 - and x_2 - coordinates are given as follows:

$$\varepsilon_{11} = \frac{\partial u_1}{\partial x_1}, \quad \varepsilon_{22} = \frac{\partial u_2}{\partial x_2}, \quad \varepsilon_{12} = \frac{1}{2} \left(\frac{\partial u_1}{\partial x_2} + \frac{\partial u_2}{\partial x_1} \right) \quad (2.2.7)$$

Using Eq.(2.2.6a), Eq.(2.2.6b) and Eq.(2.2.7), strain components in the transformed coordinates ε_{xx} , ε_{yy} and ε_{xy} can be found as follows [132]:

$$\varepsilon_{xx} = \delta_0 \varepsilon_{11}, \quad \varepsilon_{yy} = \frac{\varepsilon_{22}}{\delta_0}, \quad \varepsilon_{xy} = \varepsilon_{12} \quad (2.2.8)$$

Using Eq.(2.2.1), Eq.(2.2.6c) and Eq.(2.2.8), stress-strain relations in the transformed coordinates become:

$$\begin{bmatrix} \varepsilon_{xx} \\ \varepsilon_{yy} \\ \varepsilon_{xy} \end{bmatrix} = \frac{1}{E^*} \begin{bmatrix} (\delta^*/\delta_0)^{-2} & -\nu^* & 0 \\ -\nu^* & (\delta^*/\delta_0)^2 & 0 \\ 0 & 0 & (\kappa^* + \nu^*) \end{bmatrix} \begin{bmatrix} \sigma_{xx} \\ \sigma_{yy} \\ \sigma_{xy} \end{bmatrix} \quad (2.2.9)$$

where $E^*(x, y) = E(x_1, x_2)$, $\nu^*(x, y) = \nu(x_1, x_2)$, $\delta^*(x, y) = \delta(x_1, x_2)$ and $\kappa^*(x, y) = \kappa(x_1, x_2)$.

Strain-displacement equations in the transformed coordinates are expressed as:

$$\varepsilon_{xx} = \frac{\partial u}{\partial x}, \quad \varepsilon_{yy} = \frac{\partial v}{\partial y}, \quad \varepsilon_{xy} = \frac{1}{2} \left(\frac{\partial u}{\partial y} + \frac{\partial v}{\partial x} \right) \quad (2.2.10)$$

Then, stress components σ_{xx} , σ_{yy} and σ_{xy} can be obtained as follows:

$$\sigma_{xx} = \frac{E^*}{1 - (\nu^*)^2} \left[\left(\frac{\delta^*}{\delta_0} \right)^2 \frac{\partial u}{\partial x} + \nu^* \frac{\partial v}{\partial y} \right] \quad (2.2.11a)$$

$$\sigma_{yy} = \frac{E^*}{1 - (\nu^*)^2} \left[\nu^* \frac{\partial u}{\partial x} + \left(\frac{\delta_0}{\delta^*} \right)^2 \frac{\partial v}{\partial y} \right] \quad (2.2.11b)$$

$$\sigma_{xy} = \frac{E^*}{2(\kappa^* + \nu^*)} \left(\frac{\partial u}{\partial y} + \frac{\partial v}{\partial x} \right) \quad (2.2.11c)$$

Using Eq.(2.2.6a), the material parameters of the orthotropic FGM coating take the following form in the transformed coordinates:

$$E_1^*(x, y) = E_0 \exp(\gamma y), \quad \kappa_1^*(x, y) = \kappa_0, \quad \delta_1^*(x, y) = \delta_0, \quad \nu_1^*(x, y) = \nu_0 \quad (2.2.12)$$

where $\gamma = \beta / (\delta_0)^{0.5}$ is the material nonhomogeneity parameter in the transformed coordinates.

For the homogeneous orthotropic bond-coat, the material parameters in the transformed coordinates are written as:

$$E_3^*(x, y) = E_3, \quad \kappa_3^*(x, y) = \kappa_3, \quad \delta_3^*(x, y) = \delta_3, \quad \nu_3^*(x, y) = \nu_3 \quad (2.2.13)$$

For the homogeneous orthotropic substrate, the material parameters in the transformed coordinates are written as:

$$E_4^*(x, y) = E_4, \quad \kappa_4^*(x, y) = \kappa_4, \quad \delta_4^*(x, y) = \delta_4, \quad \nu_4^*(x, y) = \nu_4 \quad (2.2.14)$$

Governing equations for each medium are derived using the equilibrium and stress-displacement equations. Equilibrium equations in the transformed coordinates considering no body force components are expressed as follows:

$$\sigma_{ij,i} = 0, \quad (i, j = x, y) \quad (2.2.15)$$

Substituting the stress expressions given by Eq.(2.2.11) in the equilibrium equations given above and using the material parameters given by Eq.(2.2.12), governing equations for the orthotropic FGM coating are obtained as [115]:

$$\frac{\partial^2 u^{(i)}}{\partial y^2} + \beta_1 \frac{\partial^2 u^{(i)}}{\partial x^2} + \beta_2 \frac{\partial^2 v^{(i)}}{\partial x \partial y} + \gamma \left(\frac{\partial u^{(i)}}{\partial y} + \frac{\partial v^{(i)}}{\partial x} \right) = 0 \quad (2.2.16a)$$

$$\frac{\partial^2 v^{(i)}}{\partial x^2} + \beta_1 \frac{\partial^2 v^{(i)}}{\partial y^2} + \beta_2 \frac{\partial^2 u^{(i)}}{\partial x \partial y} + \beta_1 \gamma \left(\frac{\partial v^{(i)}}{\partial y} + \nu_0 \frac{\partial u^{(i)}}{\partial x} \right) = 0 \quad (2.2.16b)$$

where the superscript (i) is (1) for the region of the orthotropic FGM coating above the crack line where $h_1 \sqrt{\delta_0} > y > 0$ and (2) for the region of the orthotropic FGM coating below the crack line where $-h_2 \sqrt{\delta_0} < y < 0$. β_1 and β_2 are defined as:

$$\beta_1 = \frac{2(\kappa_0 + \nu_0)}{1 - \nu_0^2}, \quad \beta_2 = 1 + \nu_0 \beta_1 \quad (2.2.17)$$

For the homogeneous orthotropic bond-coat where $-(h_3 + h_2) \sqrt{\delta_0} < y < -h_2 \sqrt{\delta_0}$, governing equations are obtained using Eq.(2.2.11), Eq.(2.2.15) and Eq.(2.2.13) as follows:

$$\frac{\partial^2 u^{(3)}}{\partial y^2} + \beta_3 \left(\frac{\delta_3}{\delta_0} \right)^2 \frac{\partial^2 u^{(3)}}{\partial x^2} + \beta_4 \frac{\partial^2 v^{(3)}}{\partial x \partial y} = 0 \quad (2.2.18a)$$

$$\frac{\partial^2 v^{(3)}}{\partial x^2} + \beta_3 \left(\frac{\delta_0}{\delta_3} \right)^2 \frac{\partial^2 v^{(3)}}{\partial y^2} + \beta_4 \frac{\partial^2 u^{(3)}}{\partial x \partial y} = 0 \quad (2.2.18b)$$

where the superscript (3) denotes the bond-coat and β_3 and β_4 are defined as:

$$\beta_3 = \frac{2(\kappa_3 + \nu_3)}{1 - \nu_3^2}, \quad \beta_4 = 1 + \nu_3\beta_3 \quad (2.2.19)$$

Governing equations for the homogeneous orthotropic substrate where $-(h_4 + h_3 + h_2)\sqrt{\delta_0} < y < -(h_3 + h_2)\sqrt{\delta_0}$ are obtained using Eq.(2.2.11), Eq.(2.2.15) and Eq.(2.2.14) as follows:

$$\frac{\partial^2 u^{(4)}}{\partial y^2} + \beta_5 \left(\frac{\delta_4}{\delta_0} \right)^2 \frac{\partial^2 u^{(4)}}{\partial x^2} + \beta_6 \frac{\partial^2 v^{(4)}}{\partial x \partial y} = 0 \quad (2.2.20a)$$

$$\frac{\partial^2 v^{(4)}}{\partial x^2} + \beta_5 \left(\frac{\delta_0}{\delta_4} \right)^2 \frac{\partial^2 v^{(4)}}{\partial y^2} + \beta_6 \frac{\partial^2 u^{(4)}}{\partial x \partial y} = 0 \quad (2.2.20b)$$

where the superscript (4) denotes the substrate and β_5 and β_6 are defined as:

$$\beta_5 = \frac{2(\kappa_4 + \nu_4)}{1 - \nu_4^2}, \quad \beta_6 = 1 + \nu_4\beta_5 \quad (2.2.21)$$

Displacement components for the region of the orthotropic FGM coating above the crack line where $h_1\sqrt{\delta_0} > y > 0$ can be written in the following form using Fourier transform integrals:

$$u^{(1)}(x, y) = \frac{1}{2\pi} \int_{-\infty}^{\infty} U_1(\omega, y) \exp(i\omega x) d\omega \quad (2.2.22a)$$

$$v^{(i)}(x, y) = \frac{1}{2\pi} \int_{-\infty}^{\infty} V_1(\omega, y) \exp(i\omega x) d\omega \quad (2.2.22b)$$

where $U_1(\omega, y)$ and $V_1(\omega, y)$ are Fourier transforms of $u^{(i)}(x, y)$ and $v^{(i)}(x, y)$ in x , respectively.

Using Eq.(2.2.22), governing equations given by Eq.(2.2.16) become:

$$\frac{d^2 U_1}{dy^2} - \beta_1 \omega^2 U_1 + i\omega \beta_2 \frac{dV_1}{dy} + \gamma \left(\frac{dU_1}{dy} + i\omega V_1 \right) = 0 \quad (2.2.23a)$$

$$-\omega^2 V_1 + \beta_1 \frac{d^2 V_1}{dy^2} + i\omega \beta_2 \frac{dU_1}{dy} + \beta_1 \gamma \left(\frac{dV_1}{dy} + v_0 i\omega U_1 \right) = 0 \quad (2.2.23b)$$

Solving the above system of ordinary differential equations, $U_1(\omega, y)$ and $V_1(\omega, y)$ can be written in the following form:

$$U_1(\omega, y) = \sum_{j=1}^4 M_j(\omega) \exp(s_j(\omega)y), \quad (j = 1, 2, 3, 4) \quad (2.2.24a)$$

$$V_1(\omega, y) = \sum_{j=1}^4 M_j(\omega) N_j(\omega) \exp(s_j(\omega)y), \quad (j = 1, 2, 3, 4) \quad (2.2.24b)$$

where

$$s_1(\omega) = -(\gamma/2) - \sqrt{(\gamma/2)^2 + \omega^2 \kappa_0 + \omega \sqrt{\omega^2 \kappa_0^2 - \omega^2 - \gamma^2 v_0}} \quad (2.2.25a)$$

$$s_2(\omega) = -(\gamma/2) - \sqrt{(\gamma/2)^2 + \omega^2 \kappa_0 - \omega \sqrt{\omega^2 \kappa_0^2 - \omega^2 - \gamma^2 v_0}} \quad (2.2.25b)$$

$$s_3(\omega) = -(\gamma/2) + \sqrt{(\gamma/2)^2 + \omega^2 \kappa_0 + \omega \sqrt{\omega^2 \kappa_0^2 - \omega^2 - \gamma^2 \nu_0}} \quad (2.2.25c)$$

$$s_4(\omega) = -(\gamma/2) + \sqrt{(\gamma/2)^2 + \omega^2 \kappa_0 - \omega \sqrt{\omega^2 \kappa_0^2 - \omega^2 - \gamma^2 \nu_0}} \quad (2.2.25d)$$

$M_j(\omega)$, ($j=1, 2, 3, 4$), are unknown functions of ω and $N_j(\omega)$, ($j=1, 2, 3, 4$), are found by using Eq.(2.2.23a) and Eq.(2.2.24) as follows:

$$N_j(\omega) = \frac{-i((\nu_0^2 - 1)(s_j(\omega))^2 + \gamma s_j(\omega)) + 2\omega^2(\kappa_0 + \nu_0)}{\omega(s_j(\omega)(1 + \nu_0^2 + 2\nu_0 \kappa_0) + \gamma(1 - \nu_0^2))}, \quad (j=1, 2, 3, 4) \quad (2.2.26)$$

Substituting Eq.(2.2.24) into Eq.(2.2.22), displacement components can be obtained as:

$$u^{(1)}(x, y) = \frac{1}{2\pi} \int \sum_{-\infty}^{\infty} M_j(\omega) \exp(s_j(\omega)y + i\omega x) d\omega \quad (2.2.27a)$$

$$v^{(1)}(x, y) = \frac{1}{2\pi} \int \sum_{-\infty}^{\infty} M_j(\omega) N_j(\omega) \exp(s_j(\omega)y + i\omega x) d\omega \quad (2.2.27b)$$

Then, stress components σ_{yy} and σ_{xy} can be found using Eq.(2.2.11b), Eq.(2.2.11c), Eq.(2.2.12) and Eq.(2.2.27) as follows:

$$\sigma_{yy}^{(1)}(x, y) = \frac{E_0 \exp(\gamma y)}{1 - \nu_0^2} \left\{ \frac{1}{2\pi} \int \sum_{-\infty}^{\infty} M_j(\omega) (\nu_0 i \omega + N_j(\omega) s_j(\omega)) \exp(s_j(\omega)y + i\omega x) d\omega \right\} \quad (2.2.28a)$$

$$\sigma_{xy}^{(1)}(x, y) = \frac{E_0 \exp(\gamma y)}{2(\kappa_0 + \nu_0)} \left\{ \frac{1}{2\pi} \int_{-\infty}^{\infty} \sum_{j=1}^4 M_j(\omega) (N_j(\omega) i\omega + s_j(\omega)) \exp(s_j(\omega)y + i\omega x) d\omega \right\} \quad (2.2.28b)$$

Displacement components for the region of the orthotropic FGM coating below the crack line where $-h_2\sqrt{\delta_0} < y < 0$ can be written in the following form using Fourier transform integrals:

$$u^{(2)}(x, y) = \frac{1}{2\pi} \int_{-\infty}^{\infty} U_2(\omega, y) \exp(i\omega x) d\omega \quad (2.2.29a)$$

$$v^{(2)}(x, y) = \frac{1}{2\pi} \int_{-\infty}^{\infty} V_2(\omega, y) \exp(i\omega x) d\omega \quad (2.2.29b)$$

where $U_2(\omega, y)$ and $V_2(\omega, y)$ are Fourier transforms of $u^{(2)}(x, y)$ and $v^{(2)}(x, y)$ in x , respectively.

Using Eq.(2.2.29), governing equations given by Eq.(2.2.16) take the following form:

$$\frac{d^2 U_2}{dy^2} - \beta_1 \omega^2 U_2 + i\omega \beta_2 \frac{dV_2}{dy} + \gamma \left(\frac{dU_2}{dy} + i\omega V_2 \right) = 0 \quad (2.2.30a)$$

$$-\omega^2 V_2 + \beta_1 \frac{d^2 V_2}{dy^2} + i\omega \beta_2 \frac{dU_2}{dy} + \beta_1 \gamma \left(\frac{dV_2}{dy} + \nu_0 i\omega U_2 \right) = 0 \quad (2.2.30b)$$

Solving Eq.(2.2.30), $U_2(\omega, y)$ and $V_2(\omega, y)$ are found as:

$$U_2(\omega, y) = \sum_{j=1}^4 G_j(\omega) \exp(s_j(\omega)y), \quad (j = 1, 2, 3, 4) \quad (2.2.31a)$$

$$V_2(\omega, y) = \sum_{j=1}^4 G_j(\omega) N_j(\omega) \exp(s_j(\omega)y), \quad (j = 1, 2, 3, 4) \quad (2.2.31b)$$

where $G_j(\omega)$, ($j = 1, 2, 3, 4$), are unknown functions of ω .

Substituting Eq.(2.2.31) into Eq.(2.2.29), displacement components can be obtained as:

$$u^{(2)}(x, y) = \frac{1}{2\pi} \int_{-\infty}^{\infty} \sum_{j=1}^4 G_j(\omega) \exp(s_j(\omega)y + i\omega x) d\omega \quad (2.2.32a)$$

$$v^{(2)}(x, y) = \frac{1}{2\pi} \int_{-\infty}^{\infty} \sum_{j=1}^4 G_j(\omega) N_j(\omega) \exp(s_j(\omega)y + i\omega x) d\omega \quad (2.2.32b)$$

Then, stress components σ_{yy} and σ_{xy} are found using Eq.(2.2.11b), Eq.(2.2.11c), Eq.(2.2.12) and Eq.(2.2.32) as follows:

$$\sigma_{yy}^{(2)}(x, y) = \frac{E_0 \exp(\gamma y)}{1 - \nu_0^2} \left\{ \frac{1}{2\pi} \int_{-\infty}^{\infty} \sum_{j=1}^4 G_j(\omega) (\nu_0 i\omega + N_j(\omega) s_j(\omega)) \exp(s_j(\omega)y + i\omega x) d\omega \right\} \quad (2.2.33a)$$

$$\sigma_{xy}^{(2)}(x, y) = \frac{E_0 \exp(\gamma y)}{2(\kappa_0 + \nu_0)} \left\{ \frac{1}{2\pi} \int_{-\infty}^{\infty} \sum_{j=1}^4 G_j(\omega) (N_j(\omega) i\omega + s_j(\omega)) \exp(s_j(\omega)y + i\omega x) d\omega \right\} \quad (2.2.33b)$$

Displacement components for the homogeneous orthotropic bond-coat where $-(h_3 + h_2)\sqrt{\delta_0} < y < -h_2\sqrt{\delta_0}$ can be written in the following form using Fourier transform integrals:

$$u^{(3)}(x, y) = \frac{1}{2\pi} \int_{-\infty}^{\infty} U_3(\omega, y) \exp(i\omega x) d\omega \quad (2.2.34a)$$

$$v^{(3)}(x, y) = \frac{1}{2\pi} \int_{-\infty}^{\infty} V_3(\omega, y) \exp(i\omega x) d\omega \quad (2.2.34b)$$

where $U_3(\omega, y)$ and $V_3(\omega, y)$ are Fourier transforms of $u^{(3)}(x, y)$ and $v^{(3)}(x, y)$ in x , respectively.

Using Eq.(2.2.34), governing equations given by Eq.(2.2.18) can be expressed as:

$$\frac{d^2 U_3}{dy^2} - \beta_3 \omega^2 \left(\frac{\delta_3}{\delta_0} \right)^2 U_3 + i\omega \beta_4 \frac{dV_3}{dy} = 0 \quad (2.2.35a)$$

$$-\omega^2 V_3 + \beta_3 \left(\frac{\delta_0}{\delta_3} \right)^2 \frac{d^2 V_3}{dy^2} + i\omega \beta_4 \frac{dU_3}{dy} = 0 \quad (2.2.35b)$$

Solving the above system of ordinary differential equations, $U_3(\omega, y)$ and $V_3(\omega, y)$ are obtained as:

$$U_3(\omega, y) = \sum_{j=1}^4 A_j(\omega) \exp(r_j(\omega)y), \quad (j = 1, 2, 3, 4) \quad (2.2.36a)$$

$$V_3(\omega, y) = \sum_{j=1}^4 A_j(\omega) B_j(\omega) \exp(r_j(\omega)y), \quad (j = 1, 2, 3, 4) \quad (2.2.36b)$$

where

$$r_1(\omega) = |\omega| \frac{\delta_3}{\delta_0} \sqrt{\kappa_3 + \sqrt{\kappa_3^2 - 1}} \quad (2.2.37a)$$

$$r_2(\omega) = |\omega| \frac{\delta_3}{\delta_0} \sqrt{\kappa_3 - \sqrt{\kappa_3^2 - 1}} \quad (2.2.37b)$$

$$r_3(\omega) = -|\omega| \frac{\delta_3}{\delta_0} \sqrt{\kappa_3 + \sqrt{\kappa_3^2 - 1}} \quad (2.2.37c)$$

$$r_4(\omega) = -|\omega| \frac{\delta_3}{\delta_0} \sqrt{\kappa_3 - \sqrt{\kappa_3^2 - 1}} \quad (2.2.37d)$$

$A_j(\omega)$, ($j = 1, 2, 3, 4$), are unknown functions of ω and $B_j(\omega)$, ($j = 1, 2, 3, 4$), are found by substituting Eq.(2.2.36) into Eq.(2.2.35a) as:

$$B_j(\omega) = \frac{-i \left((r_j(\omega))^2 (v_3^2 - 1) + 2\omega^2 \left(\frac{\delta_3}{\delta_0} \right)^2 (\kappa_3 + v_3) \right)}{\omega r_j(\omega) (1 + v_3^2 + 2v_3 \kappa_3)}, \quad (j = 1, 2, 3, 4) \quad (2.2.38)$$

Substituting Eq.(2.2.36) into Eq.(2.2.34), displacement components are obtained as:

$$u^{(3)}(x, y) = \frac{1}{2\pi} \int \sum_{j=1}^4 A_j(\omega) \exp(r_j(\omega)y + i\omega x) d\omega \quad (2.2.39a)$$

$$v^{(3)}(x, y) = \frac{1}{2\pi} \int_{-\infty}^{\infty} \sum_{j=1}^4 A_j(\omega) B_j(\omega) \exp(r_j(\omega)y + i\omega x) d\omega \quad (2.2.39b)$$

Then, stress components σ_{yy} and σ_{xy} are found using Eq.(2.2.11b), Eq.(2.2.11c), Eq.(2.2.13) and Eq.(2.2.39) as follows:

$$\sigma_{yy}^{(3)}(x, y) = \frac{E_3}{1-\nu_3^2} \left\{ \frac{1}{2\pi} \int_{-\infty}^{\infty} \sum_{j=1}^4 A_j(\omega) \left(\nu_3 i\omega + \left(\frac{\delta_0}{\delta_3} \right)^2 r_j(\omega) \right) B_j(\omega) \exp(r_j(\omega)y + i\omega x) d\omega \right\} \quad (2.2.40a)$$

$$\sigma_{xy}^{(3)}(x, y) = \frac{E_3}{2(\kappa_3 + \nu_3)} \left\{ \frac{1}{2\pi} \int_{-\infty}^{\infty} \sum_{j=1}^4 iA_j(\omega) (-r_j(\omega)i + \omega B_j(\omega)) \exp(r_j(\omega)y + i\omega x) d\omega \right\} \quad (2.2.40b)$$

Displacement components for the homogeneous orthotropic substrate where $-(h_4 + h_3 + h_2)\sqrt{\delta_0} < y < -(h_3 + h_2)\sqrt{\delta_0}$ can be written in the following form using Fourier transform integrals:

$$u^{(4)}(x, y) = \frac{1}{2\pi} \int_{-\infty}^{\infty} U_4(\omega, y) \exp(i\omega x) d\omega \quad (2.2.41a)$$

$$v^{(4)}(x, y) = \frac{1}{2\pi} \int_{-\infty}^{\infty} V_4(\omega, y) \exp(i\omega x) d\omega \quad (2.2.41b)$$

where $U_4(\omega, y)$ and $V_4(\omega, y)$ are Fourier transforms of $u^{(4)}(x, y)$ and $v^{(4)}(x, y)$ in x , respectively.

Using Eq.(2.2.41), governing equations given by Eq.(2.2.20) can be written as:

$$\frac{d^2 U_4}{dy^2} - \beta_3 \omega^2 \left(\frac{\delta_4}{\delta_0} \right)^2 U_4 + i \omega \beta_6 \frac{dV_4}{dy} = 0 \quad (2.2.42a)$$

$$-\omega^2 V_4 + \beta_5 \left(\frac{\delta_0}{\delta_4} \right)^2 \frac{d^2 V_4}{dy^2} + i \omega \beta_6 \frac{dU_4}{dy} = 0 \quad (2.2.42b)$$

Solving the above ordinary differential equation system, $U_4(\omega, y)$ and $V_4(\omega, y)$ are obtained as:

$$U_4(\omega, y) = \sum_{j=1}^4 C_j(\omega) \exp(n_j(\omega)y), \quad (j = 1, 2, 3, 4) \quad (2.2.43a)$$

$$V_4(\omega, y) = \sum_{j=1}^4 C_j(\omega) D_j(\omega) \exp(n_j(\omega)y), \quad (j = 1, 2, 3, 4) \quad (2.2.43b)$$

where

$$n_1(\omega) = |\omega| \frac{\delta_4}{\delta_0} \sqrt{\kappa_4 + \sqrt{\kappa_4^2 - 1}} \quad (2.2.44a)$$

$$n_2(\omega) = |\omega| \frac{\delta_4}{\delta_0} \sqrt{\kappa_4 - \sqrt{\kappa_4^2 - 1}} \quad (2.2.44b)$$

$$n_3(\omega) = -|\omega| \frac{\delta_4}{\delta_0} \sqrt{\kappa_4 + \sqrt{\kappa_4^2 - 1}} \quad (2.2.44c)$$

$$n_4(\omega) = -|\omega| \frac{\delta_4}{\delta_0} \sqrt{\kappa_4 - \sqrt{\kappa_4^2 - 1}} \quad (2.2.44d)$$

$C_j(\omega)$, ($j = 1, 2, 3, 4$), are unknown functions of ω and $D_j(\omega)$, ($j = 1, 2, 3, 4$), are found by substituting Eq.(2.2.43) into Eq.(2.2.42a) as:

$$D_j(\omega) = \frac{-i \left((n_j(\omega))^2 (v_4^2 - 1) + 2\omega^2 \left(\frac{\delta_4}{\delta_0} \right)^2 (\kappa_4 + v_4) \right)}{\omega n_j(\omega) (1 + v_4^2 + 2v_4 \kappa_4)}, \quad (j = 1, 2, 3, 4) \quad (2.2.45)$$

Displacement components are obtained by substituting Eq.(2.2.43) into Eq.(2.2.41) as follows:

$$u^{(4)}(x, y) = \frac{1}{2\pi} \int_{-\infty}^{\infty} \sum_{j=1}^4 C_j(\omega) \exp(n_j(\omega)y + i\omega x) d\omega \quad (2.2.46a)$$

$$v^{(4)}(x, y) = \frac{1}{2\pi} \int_{-\infty}^{\infty} \sum_{j=1}^4 C_j(\omega) D_j(\omega) \exp(n_j(\omega)y + i\omega x) d\omega \quad (2.2.46b)$$

Then, stress components σ_{yy} and σ_{xy} are found using Eq.(2.2.11b), Eq.(2.2.11c), Eq.(2.2.14) and Eq.(2.2.46) as follows:

$$\sigma_{yy}^{(4)}(x, y) = \frac{E_4}{1 - v_4^2} \left\{ \frac{1}{2\pi} \int_{-\infty}^{\infty} \sum_{j=1}^4 C_j(\omega) \left(v_4 i \omega + \left(\frac{\delta_0}{\delta_4} \right)^2 n_j(\omega) D_j(\omega) \right) \exp(n_j(\omega)y + i\omega x) d\omega \right\} \quad (2.2.47a)$$

$$\sigma_{xy}^{(4)}(x, y) = \frac{E_4}{2(\kappa_4 + v_4)} \left\{ \frac{1}{2\pi} \int_{-\infty}^{\infty} \sum_{j=1}^4 i C_j(\omega) (-n_j(\omega) i + \omega D_j(\omega)) \exp(n_j(\omega)y + i\omega x) d\omega \right\} \quad (2.2.47b)$$

In order to determine the unknown functions $M_j(\omega)$, $G_j(\omega)$, $A_j(\omega)$ and $C_j(\omega)$, ($j=1,2,3,4$), the following boundary and continuity conditions have to be satisfied.

$$\sigma_{22}^{(1)}(x_1, h_1) = 0, \quad |x_1| < \infty \quad (2.2.48a)$$

$$\sigma_{12}^{(1)}(x_1, h_1) = 0, \quad |x_1| < \infty \quad (2.2.48b)$$

$$\sigma_{22}^{(1)}(x_1, 0) = \sigma_{22}^{(2)}(x_1, 0), \quad |x_1| < \infty \quad (2.2.48c)$$

$$\sigma_{12}^{(1)}(x_1, 0) = \sigma_{12}^{(2)}(x_1, 0), \quad |x_1| < \infty \quad (2.2.48d)$$

$$\sigma_{22}^{(2)}(x_1, -h_2) = \sigma_{22}^{(3)}(x_1, -h_2), \quad |x_1| < \infty \quad (2.2.48e)$$

$$\sigma_{12}^{(2)}(x_1, -h_2) = \sigma_{12}^{(3)}(x_1, -h_2), \quad |x_1| < \infty \quad (2.2.48f)$$

$$u_1^{(2)}(x_1, -h_2) = u_1^{(3)}(x_1, -h_2), \quad |x_1| < \infty \quad (2.2.48g)$$

$$u_2^{(2)}(x_1, -h_2) = u_2^{(3)}(x_1, -h_2), \quad |x_1| < \infty \quad (2.2.48h)$$

$$\sigma_{22}^{(3)}(x_1, -(h_2 + h_3)) = \sigma_{22}^{(4)}(x_1, -(h_2 + h_3)), \quad |x_1| < \infty \quad (2.2.48i)$$

$$\sigma_{12}^{(3)}(x_1, -(h_2 + h_3)) = \sigma_{12}^{(4)}(x_1, -(h_2 + h_3)), \quad |x_1| < \infty \quad (2.2.48j)$$

$$u_1^{(3)}(x_1, -(h_2 + h_3)) = u_1^{(4)}(x_1, -(h_2 + h_3)), \quad |x_1| < \infty \quad (2.2.48k)$$

$$u_2^{(3)}(x_1, -(h_2 + h_3)) = u_2^{(4)}(x_1, -(h_2 + h_3)), \quad |x_1| < \infty \quad (2.2.48l)$$

$$\sigma_{22}^{(4)}(x_1, -(h_2 + h_3 + h_4)) = 0, \quad |x_1| < \infty \quad (2.2.48m)$$

$$\sigma_{12}^{(4)}(x_1, -(h_2 + h_3 + h_4)) = 0, \quad |x_1| < \infty \quad (2.2.48n)$$

Then, the following equations which imply the perfect bonding condition in the crack line outside the crack are introduced by defining the derivatives of the relative displacements of the crack surfaces as unknown functions $f_1(x_1)$ and $f_2(x_1)$.

$$\frac{\partial}{\partial x_1} (u_2^{(1)}(x_1, 0) - u_2^{(2)}(x_1, 0)) = \begin{cases} f_1(x_1), & |x_1| < c \\ 0, & |x_1| > c \end{cases} \quad (2.2.49a)$$

$$\frac{\partial}{\partial x_1} (u_1^{(1)}(x_1, 0) - u_1^{(2)}(x_1, 0)) = \begin{cases} f_2(x_1), & |x_1| < c \\ 0, & |x_1| > c \end{cases} \quad (2.2.49b)$$

Expressing Eq.(2.2.48) and Eq.(2.2.49) in the transformed coordinate system and applying Fourier transformations to them, the following system of equations is obtained:

$$\sum_{j=1}^4 M_j(\omega) (N_j(\omega) s_j(\omega) + \nu_0 i \omega) \exp(s_j(\omega) h_1 \sqrt{\delta_0}) = 0 \quad (2.2.50a)$$

$$\sum_{j=1}^4 M_j(\omega) (s_j(\omega) + N_j(\omega) i \omega) \exp(s_j(\omega) h_1 \sqrt{\delta_0}) = 0 \quad (2.2.50b)$$

$$\sum_{j=1}^4 M_j(\omega)(v_0 i\omega + N_j(\omega)s_j(\omega)) - \sum_{j=1}^4 G_j(\omega)(v_0 i\omega + N_j(\omega)s_j(\omega)) = 0 \quad (2.2.50c)$$

$$\sum_{j=1}^4 M_j(\omega)(N_j(\omega)i\omega + s_j(\omega)) - \sum_{j=1}^4 G_j(\omega)(N_j(\omega)i\omega + s_j(\omega)) = 0 \quad (2.2.50d)$$

$$\begin{aligned} & \frac{E_0 \exp(-\mathcal{H}_2 \sqrt{\delta_0})}{1 - v_0^2} \left(\sum_{j=1}^4 G_j(\omega)(v_0 i\omega + N_j(\omega)s_j(\omega)) \exp(-s_j(\omega)h_2 \sqrt{\delta_0}) \right) \\ & - \frac{E_3}{1 - v_3^2} \left(\sum_{j=1}^4 A_j(\omega) \left(v_3 i\omega + \left(\frac{\delta_0}{\delta_3} \right)^2 B_j(\omega)r_j(\omega) \right) \exp(-r_j(\omega)h_2 \sqrt{\delta_0}) \right) = 0 \end{aligned} \quad (2.2.50e)$$

$$\begin{aligned} & \frac{E_0 \exp(-\mathcal{H}_2 \sqrt{\delta_0})}{2(\kappa_0 + v_0)} \left(\sum_{j=1}^4 G_j(\omega)(s_j(\omega) + N_j(\omega)i\omega) \exp(-s_j(\omega)h_2 \sqrt{\delta_0}) \right) \\ & - \frac{E_3}{2(\kappa_3 + v_3)} \left(\sum_{j=1}^4 iA_j(\omega)(-r_j(\omega)i + \omega B_j(\omega)) \exp(-r_j(\omega)h_2 \sqrt{\delta_0}) \right) = 0 \end{aligned} \quad (2.2.50f)$$

$$\sum_{j=1}^4 G_j(\omega) \exp(-s_j(\omega)h_2 \sqrt{\delta_0}) - \sum_{j=1}^4 A_j(\omega) \exp(-r_j(\omega)h_2 \sqrt{\delta_0}) = 0 \quad (2.2.50g)$$

$$\sum_{j=1}^4 G_j(\omega)N_j(\omega) \exp(-s_j(\omega)h_2 \sqrt{\delta_0}) - \sum_{j=1}^4 A_j(\omega)B_j(\omega) \exp(-r_j(\omega)h_2 \sqrt{\delta_0}) = 0 \quad (2.2.50h)$$

$$\begin{aligned} & \frac{E_3}{1 - v_3^2} \left(\sum_{j=1}^4 A_j(\omega) \left(v_3 i\omega + \left(\frac{\delta_0}{\delta_3} \right)^2 B_j(\omega)r_j(\omega) \right) \exp(-r_j(\omega)(h_3 + h_2) \sqrt{\delta_0}) \right) \\ & - \frac{E_4}{1 - v_4^2} \left(\sum_{j=1}^4 C_j(\omega) \left(v_4 i\omega + \left(\frac{\delta_0}{\delta_4} \right)^2 D_j(\omega)n_j(\omega) \right) \exp(-n_j(\omega)(h_3 + h_2) \sqrt{\delta_0}) \right) = 0 \end{aligned} \quad (2.2.50i)$$

$$\begin{aligned} & \frac{E_3}{2(\kappa_3 + \nu_3)} \left(\sum_{j=1}^4 iA_j(\omega)(-r_j(\omega)i + \omega B_j(\omega)) \exp(-r_j(\omega)(h_3 + h_2)\sqrt{\delta_0}) \right) \\ & - \frac{E_4}{2(\kappa_4 + \nu_4)} \left(\sum_{j=1}^4 iC_j(\omega)(-n_j(\omega)i + \omega D_j(\omega)) \exp(-n_j(\omega)(h_3 + h_2)\sqrt{\delta_0}) \right) = 0 \end{aligned} \quad (2.2.50j)$$

$$\sum_{j=1}^4 A_j(\omega) \exp(-r_j(\omega)(h_3 + h_2)\sqrt{\delta_0}) - \sum_{j=1}^4 C_j(\omega) \exp(-n_j(\omega)(h_3 + h_2)\sqrt{\delta_0}) = 0 \quad (2.2.50k)$$

$$\begin{aligned} & \sum_{j=1}^4 A_j(\omega) B_j(\omega) \exp(-r_j(\omega)(h_3 + h_2)\sqrt{\delta_0}) \\ & - \sum_{j=1}^4 C_j(\omega) D_j(\omega) \exp(-n_j(\omega)(h_3 + h_2)\sqrt{\delta_0}) = 0 \end{aligned} \quad (2.2.50l)$$

$$\sum_{j=1}^4 C_j(\omega) \left(i\omega \nu_4 + \left(\frac{\delta_0}{\delta_4} \right)^2 n_j(\omega) D_j(\omega) \right) \exp(-n_j(\omega)(h_4 + h_3 + h_2)\sqrt{\delta_0}) = 0 \quad (2.2.50m)$$

$$\sum_{j=1}^4 iC_j(\omega)(-n_j(\omega)i + \omega D_j(\omega)) \exp(-n_j(\omega)(h_4 + h_3 + h_2)\sqrt{\delta_0}) = 0 \quad (2.2.50n)$$

$$i\omega \left(\sum_{j=1}^4 M_j(\omega) N_j(\omega) - \sum_{j=1}^4 G_j(\omega) N_j(\omega) \right) = \int_{-c/\sqrt{\delta_0}}^{c/\sqrt{\delta_0}} \phi_1(t) \exp(-i\omega t) dt \quad (2.2.50p)$$

$$i\omega \left(\sum_{j=1}^4 M_j(\omega) - \sum_{j=1}^4 G_j(\omega) \right) = \int_{-c/\sqrt{\delta_0}}^{c/\sqrt{\delta_0}} \phi_2(t) \exp(-i\omega t) dt \quad (2.2.50r)$$

where $\phi_1(t) = f_1(\sqrt{\delta_0}t)$ and $\phi_2(t) = \delta_0 f_2(\sqrt{\delta_0}t)$.

From Eq.(2.2.50), the unknown functions $M_j(\omega)$, $G_j(\omega)$, $A_j(\omega)$ and $C_j(\omega)$, ($j = 1, 2, 3, 4$), can be written in the following form.

$$M_j(\omega) = Y_j(\omega) \int_{-c/\sqrt{\delta_0}}^{c/\sqrt{\delta_0}} \phi_1(t) \exp(-i\omega t) dt + Z_j(\omega) \int_{-c/\sqrt{\delta_0}}^{c/\sqrt{\delta_0}} \phi_2(t) \exp(-i\omega t) dt, \quad (j = 1, 2, 3, 4) \quad (2.2.51a)$$

$$G_j(\omega) = V_j(\omega) \int_{-c/\sqrt{\delta_0}}^{c/\sqrt{\delta_0}} \phi_1(t) \exp(-i\omega t) dt + W_j(\omega) \int_{-c/\sqrt{\delta_0}}^{c/\sqrt{\delta_0}} \phi_2(t) \exp(-i\omega t) dt, \quad (j = 1, 2, 3, 4) \quad (2.2.51b)$$

$$A_j(\omega) = X_j(\omega) \int_{-c/\sqrt{\delta_0}}^{c/\sqrt{\delta_0}} \phi_1(t) \exp(-i\omega t) dt + L_j(\omega) \int_{-c/\sqrt{\delta_0}}^{c/\sqrt{\delta_0}} \phi_2(t) \exp(-i\omega t) dt, \quad (j = 1, 2, 3, 4) \quad (2.2.51c)$$

$$C_j(\omega) = P_j(\omega) \int_{-a}^a \phi_1(t) \exp(-i\omega t) dt + Q_j(\omega) \int_{-a}^a \phi_2(t) \exp(-i\omega t) dt, \quad (j = 1, 2, 3, 4) \quad (2.2.51d)$$

where $Y_j(\omega)$, $Z_j(\omega)$, $V_j(\omega)$, $W_j(\omega)$, $X_j(\omega)$, $L_j(\omega)$, $P_j(\omega)$ and $Q_j(\omega)$, ($j = 1, 2, 3, 4$), are found numerically as described in Appendix A.

Assuming that $p(x_1)$ is normal traction and $q(x_1)$ is shear traction at the crack surfaces, the following boundary conditions are written.

$$\sigma_{22}(x_1, 0) = -p(x_1), \quad |x_1| < c \quad (2.2.52a)$$

$$\sigma_{12}(x_1, 0) = -q(x_1), \quad |x_1| < c \quad (2.2.52b)$$

They are written in the transformed coordinates as follows:

$$\sigma_{yy}(x, 0) = \bar{p}(x) = -\delta_0 p(\sqrt{\delta_0} x), \quad |x| < c/\sqrt{\delta_0} \quad (2.2.53a)$$

$$\sigma_{xy}(x, 0) = \bar{q}(x) = -q(\sqrt{\delta_0} x), \quad |x| < c/\sqrt{\delta_0} \quad (2.2.53b)$$

Using the stress expressions obtained by substituting Eq.(2.2.51a) into Eq.(2.2.28) and doing some manipulations, Eq.(2.2.53) yields the following integral equations:

$$\begin{aligned} \lim_{y \rightarrow 0^+} & \left\{ \int_{-c/\sqrt{\delta_0}}^{c/\sqrt{\delta_0}} \phi_1(t) dt \frac{1}{2\pi} \int_0^\infty F_{11}(\omega, y) \cos(\omega(x-t)) d\omega \right. \\ & + \int_{-c/\sqrt{\delta_0}}^{c/\sqrt{\delta_0}} \phi_1(t) dt \frac{1}{2\pi} \int_0^\infty F_{11}(-\omega, y) \cos(\omega(x-t)) d\omega \\ & + \int_{-c/\sqrt{\delta_0}}^{c/\sqrt{\delta_0}} \phi_1(t) dt \frac{1}{2\pi} \int_0^\infty iF_{11}(\omega, y) \sin(\omega(x-t)) d\omega \\ & + \int_{-c/\sqrt{\delta_0}}^{c/\sqrt{\delta_0}} \phi_1(t) dt \frac{1}{2\pi} \int_0^\infty -iF_{11}(-\omega, y) \sin(\omega(x-t)) d\omega \\ & + \int_{-c/\sqrt{\delta_0}}^{c/\sqrt{\delta_0}} \phi_2(t) dt \frac{1}{2\pi} \int_0^\infty F_{12}(\omega, y) \cos(\omega(x-t)) d\omega \\ & + \int_{-c/\sqrt{\delta_0}}^{c/\sqrt{\delta_0}} \phi_2(t) dt \frac{1}{2\pi} \int_0^\infty F_{12}(-\omega, y) \cos(\omega(x-t)) d\omega \\ & \left. + \int_{-c/\sqrt{\delta_0}}^{c/\sqrt{\delta_0}} \phi_2(t) dt \frac{1}{2\pi} \int_0^\infty iF_{12}(\omega, y) \sin(\omega(x-t)) d\omega \right\} \end{aligned}$$

$$+ \int_{-c/\sqrt{\delta_0}}^{c/\sqrt{\delta_0}} \phi_2(t) dt \frac{1}{2\pi} \int_0^\infty -iF_{12}(-\omega, y) \sin(\omega(x-t)) d\omega \left\} = \frac{1-v_0^2}{E_0} \bar{p}(x) \quad (2.2.54a)$$

$$\begin{aligned} \lim_{y \rightarrow 0^+} & \left\{ \int_{-c/\sqrt{\delta_0}}^{c/\sqrt{\delta_0}} \phi_1(t) dt \frac{1}{2\pi} \int_0^\infty D_{11}(\omega, y) \cos(\omega(x-t)) d\omega \right. \\ & + \int_{-c/\sqrt{\delta_0}}^{c/\sqrt{\delta_0}} \phi_1(t) dt \frac{1}{2\pi} \int_0^\infty D_{11}(-\omega, y) \cos(\omega(x-t)) d\omega \\ & + \int_{-c/\sqrt{\delta_0}}^{c/\sqrt{\delta_0}} \phi_1(t) dt \frac{1}{2\pi} \int_0^\infty iD_{11}(\omega, y) \sin(\omega(x-t)) d\omega \\ & + \int_{-c/\sqrt{\delta_0}}^{c/\sqrt{\delta_0}} \phi_1(t) dt \frac{1}{2\pi} \int_0^\infty -iD_{11}(-\omega, y) \sin(\omega(x-t)) d\omega \\ & + \int_{-c/\sqrt{\delta_0}}^{c/\sqrt{\delta_0}} \phi_2(t) dt \frac{1}{2\pi} \int_0^\infty D_{12}(\omega, y) \cos(\omega(x-t)) d\omega \\ & + \int_{-c/\sqrt{\delta_0}}^{c/\sqrt{\delta_0}} \phi_2(t) dt \frac{1}{2\pi} \int_0^\infty D_{12}(-\omega, y) \cos(\omega(x-t)) d\omega \\ & + \int_{-c/\sqrt{\delta_0}}^{c/\sqrt{\delta_0}} \phi_2(t) dt \frac{1}{2\pi} \int_0^\infty iD_{12}(\omega, y) \sin(\omega(x-t)) d\omega \\ & \left. + \int_{-c/\sqrt{\delta_0}}^{c/\sqrt{\delta_0}} \phi_2(t) dt \frac{1}{2\pi} \int_0^\infty -iD_{12}(-\omega, y) \sin(\omega(x-t)) d\omega \right\} = \frac{2(\kappa_0 + v_0)}{E_0} \bar{q}(x) \quad (2.2.54b) \end{aligned}$$

where $|x| < c/\sqrt{\delta_0}$ and,

$$F_{11}(\omega, y) = \sum_{j=1}^4 (i\omega v_0 + N_j(\omega) s_j(\omega)) Y_j(\omega) \exp(s_j(\omega) y) \quad (2.2.55a)$$

$$F_{12}(\omega, y) = \sum_{j=1}^4 (i\omega v_0 + N_j(\omega)s_j(\omega))Z_j(\omega)\exp(s_j(\omega)y) \quad (2.2.55b)$$

$$D_{11}(\omega, y) = \sum_{j=1}^4 (s_j(\omega) + N_j(\omega)i\omega)Y_j(\omega)\exp(s_j(\omega)y) \quad (2.2.55c)$$

$$D_{12}(\omega, y) = \sum_{j=1}^4 (s_j(\omega) + N_j(\omega)i\omega)Z_j(\omega)\exp(s_j(\omega)y) \quad (2.2.55d)$$

Using the symbolic manipulator MAPLE, asymptotic behaviors of the integrands $F_{11}(\omega, 0)$, $F_{11}(-\omega, 0)$, $F_{12}(\omega, 0)$, $F_{12}(-\omega, 0)$, $D_{11}(\omega, 0)$, $D_{11}(-\omega, 0)$, $D_{12}(\omega, 0)$ and $D_{12}(-\omega, 0)$ are determined in the following form as ω approaches infinity as described in Appendix B.

$$F_{11}^{\infty}(\omega, 0) = a_0 + b_0 + \frac{a_2 + b_2}{\omega^2} \quad (2.2.56a)$$

$$F_{11}^{\infty}(-\omega, 0) = c_0 + d_0 + \frac{c_2 + d_2}{\omega^2} \quad (2.2.56b)$$

$$F_{12}^{\infty}(\omega, 0) = e_0 + f_0 + \frac{e_1 + f_1}{\omega} + \frac{e_2 + f_2}{\omega^2} \quad (2.2.56c)$$

$$F_{12}^{\infty}(-\omega, 0) = g_0 + h_0 + \frac{g_1 + h_1}{\omega} + \frac{g_2 + h_2}{\omega^2} \quad (2.2.56d)$$

$$D_{11}^{\infty}(\omega, 0) = a_{10} + b_{10} + \frac{a_{11} + b_{11}}{\omega} + \frac{a_{12} + b_{12}}{\omega^2} + \frac{a_{13} + b_{13}}{\omega^3} \quad (2.2.56e)$$

$$D_{11}^{\infty}(-\omega, 0) = c_{10} + d_{10} + \frac{c_{11} + d_{11}}{\omega} + \frac{c_{12} + d_{12}}{\omega^2} + \frac{c_{13} + d_{13}}{\omega^3} \quad (2.2.56f)$$

$$D_{12}^{\infty}(\omega, 0) = e_{10} + f_{10} + \frac{e_{12} + f_{12}}{\omega^2} \quad (2.2.56g)$$

$$D_{12}^{\infty}(-\omega, 0) = g_{10} + h_{10} + \frac{g_{12} + h_{12}}{\omega^2} \quad (2.2.56h)$$

where the superscript ∞ denotes the asymptotic expansion as ω approaches infinity and $a_0, a_2, b_0, b_2, c_0, c_2, d_0, d_2, e_0, e_1, e_2, f_0, f_1, f_2, g_0, g_1, g_2, h_0, h_1, h_2, a_{10}, a_{11}, a_{12}, a_{13}, b_{10}, b_{11}, b_{12}, b_{13}, c_{10}, c_{11}, c_{12}, c_{13}, d_{10}, d_{11}, d_{12}, d_{13}, e_{10}, e_{12}, f_{10}, f_{12}, g_{10}, g_{12}, h_{10}, h_{12}$ are the functions of the constants $\beta, \delta_0, \kappa_0$ and ν_0 . Expressions for these asymptotic expansion coefficients are given in Appendix B.

Subtracting and adding the asymptotic expansion terms, evaluating some of the integrals in closed form and taking the limit as y approaches 0^+ , the integral equations can be rearranged as:

$$\begin{aligned} & \int_{-c/\sqrt{\delta_0}}^{c/\sqrt{\delta_0}} \left[\frac{i((a_0 + b_0) - (c_0 + d_0))}{2\pi(x-t)} + H_{11}(x, t) + H_{12}(x, t) + H_{13}(x, t) - H_{14}(x, t) \right] \phi_1(t) dt \\ & + \int_{-c/\sqrt{\delta_0}}^{c/\sqrt{\delta_0}} \left[H_{15}(x, t) + H_{16}(x, t) + H_{17}(x, t) - H_{18}(x, t) - \frac{e_1 + f_1}{2\pi} \ln(A_{15}|x-t|) \right. \\ & - \frac{g_1 + h_1}{2\pi} \ln(A_{16}|x-t|) + \frac{i(e_0 + f_0)}{2\pi(x-t)} - \frac{i(g_0 + h_0)}{2\pi(x-t)} \\ & \left. + \frac{i(e_1 + f_1 - (g_1 + h_1))}{4} \text{sign}(x-t) \right] \phi_2(t) dt = \frac{(1 - \nu_0^2)}{E_0} \bar{p}(x), \quad |x| < c/\sqrt{\delta_0} \quad (2.2.57a) \end{aligned}$$

$$\begin{aligned}
& \int_{-c/\sqrt{\delta_0}}^{c/\sqrt{\delta_0}} \left[\frac{i((e_{10} + f_{10}) - (g_{10} + h_{10}))}{2\pi(x-t)} + H_{25}(x,t) + H_{26}(x,t) + H_{27}(x,t) - H_{28}(x,t) \right] \phi_2(t) dt \\
& + \int_{-c/\sqrt{\delta_0}}^{c/\sqrt{\delta_0}} \left[H_{21}(x,t) + H_{22}(x,t) + H_{23}(x,t) - H_{24}(x,t) - \frac{a_{11} + b_{11}}{2\pi} \ln(A_{21}|x-t|) \right. \\
& - \frac{c_{11} + d_{11}}{2\pi} \ln(A_{22}|x-t|) + \frac{i(a_{10} + b_{10})}{2\pi(x-t)} - \frac{i(c_{10} + d_{10})}{2\pi(x-t)} \\
& \left. + \frac{i(a_{11} + b_{11} - (c_{11} + d_{11}))}{4} \text{sign}(x-t) \right] \phi_1(t) dt = \frac{2(\kappa_0 + \nu_0)}{E_0} \bar{q}(x), \quad |x| < c/\sqrt{\delta_0}
\end{aligned} \tag{2.2.57b}$$

where A_{15} , A_{16} , A_{21} , A_{22} are integration cut-off points and the functions $H_{ij}(x,t)$, ($i=1, 2$ and $j=1, 2, \dots, 8$), are given in Appendix C.

Then, the following transformations are introduced:

$$s = \frac{x\sqrt{\delta_0}}{c}, \quad |x| < c/\sqrt{\delta_0}, \quad |s| < 1 \tag{2.2.58a}$$

$$r = \frac{t\sqrt{\delta_0}}{c}, \quad |t| < c/\sqrt{\delta_0}, \quad |r| < 1 \tag{2.2.58b}$$

Using the above transformations, Eq.(2.2.57) can be written in the following normalized form:

$$\begin{aligned}
& \int_{-1}^1 \left[\frac{i((a_0 + b_0) - (c_0 + d_0))}{2\pi(s-r)} + \hat{H}_{11}(s, r) + \hat{H}_{12}(s, r) + \hat{H}_{13}(s, r) - \hat{H}_{14}(s, r) \right] \hat{\phi}(r) dr \\
& + \int_{-1}^1 \left[-\frac{\hat{e}_1 + \hat{f}_1}{2\pi} \ln(A_{15}^* |s-r|) - \frac{\hat{g}_1 + \hat{h}_1}{2\pi} \ln(A_{16}^* |s-r|) + \frac{i(e_0 + f_0 - (g_0 + h_0))}{2\pi(s-r)} \right. \\
& \left. + \frac{i(\hat{e}_1 + \hat{f}_1 - (\hat{g}_1 + \hat{h}_1))}{4} \text{sign}(s-r) + \hat{H}_{15}(s, r) + \hat{H}_{16}(s, r) + \hat{H}_{17}(s, r) - \hat{H}_{18}(s, r) \right] \hat{\phi}(r) dr \\
& = \frac{(1 - \nu_0^2)}{E_0} \bar{p}(sc/\sqrt{\delta_0}), \quad |s| < 1 \quad (2.2.59a)
\end{aligned}$$

$$\begin{aligned}
& \int_{-1}^1 \left[-\frac{\hat{a}_{11} + \hat{b}_{11}}{2\pi} \ln(A_{21}^* |s-r|) - \frac{\hat{c}_{11} + \hat{d}_{11}}{2\pi} \ln(A_{22}^* |s-r|) + \frac{i(a_{10} + b_{10} - (c_{10} + d_{10}))}{2\pi(s-r)} + \right. \\
& \left. \frac{i(\hat{a}_{11} + \hat{b}_{11} - (\hat{c}_{11} + \hat{d}_{11}))}{4} \text{sign}(s-r) + \hat{H}_{21}(s, r) + \hat{H}_{22}(s, r) + \hat{H}_{23}(s, r) - \hat{H}_{24}(s, r) \right] \hat{\phi}(r) dr \\
& + \int_{-1}^1 \left[\frac{i((e_{10} + f_{10}) - (g_{10} + h_{10}))}{2\pi(s-r)} + \hat{H}_{25}(s, r) + \hat{H}_{26}(s, r) + \hat{H}_{27}(s, r) - \hat{H}_{28}(s, r) \right] \hat{\phi}(r) dr \\
& = \frac{2(\kappa_0 + \nu_0)}{E_0} \bar{q}(sc/\sqrt{\delta_0}), \quad |s| < 1 \quad (2.2.59b)
\end{aligned}$$

where

$$\hat{\phi}(r) = \phi_1(r c/\sqrt{\delta_0}), \quad \bar{\phi}(r) = \phi_2(r c/\sqrt{\delta_0}) \quad (2.2.60a)$$

$$\hat{H}_{ij}(s, r) = H_{ij}(sc/\sqrt{\delta_0}, rc/\sqrt{\delta_0})c/\sqrt{\delta_0}, \quad (i=1, 2 \text{ and } j=1, 2, \dots, 8) \quad (2.2.60b)$$

$$\hat{e}_1 = e_1 c/\sqrt{\delta_0}, \quad \hat{f}_1 = f_1 c/\sqrt{\delta_0}, \quad \hat{g}_1 = g_1 c/\sqrt{\delta_0}, \quad \hat{h}_1 = h_1 c/\sqrt{\delta_0} \quad (2.2.60c)$$

$$\hat{a}_{11} = a_{11} c/\sqrt{\delta_0}, \quad \hat{b}_{11} = b_{11} c/\sqrt{\delta_0}, \quad \hat{c}_{11} = c_{11} c/\sqrt{\delta_0}, \quad \hat{d}_{11} = d_{11} c/\sqrt{\delta_0} \quad (2.2.60d)$$

$$A_{15}^* = A_{15} c/\sqrt{\delta_0}, \quad A_{16}^* = A_{16} c/\sqrt{\delta_0}, \quad A_{21}^* = A_{21} c/\sqrt{\delta_0}, \quad A_{22}^* = A_{22} c/\sqrt{\delta_0} \quad (2.2.60e)$$

Then the solution can be expressed in the following form:

$$\hat{\phi}(r) = \frac{1}{\sqrt{1-r^2}} \sum_{n=0}^{\infty} \hat{A}_n T_n(r) \quad (2.2.61a)$$

$$\hat{\phi}(r) = \frac{1}{\sqrt{1-r^2}} \sum_{n=0}^{\infty} \hat{B}_n T_n(r) \quad (2.2.61b)$$

where T_n is the Chebyshev polynomial of the first kind of order n and its definition is given in Appendix D. \hat{A}_n and \hat{B}_n are unknown constants.

It is known that relative displacements at the crack tips are zero. Using this condition and Eq.(2.2.49), the following expressions can be written.

$$\int_{-c}^c f_1(x_1) dx_1 = 0 \quad (2.2.62a)$$

$$\int_{-c}^c f_2(x_1) dx_1 = 0 \quad (2.2.62b)$$

Making use of the above expressions, the following equations can be obtained:

$$\int_{-1}^1 \hat{\phi}(s) ds = 0 \quad (2.2.63a)$$

$$\int_{-1}^1 \hat{\phi}(s) ds = 0 \quad (2.2.63b)$$

Substituting Eq.(2.2.61) into Eq.(2.2.63) and using the orthogonality condition of the Chebyshev polynomials of the first kind given in Appendix D, \hat{A}_0 and \hat{B}_0 are found to be zero.

Then, the series given by Eq.(2.2.61) are truncated at $n = N$ as follows:

$$\hat{\phi}(r) = \frac{1}{\sqrt{1-r^2}} \sum_{n=1}^N \hat{A}_n T_n(r) \quad (2.2.64a)$$

$$\hat{\phi}(r) = \frac{1}{\sqrt{1-r^2}} \sum_{n=1}^N \hat{B}_n T_n(r) \quad (2.2.64b)$$

It can be shown that,

$$e_0 + f_0 - g_0 - h_0 = 0 \quad (2.2.65a)$$

$$\hat{e}_1 + \hat{f}_1 - \hat{g}_1 - \hat{h}_1 = 0 \quad (2.2.65b)$$

$$a_{10} + b_{10} - c_{10} - d_{10} = 0 \quad (2.2.65c)$$

$$\hat{a}_{11} + \hat{b}_{11} - \hat{c}_{11} - \hat{d}_{11} = 0 \quad (2.2.65d)$$

Substituting Eq.(2.2.64) and Eq.(2.2.65) into Eq.(2.2.59) and evaluating some of the integrals in closed form as given in Appendix E, the integral equations can be rearranged as:

$$\begin{aligned}
& \sum_{n=1}^N \hat{A}_n \left\{ -\frac{i(a_0 + b_0 - c_0 - d_0)}{2} U_{n-1}(s) + k_{11n}(s) + k_{12n}(s) + k_{13n}(s) - k_{14n}(s) \right\} \\
& + \sum_{n=1}^N \hat{B}_n \left\{ \frac{\hat{e}_1 + \hat{f}_1 + \hat{g}_1 + \hat{h}_1}{2} \frac{T_n(s)}{n} + k_{15n}(s) + k_{16n}(s) + k_{17n}(s) - k_{18n}(s) \right\} \\
& = \frac{(1 - \nu_0^2)}{E_0} \bar{p}(s c / \sqrt{\delta_0}), \quad |s| < 1 \quad (2.2.66a)
\end{aligned}$$

$$\begin{aligned}
& \sum_{n=1}^N \hat{A}_n \left\{ \frac{\hat{a}_{11} + \hat{b}_{11} + \hat{c}_{11} + \hat{d}_{11}}{2} \frac{T_n(s)}{n} + k_{21n}(s) + k_{22n}(s) + k_{23n}(s) - k_{24n}(s) \right\} \\
& + \sum_{n=1}^N \hat{B}_n \left\{ -\frac{i(e_{10} + f_{10} - g_{10} - h_{10})}{2} U_{n-1}(s) + k_{25n}(s) + k_{26n}(s) + k_{27n}(s) - k_{28n}(s) \right\} \\
& = \frac{2(\kappa_0 + \nu_0)}{E_0} \bar{q}(s c / \sqrt{\delta_0}), \quad |s| < 1 \quad (2.2.66b)
\end{aligned}$$

Where U_n is the Chebyshev polynomial of the second kind of order n and the functions $k_{ijn}(s)$, ($i = 1, 2$ and $j = 1, 2, \dots, 8$), are defined by:

$$k_{ijn}(s) = \int_{-1}^1 \frac{\hat{H}_{ij}(s, r)}{\sqrt{1-r^2}} T_n(r) dr \quad (2.2.67)$$

To find the unknown constants \hat{A}_n and \hat{B}_n , ($n = 1, \dots, N$), suitable collocation points are defined for Eq.(2.2.66) which leads to a $2N \times 2N$ linear system of equations. The collocation points are chosen as the roots of the Chebyshev polynomials of the first kind which are given in Appendix D.

Definitions of the stress intensity factors are given by the following expressions:

$$k_1(\pm c) = \lim_{x_1 \rightarrow \pm c^\pm} \sqrt{\pm 2(x_1 \mp c)} \sigma_{22}(x_1, 0) \quad (2.2.68a)$$

$$k_2(\pm c) = \lim_{x_1 \rightarrow \pm c^\pm} \sqrt{\pm 2(x_1 \mp c)} \sigma_{12}(x_1, 0) \quad (2.2.68b)$$

The dominant parts of the stress components $\sigma_{yy}(x, 0)$ and $\sigma_{xy}(x, 0)$ are expressed as follows:

$$\sigma_{yy}(x, 0) \cong \frac{E_0}{1-\nu_0^2} \frac{1}{\pi} \int_{-c/\sqrt{\delta_0}}^{c/\sqrt{\delta_0}} \frac{i(a_0 + b_0 - c_0 - d_0)}{2(x-t)} \phi_1(t) dt \quad (2.2.69a)$$

$$\sigma_{xy}(x, 0) \cong \frac{E_0}{2(\kappa_0 + \nu_0)} \frac{1}{\pi} \int_{-c/\sqrt{\delta_0}}^{c/\sqrt{\delta_0}} \frac{i(e_{10} + f_{10} - g_{10} - h_{10})}{2(x-t)} \phi_2(t) dt \quad (2.2.69b)$$

Using Eq.(2.2.69), the stress intensity factors are obtained as:

$$k_1(\pm c) = \pm \frac{i(a_0 + b_0 - c_0 - d_0)E_0 \sqrt{c}}{2\delta_0(1-\nu_0^2)} \sum_{n=1}^N \hat{A}_n T_n(\pm 1) \quad (2.2.70a)$$

$$k_2(\pm c) = \pm \frac{i(e_{10} + f_{10} - g_{10} - h_{10})E_0 \sqrt{c}}{4(\kappa_0 + \nu_0)} \sum_{n=1}^N \hat{B}_n T_n(\pm 1) \quad (2.2.70b)$$

Expressions for the normal and tangential crack opening displacements can be written using Eq.(2.2.49) as follows:

$$u_2(x_1, 0^+) - u_2(x_1, 0^-) = \int_{-c}^{x_1} f_1(x_1) dx_1, \quad |x_1| < c \quad (2.2.71a)$$

$$u_1(x_1, 0^+) - u_1(x_1, 0^-) = \int_{-c}^{x_1} f_2(x_1) dx_1, \quad |x_1| < c \quad (2.2.71b)$$

Then, they can be rearranged in the form given in Eq.(2.2.72) using Eq.(2.2.64) and the closed form integral [115] given in Eq.(2.2.73) .

$$u_2(x_1, 0^+) - u_2(x_1, 0^-) = -c \sqrt{1 - \left(\frac{x_1}{c}\right)^2} \sum_{n=1}^N \frac{\hat{A}_n}{n} U_{n-1}\left(\frac{x_1}{c}\right), \quad |x_1| < c \quad (2.2.72a)$$

$$u_1(x_1, 0^+) - u_1(x_1, 0^-) = -\frac{c}{\delta_0} \sqrt{1 - \left(\frac{x_1}{c}\right)^2} \sum_{n=1}^N \frac{\hat{B}_n}{n} U_{n-1}\left(\frac{x_1}{c}\right), \quad |x_1| < c \quad (2.2.72b)$$

$$\int_{-1}^{x_1/c} \frac{T_n(s)}{\sqrt{1-s^2}} ds = -\frac{1}{n} \sqrt{1 - \left(\frac{x_1}{c}\right)^2} U_{n-1}\left(\frac{x_1}{c}\right), \quad \left|\frac{x_1}{c}\right| < 1 \quad (2.2.73)$$

It is known that the relatively weak fracture planes correspond to the principal planes of orthotropy in the graded medium [115]. So, the energy release rates at the crack tips can be obtained assuming the crack extension along x_1 - axis. Using the crack closure energy concept, the energy release rate per tip can be expressed as follows:

$$G = \lim_{\Delta c \rightarrow 0} \frac{\Delta W}{B \Delta c} \quad (2.2.74)$$

where ΔW is the necessary work to close the crack extension per tip. B is the thickness of the plate and Δc is the length of the crack propagation at the crack tip. Considering the mode I and mode II loading conditions, ΔW can be written as follows for the crack tips where $x_1 = c$ and $x_1 = -c$, respectively.

$$\begin{aligned} \Delta W(c) = & \int_c^{c+\Delta c} \frac{B}{2} \sigma_{22}(x_1, 0) [u_2(x_1, 0^+) - u_2(x_1, 0^-)] dx_1 \\ & + \int_c^{c+\Delta c} \frac{B}{2} \sigma_{12}(x_1, 0) [u_1(x_1, 0^+) - u_1(x_1, 0^-)] dx_1 \end{aligned} \quad (2.2.75a)$$

$$\begin{aligned} \Delta W(-c) = & \int_{-c-\Delta c}^{-c} \frac{B}{2} \sigma_{22}(x_1, 0) [u_2(x_1, 0^+) - u_2(x_1, 0^-)] dx_1 \\ & + \int_{-c-\Delta c}^{-c} \frac{B}{2} \sigma_{12}(x_1, 0) [u_1(x_1, 0^+) - u_1(x_1, 0^-)] dx_1 \end{aligned} \quad (2.2.75b)$$

Then, strain energy release rate is obtained in the following form:

$$G(\pm c) = -\frac{\pi}{2E_0} \left(\frac{\delta_0(1-\nu_0^2)k_1^2(\pm c)}{i(a_0 + b_0 - c_0 - d_0)} + \frac{2(\kappa_0 + \nu_0)k_2^2(\pm c)}{i(e_{10} + f_{10} - g_{10} - h_{10})\delta_0} \right) \quad (2.2.76)$$

CHAPTER 3

COMPUTATIONAL SOLUTION FOR THE CRACK PROBLEMS IN AN ORTHOTROPIC FGM COATING

3.1 Computational Solution

Computational approaches are very useful for investigation of analytically untractable fracture problems. In this chapter, the employed computational approach is described.

In the adopted computational approach, finite element method is used in conjunction with the displacement correlation technique (DCT) to investigate the fracture behavior of the orthotropic FGM coating bonded to a homogeneous substrate through a homogeneous bond-coat.

Results of the finite element method are obtained using the general purpose finite element analysis software ANSYS. The finite element models are created using quarter point singular elements around the crack tips and regular 6-noded triangular and 8-noded quadrilateral elements in the other regions. To represent the variations in the material properties of the orthotropic FGM coating, material properties of each element are assigned according to the centroidal position of the element.

3.2 Review of Displacement Correlation Technique

In this section, a review is made for the displacement correlation technique (DCT) that is used in a previous study by Kim and Paulino [120] for the mixed-mode two-

dimensional crack problems in orthotropic FGMs. In this technique, stress intensity factors are calculated by correlating the displacements at specific nodal locations of the singular elements located around the crack tips with the known analytical solutions. An illustration describing the quarter-point singular elements located at the crack tip is shown in Figure-3.2.1.

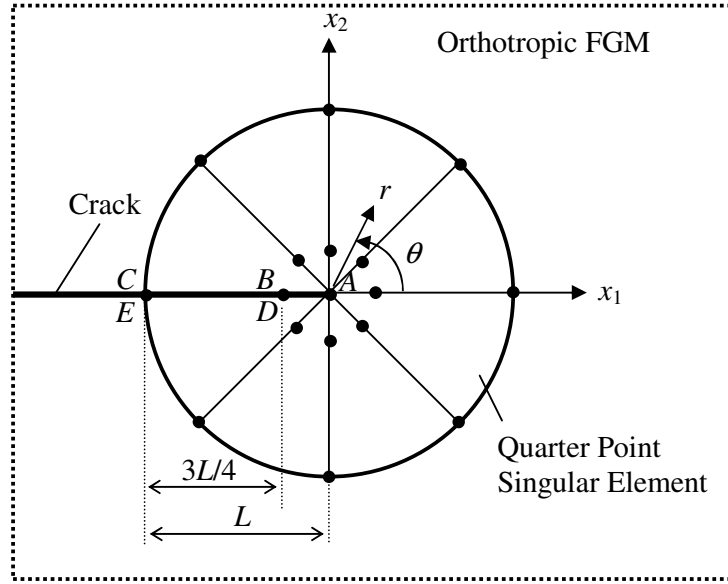


Figure-3.2.1 Quarter-point singular elements located at the crack tip.

Considering the crack tip polar coordinate system and definitions of stress intensity factors given by Eq.(2.2.68), displacement equations in the close vicinity of the crack tip can be written as given in Eq.(3.2.1) for pure mode I and as given in Eq.(3.2.2) for pure mode II [120].

$$u_1 = k_1 \sqrt{2r} \operatorname{Re} \left[\mu_1^{ip} p_2 \frac{\sqrt{\cos \theta + \mu_2^{ip} \sin \theta}}{\mu_1^{ip} - \mu_2^{ip}} - \mu_2^{ip} p_1 \frac{\sqrt{\cos \theta + \mu_1^{ip} \sin \theta}}{\mu_1^{ip} - \mu_2^{ip}} \right] \quad (3.2.1a)$$

$$u_2 = k_1 \sqrt{2r} \operatorname{Re} \left[\mu_1^{ip} q_2 \frac{\sqrt{\cos \theta + \mu_2^{ip} \sin \theta}}{\mu_1^{ip} - \mu_2^{ip}} - \mu_2^{ip} q_1 \frac{\sqrt{\cos \theta + \mu_1^{ip} \sin \theta}}{\mu_1^{ip} - \mu_2^{ip}} \right] \quad (3.2.1b)$$

$$u_1 = k_2 \sqrt{2r} \operatorname{Re} \left[p_2 \frac{\sqrt{\cos \theta + \mu_2^{ip} \sin \theta}}{\mu_1^{ip} - \mu_2^{ip}} - p_1 \frac{\sqrt{\cos \theta + \mu_1^{ip} \sin \theta}}{\mu_1^{ip} - \mu_2^{ip}} \right] \quad (3.2.2a)$$

$$u_2 = k_2 \sqrt{2r} \operatorname{Re} \left[q_2 \frac{\sqrt{\cos \theta + \mu_2^{ip} \sin \theta}}{\mu_1^{ip} - \mu_2^{ip}} - q_1 \frac{\sqrt{\cos \theta + \mu_1^{ip} \sin \theta}}{\mu_1^{ip} - \mu_2^{ip}} \right] \quad (3.2.2b)$$

where k_1 and k_2 are the mode I and mode II stress intensity factors, respectively. u_1 and u_2 are the displacement components along x_1 - and x_2 - directions, respectively. $\mu_1^{ip} = \alpha_1 + i\hat{\beta}_1$ and $\mu_2^{ip} = \alpha_2 + i\hat{\beta}_2$ are the crack tip parameters and found as the roots of the following characteristic equation such that $\hat{\beta}_j > 0$ ($j = 1, 2$):

$$a_{11}\mu^4 - 2a_{16}\mu^3 + (2a_{12} + a_{66})\mu^2 - 2a_{26}\mu + a_{22} = 0 \quad (3.2.3)$$

where a_{11} , a_{12} , a_{16} , a_{22} , a_{26} and a_{66} are the terms of the compliance matrix considering the crack tip Cartesian coordinate system. For plane elasticity problems in orthotropic materials, they are introduced as follows:

$$\begin{bmatrix} \varepsilon_{x_1 x_1} \\ \varepsilon_{x_2 x_2} \\ 2\varepsilon_{x_1 x_2} \end{bmatrix} = \begin{bmatrix} a_{11} & a_{12} & a_{16} \\ a_{12} & a_{22} & a_{26} \\ a_{16} & a_{26} & a_{66} \end{bmatrix} \begin{bmatrix} \sigma_{x_1 x_1} \\ \sigma_{x_2 x_2} \\ \sigma_{x_1 x_2} \end{bmatrix} \quad (3.2.4)$$

where $\varepsilon_{x_1 x_1}$, $\varepsilon_{x_2 x_2}$, $\varepsilon_{x_1 x_2}$ are the strain components and $\sigma_{x_1 x_1}$, $\sigma_{x_2 x_2}$, $\sigma_{x_1 x_2}$ are the stress components with respect to the crack tip Cartesian coordinate system.

p_j and q_j , ($j = 1, 2$), are given by:

$$p_j = a_{11}(\mu_j^{ip})^2 + a_{12} - a_{16}\mu_j^{ip}, \quad (j = 1, 2) \quad (3.2.5)$$

$$q_j = a_{12}\mu_j^{ip} + \frac{a_{22}}{\mu_j^{ip}} - a_{26}, \quad (j = 1, 2) \quad (3.2.6)$$

For quadratic isoparametric quarter point singular elements, normal crack opening displacement along the edge ABC , COD_{ABC}^n , is given by the following equation [128].

$$COD_{ABC}^n = (4u_2^B - u_2^C)\sqrt{\frac{r}{L}} + (-4u_2^B + 2u_2^C)\frac{r}{L} \quad (3.2.7)$$

where u_2^B and u_2^C are the displacement components along x_2 - direction at point B and point C , respectively.

The tangential crack opening displacement along the edge ABC , COD'_{ABC} , is written as follows [133]:

$$COD'_{ABC} = (4u_1^B - u_1^C)\sqrt{\frac{r}{L}} + (-4u_1^B + 2u_1^C)\frac{r}{L} \quad (3.2.8)$$

where u_1^B and u_1^C are the displacement components along x_1 - direction at point B and point C , respectively.

Considering both edge ABC and edge ADE , resultant normal crack opening displacement, COD^n , and resultant tangential crack opening displacement, COD^t , are written as follows:

$$COD^n = COD_{ABC}^n - COD_{ADE}^n = \left(4(u_2^B - u_2^D) - (u_2^C - u_2^E)\right) \sqrt{\frac{r}{L}} + \left(-4(u_2^B - u_2^D) + 2(u_2^C - u_2^E)\right) \frac{r}{L} \quad (3.2.9)$$

$$COD^t = COD_{ABC}^t - COD_{ADE}^t = \left(4(u_1^B - u_1^D) - (u_1^C - u_1^E)\right) \sqrt{\frac{r}{L}} + \left(-4(u_1^B - u_1^D) + 2(u_1^C - u_1^E)\right) \frac{r}{L} \quad (3.2.10)$$

where u_2^D and u_2^E are the displacement components along x_2 - direction at point D and point E , u_1^D and u_1^E are the displacement components along x_1 - direction at point D and point E , respectively.

Then, using Eq.(3.2.1), Eq.(3.2.2), Eq.(3.2.9) and Eq.(3.2.10), mode I and mode II stress intensity factors at the considered crack tip can be obtained as follows [120]:

$$k_1 = \frac{1}{4} \sqrt{\frac{2}{L}} \frac{F_4 \left(4(u_1^B - u_1^D) - (u_1^C - u_1^E)\right) - F_2 \left(4(u_2^B - u_2^D) - (u_2^C - u_2^E)\right)}{F_1 F_4 - F_2 F_3} \quad (3.2.11a)$$

$$k_2 = \frac{1}{4} \sqrt{\frac{2}{L}} \frac{F_1 \left(4(u_2^B - u_2^D) - (u_2^C - u_2^E)\right) - F_3 \left(4(u_1^B - u_1^D) - (u_1^C - u_1^E)\right)}{F_1 F_4 - F_2 F_3} \quad (3.2.11b)$$

where

$$F_1 = \text{Re} \left[\frac{i}{\mu_1^{ip} - \mu_2^{ip}} \left(\mu_1^{ip} p_2 - \mu_2^{ip} p_1 \right) \right] \quad (3.2.12a)$$

$$F_2 = \operatorname{Re} \left[\frac{i}{\mu_1^{ip} - \mu_2^{ip}} (p_2 - p_1) \right] \quad (3.2.12b)$$

$$F_3 = \operatorname{Re} \left[\frac{i}{\mu_1^{ip} - \mu_2^{ip}} (\mu_1^{ip} q_2 - \mu_2^{ip} q_1) \right] \quad (3.2.12c)$$

$$F_4 = \operatorname{Re} \left[\frac{i}{\mu_1^{ip} - \mu_2^{ip}} (q_2 - q_1) \right] \quad (3.2.12d)$$

CHAPTER 4

NUMERICAL RESULTS

4.1 Verification of the Analytical Study

Verification of the analytical study presented in Chapter 2 is performed considering an embedded crack in a homogeneous orthotropic strip. Cinar and Erdogan [134] presented the results of a plane elasticity problem for an orthotropic strip containing a crack parallel to the boundaries. Illustration of the problem is shown in Figure-4.1.1. This problem is solved using the present formulation by taking each of the material parameters E , ν , δ^4 and κ for coating, bond-coat and substrate as the same and material nonhomogeneity parameter β of the FGM coating as equal to 0. For the case of $\kappa = 1$, the value of κ is taken as 0.9999999.

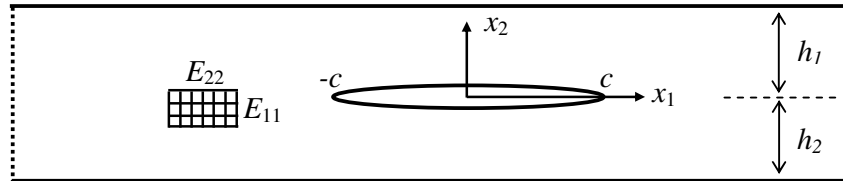


Figure-4.1.1 Illustration of the crack problem solved by Cinar and Erdogan [134].

Assuming that the crack surfaces are under uniform normal stress ($\sigma_{22}(x_1, 0) = -\sigma_0$, $|x_1| < c$), stress intensity factors obtained by both studies are given in Table-4.1.1 for $2h_1/(h_1 + h_2) = 1.0$ and $\delta(h_1 + h_2)/(2c) = 0.35$ and in Table-4.1.2 for $2h_1/(h_1 + h_2) = 0.4$ and $\delta(h_1 + h_2)/(2c) = 0.35$. Assuming that the

crack surfaces are under uniform shear stress ($\sigma_{12}(x_1,0) = -\tau_0, |x_1| < c$), stress intensity factors obtained by both studies are given in Table-4.1.3 for $2h_1/(h_1 + h_2) = 1.0$ and $\delta(h_1 + h_2)/(2c) = 0.35$ and in Table-4.1.4 for $2h_1/(h_1 + h_2) = 0.4$ and $\delta(h_1 + h_2)/(2c) = 0.35$. It is shown that results of the present study agree very well with the results given by Cinar and Erdogan [134].

Table-4.1.1 Comparison of the stress intensity factors, $2h_1/(h_1 + h_2) = 1.0$,

$$\delta(h_1 + h_2)/(2c) = 0.35, \sigma_{22}(x_1,0) = -\sigma_0 \text{ for } |x_1| < c.$$

κ	Cinar and Erdogan [134]	Present Study
	$k_1(c)/(\sigma_0 \sqrt{c})$	$k_1(c)/(\sigma_0 \sqrt{c})$
1	4.801	4.801
2	4.657	4.654
4	4.564	4.553

Table-4.1.2 Comparison of the stress intensity factors, $2h_1/(h_1 + h_2) = 0.4$,

$$\delta(h_1 + h_2)/(2c) = 0.35, \sigma_{22}(x_1,0) = -\sigma_0 \text{ for } |x_1| < c.$$

κ	Cinar and Erdogan [134]		Present Study	
	$k_1(c)/(\sigma_0 \sqrt{c})$	$k_2(c)/(\delta\sigma_0 \sqrt{c})$	$k_1(c)/(\sigma_0 \sqrt{c})$	$k_2(c)/(\delta\sigma_0 \sqrt{c})$
1	9.519	-4.855	9.526	-4.850
2	8.986	-4.404	8.989	-4.386
4	8.447	-3.908	8.470	-3.882

Table-4.1.3 Comparison of the stress intensity factors, $2h_1/(h_1 + h_2) = 1.0$,

$$\delta(h_1 + h_2)/(2c) = 0.35, \sigma_{12}(x_1,0) = -\tau_0 \text{ for } |x_1| < c.$$

κ	Cinar and Erdogan [134]	Present Study
	$k_2(c)/(\tau_0 \sqrt{c})$	$k_2(c)/(\tau_0 \sqrt{c})$
1	2.047	2.047
2	1.890	1.889
4	1.717	1.716

Table-4.1.4 Comparison of the stress intensity factors, $2h_1/(h_1 + h_2) = 0.4$,

$$\delta(h_1 + h_2)/(2c) = 0.35, \sigma_{12}(x_1, 0) = -\tau_0 \text{ for } |x_1| < c.$$

κ	Cinar and Erdogan [134]		Present Study	
	$\delta k_1(c)/(\tau_0 \sqrt{c})$	$k_2(c)/(\tau_0 \sqrt{c})$	$\delta k_1(c)/(\tau_0 \sqrt{c})$	$k_2(c)/(\tau_0 \sqrt{c})$
1	0.846	1.658	0.845	1.659
2	0.761	1.553	0.758	1.554
4	0.666	1.441	0.661	1.441

4.2 Numerical Results Based on Analytical and Computational Approaches

In this section, some numerical results obtained using analytical and computational approaches are presented for the embedded crack problems in the orthotropic FGM coating bonded to the homogeneous substrate through the homogeneous bond-coat.

First, the analytical and computational results for the normalized fracture related parameters of the single embedded crack problem are given considering the pure uniform normal stress ($p(x_1) = \sigma_0$ and $q(x_1) = 0$) on crack surfaces. The reason of giving the results of the two methods is to verify the computational approach. Then, analytical results are given for the single embedded crack problem considering the pure uniform shear stress ($p(x_1) = 0$ and $q(x_1) = \tau_0$) on crack surfaces. Finally, the computational results for the fracture related parameters of the periodic cracks in the orthotropic FGM coating are presented.

Under the applied loading conditions, the following relations exist:

$$k_1(c) = k_1(-c), k_2(c) = -k_2(-c) \text{ for } q(x_1) = 0, p(x_1) = \sigma_0 \quad (4.2.1a)$$

$$k_1(c) = -k_1(-c), k_2(c) = k_2(-c) \text{ for } q(x_1) = \tau_0, p(x_1) = 0 \quad (4.2.1b)$$

So, the tip at which $x_1 = c$ is selected to give the results for the normalized mixed-mode stress intensity factors and energy release rate.

The presented results consist of normalized mode I and mode II stress intensity factors, normalized energy release rate and normalized normal and tangential crack opening displacements.

Expressions for the normalized mode I stress intensity factors under pure uniform normal and pure uniform shear crack surface tractions are given in Eq.(4.2.2a) and Eq.(4.2.2b), respectively.

$$k_1(c)/(\sigma_0 c^{0.5}) \quad (4.2.2a)$$

$$k_1(c)/(\tau_0 c^{0.5}) \quad (4.2.2b)$$

Expressions for the normalized mode II stress intensity factors under pure uniform normal and pure uniform shear crack surface tractions are given in Eq.(4.2.3a) and Eq.(4.2.3b), respectively.

$$k_2(c)/(\sigma_0 c^{0.5}) \quad (4.2.3a)$$

$$k_2(c)/(\tau_0 c^{0.5}) \quad (4.2.3b)$$

Expression for the normalized energy release rate under pure uniform normal crack surface traction is given in Eq.(4.2.4).

$$G(c)/(\pi c \sigma_0^2 / E_0) \quad (4.2.4)$$

Expressions for the normalized normal crack opening displacements under pure uniform normal and pure uniform shear crack surface tractions are given in Eq.(4.2.5a) and Eq.(4.2.5b), respectively. Expressions for the normalized tangential crack opening displacements under pure uniform normal and pure uniform shear crack surface tractions are given in Eq.(4.2.6a) and Eq.(4.2.6b), respectively.

$$v^*(x_1)/\Delta_\sigma \quad (4.2.5a)$$

$$v^*(x_1)/\Delta_\tau \quad (4.2.5b)$$

$$u^*(x_1)/\Delta_\sigma \quad (4.2.6a)$$

$$u^*(x_1)/\Delta_\tau \quad (4.2.6b)$$

where

$$v^*(x_1) = u_2^{(1)}(x_1, 0) - u_2^{(2)}(x_1, 0) \quad (4.2.7a)$$

$$u^*(x_1) = u_1^{(1)}(x_1, 0) - u_1^{(2)}(x_1, 0) \quad (4.2.7b)$$

$$\Delta_\sigma = 2c(\kappa_0 + \nu_0)(\sigma_0/E_0) \quad (4.2.7c)$$

$$\Delta_\tau = 2c(\kappa_0 + \nu_0)(\tau_0/E_0) \quad (4.2.7d)$$

In all of the examined cases, it is assumed that material properties are continuous with discontinuous derivatives at the interface between the FGM coating and the homogeneous bond-coat. The homogeneous substrate material is assumed to be isotropic.

In the presented results, the examined values of material parameters are changing such that κ_0 is from -0.2 to 5.0 , δ_0^4 is from 0.25 to 6.0 and ν_0 is from 0.05 to 0.95 . The minimum value of κ_0 is taken as -0.2 because $(\kappa_0 + \nu_0)$ has to be greater than zero.

In this section, all results are based on the parametric values of the material properties. For an example about the orthotropic FGM coatings used in real applications, the FGM consisting of nickel and alumina can be given. When the FGM coating is 100% alumina, its elastic properties which are given as $E_{11} = 116.36$ GPa, $E_{22} = 90.43$ GPa, $G_{12} = 38.21$ GPa and $\nu_{12} = 0.28$ [126, 135] lead to the material parameters of $E \cong 102.58$ GPa, $\nu \cong 0.25$, $\delta^4 \cong 1.29$ and $\kappa \cong 1.10$ under generalized plane stress state.

4.2.1 Single Embedded Crack Problem Considering Uniform Normal Stress on Crack Surfaces

In this subsection, some numerical results are presented for the single embedded crack problem in the orthotropic FGM coating bonded to the homogeneous substrate through the homogeneous bond-coat considering the uniform normal stress on crack surfaces such that $p(x_1) = \sigma_0$. For this problem, both analytical and computational results are given to verify the displacement correlation technique (DCT).

For the computational analysis, the finite element model of the problem is created considering half of the structure with the appropriate symmetry boundary conditions. The structure is taken sufficiently long to satisfy the assumption of infinite length in x_1 - direction. The deformed shape of the structure, close-up view of the crack faces and applied displacement boundary conditions are shown in

Figure-4.2.1.1 for a typical run. To satisfy the symmetry about x_2 - axis, the displacement component u_1 is fixed as zero at $x_1 = 0$.

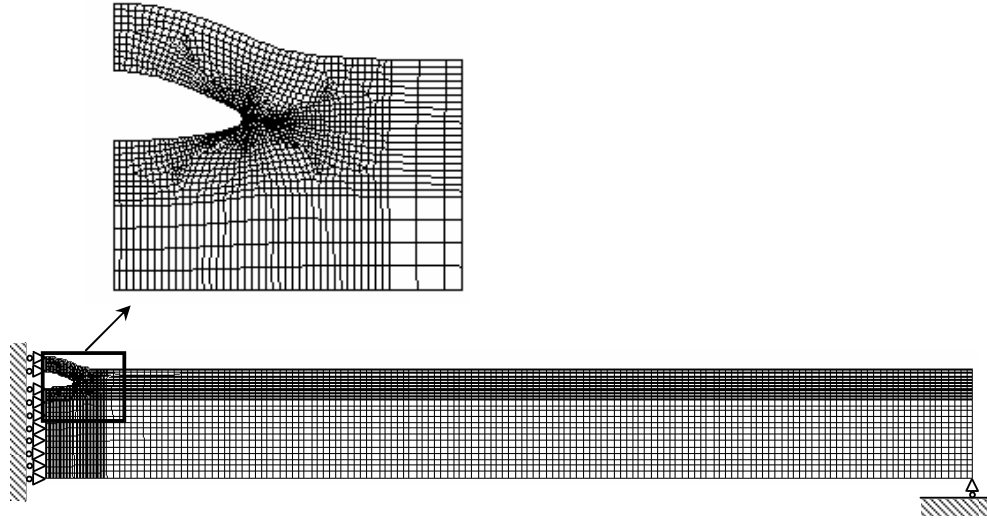


Figure-4.2.1.1 Finite element model of the single embedded crack problem under uniform normal crack surface tractions.

The normalized mode I and mode II stress intensity factors, normalized energy release rate and normalized crack opening displacements are obtained by varying the nonhomogeneity constant βc for various values of the material parameters of the orthotropic FGM coating and geometric parameters of the structure.

The effects of relative coating thickness above the crack, h_1/c , on normalized mode I and mode II stress intensity factors and normalized energy release rates are plotted in Figure-4.2.1.2, Figure-4.2.1.3 and Figure-4.2.1.4, respectively, for various values of material nonhomogeneity constant βc . In the examined cases, h_1/c values are changing from 0.25 to 2.0 and geometric parameters are taken as $2h_2 = 2h_3 = h_4/2 = c$.

Taking the geometric parameters as $2h_1 = 2h_2 = 2h_3 = h_4/2 = c$, normalized mode I and mode II stress intensity factors and normalized energy release rates are plotted with respect to the shear parameter κ_0 in Figure-4.2.1.5, Figure-4.2.1.6 and Figure-4.2.1.7, with respect to the stiffness ratio δ_0^4 in Figure-4.2.1.8, Figure-4.2.1.9 and Figure-4.2.1.10 and with respect to the effective Poisson's ratio ν_0 in Figure-4.2.1.11, Figure-4.2.1.12 and Figure-4.2.1.13, respectively, by changing the values of βc . For the same geometry, normalized normal and tangential crack opening displacements are given in Figure-4.2.1.14 and Figure-4.2.1.15 for various values of κ_0 , in Figure-4.2.1.16 and Figure-4.2.1.17 for various values of δ_0^4 and in Figure-4.2.1.18 and Figure-4.2.1.19 for various values of ν_0 , respectively, taking βc as -1 or 1 . Since the half of the structure is considered in the computational approach, finite element method (FEM) results of normalized normal and tangential crack opening displacements are given for the half crack length.

To investigate the effect of relative bond-coat thickness, h_3/c , on the fracture related parameters, normalized mode I and mode II stress intensity factors and normalized energy release rates are plotted with respect to h_3/c in Figure-4.2.1.20, Figure-4.2.1.21 and Figure-4.2.1.22, respectively, for various values of material nonhomogeneity constant βc assuming that the crack lies very close to the bond-coat such that $h_1/0.95 = h_2/0.05 = h_4/2 = c$. The examined values of h_3/c are changing from 0.025 to 0.5.

From Figure-4.2.1.2 to Figure-4.2.1.19, the plotted data is obtained assuming $E_0 \exp(-\beta h_2) = E_3 = E_4/1.5$. In Figure-4.2.1.20, Figure-4.2.1.21 and Figure-4.2.1.22, it is assumed that $E_0 \exp(-\beta h_2) = E_3 = E_4/3$.

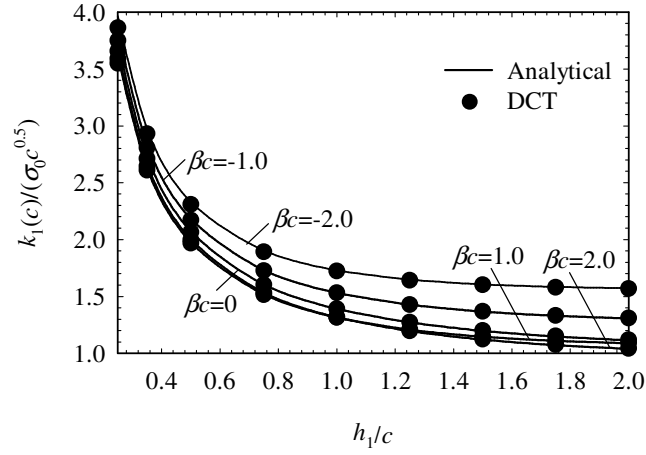


Figure-4.2.1.2 Normalized mode I stress intensity factor versus h_1/c and nonhomogeneity constant βc , $E_0 \exp(-\beta h_2) = E_3 = E_4/1.5$, $\nu_0 = \nu_3 = 0.25$, $\nu_4 = 0.3$, $\kappa_0 = \kappa_3 = 2$, $\kappa_4 = 1$, $\delta_0^4 = \delta_3^4 = 2$, $\delta_4^4 = 1$, $2h_2 = 2h_3 = h_4/2 = c$, $p(x_1) = \sigma_0$, $q(x_1) = 0$.

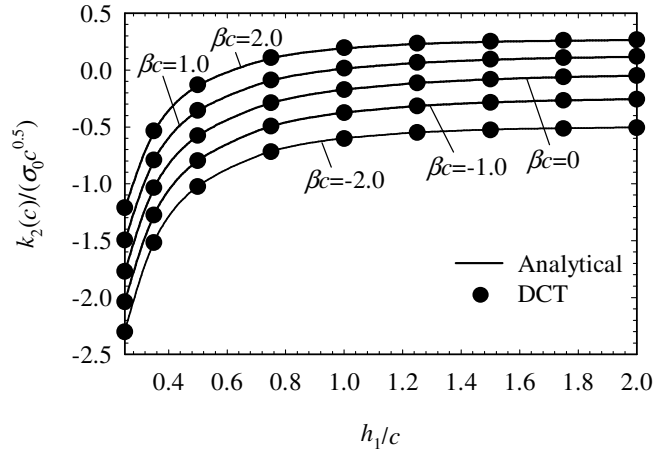


Figure-4.2.1.3 Normalized mode II stress intensity factor versus h_1/c and nonhomogeneity constant βc , $E_0 \exp(-\beta h_2) = E_3 = E_4/1.5$, $\nu_0 = \nu_3 = 0.25$, $\nu_4 = 0.3$, $\kappa_0 = \kappa_3 = 2$, $\kappa_4 = 1$, $\delta_0^4 = \delta_3^4 = 2$, $\delta_4^4 = 1$, $2h_2 = 2h_3 = h_4/2 = c$, $p(x_1) = \sigma_0$, $q(x_1) = 0$.

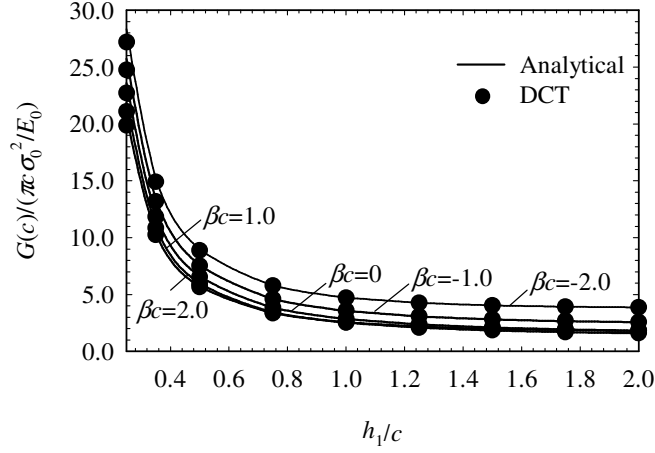


Figure-4.2.1.4 Normalized energy release rate versus h_1/c and nonhomogeneity constant βc , $E_0 \exp(-\beta h_2) = E_3 = E_4/1.5$, $\nu_0 = \nu_3 = 0.25$, $\nu_4 = 0.3$, $\kappa_0 = \kappa_3 = 2$, $\kappa_4 = 1$, $\delta_0^4 = \delta_3^4 = 2$, $\delta_4^4 = 1$, $2h_2 = 2h_3 = h_4/2 = c$, $p(x_1) = \sigma_0$, $q(x_1) = 0$.

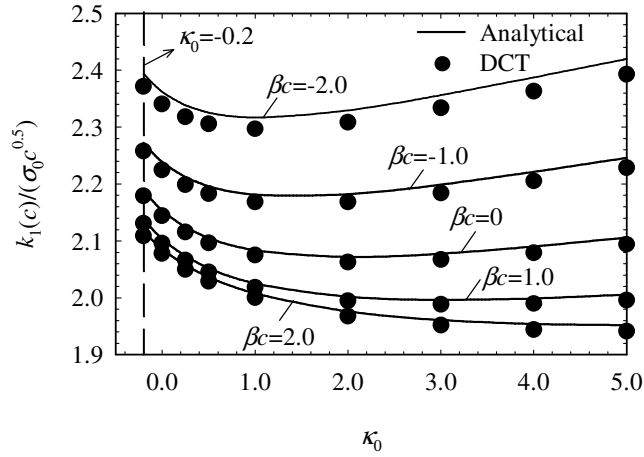


Figure-4.2.1.5 Normalized mode I stress intensity factor versus shear parameter κ_0 and nonhomogeneity constant βc , $E_0 \exp(-\beta h_2) = E_3 = E_4/1.5$, $\nu_0 = \nu_3 = 0.25$, $\nu_4 = 0.3$, $\kappa_0 = \kappa_3$, $\kappa_4 = 1$, $\delta_0^4 = \delta_3^4 = 2$, $\delta_4^4 = 1$, $2h_1 = 2h_2 = 2h_3 = h_4/2 = c$, $p(x_1) = \sigma_0$, $q(x_1) = 0$.

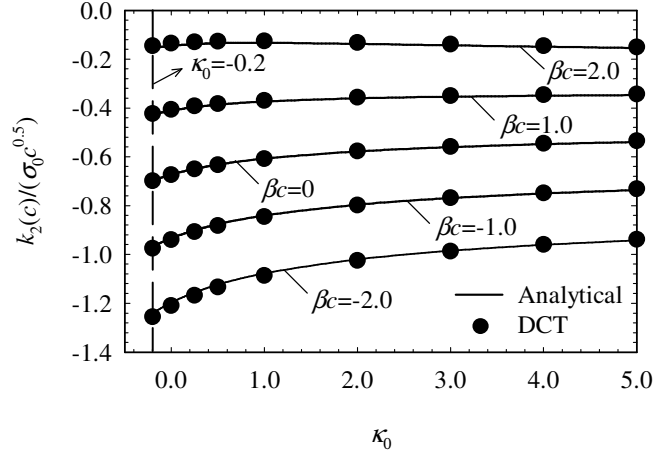


Figure-4.2.1.6 Normalized mode II stress intensity factor versus shear parameter κ_0 and nonhomogeneity constant βc , $E_0 \exp(-\beta h_2) = E_3 = E_4/1.5$, $\nu_0 = \nu_3 = 0.25$, $\nu_4 = 0.3$, $\kappa_0 = \kappa_3$, $\kappa_4 = 1$, $\delta_0^4 = \delta_3^4 = 2$, $\delta_4^4 = 1$, $2h_1 = 2h_2 = 2h_3 = h_4/2 = c$, $p(x_1) = \sigma_0$, $q(x_1) = 0$.

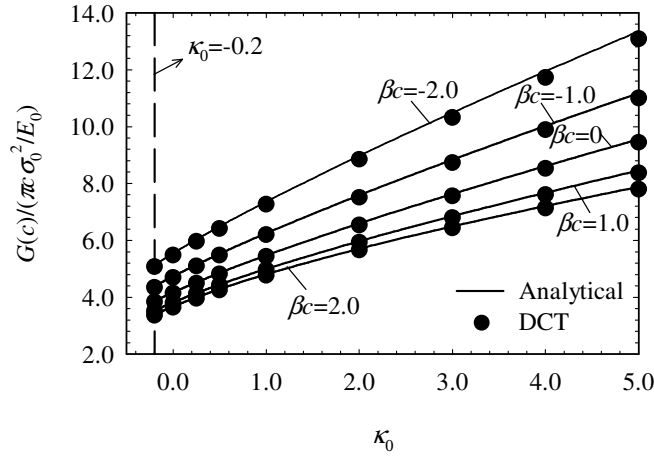


Figure-4.2.1.7 Normalized energy release rate versus shear parameter κ_0 and nonhomogeneity constant βc , $E_0 \exp(-\beta h_2) = E_3 = E_4/1.5$, $\nu_0 = \nu_3 = 0.25$, $\nu_4 = 0.3$, $\kappa_0 = \kappa_3$, $\kappa_4 = 1$, $\delta_0^4 = \delta_3^4 = 2$, $\delta_4^4 = 1$, $2h_1 = 2h_2 = 2h_3 = h_4/2 = c$, $p(x_1) = \sigma_0$, $q(x_1) = 0$.

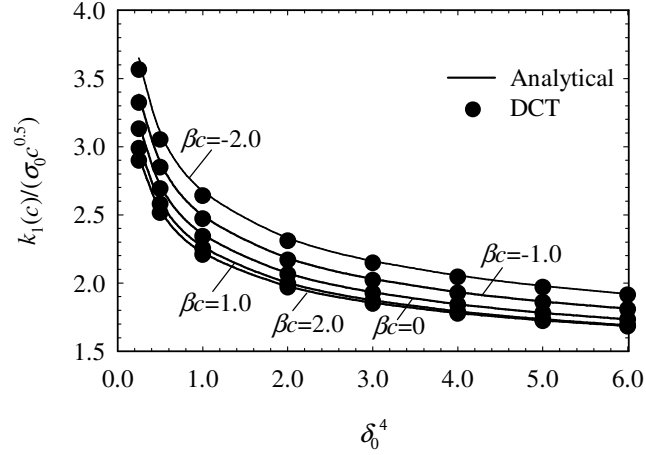


Figure-4.2.1.8 Normalized mode I stress intensity factor versus stiffness ratio δ_0^4 and nonhomogeneity constant βc , $E_0 \exp(-\beta h_2) = E_3 = E_4/1.5$, $\nu_0 = \nu_3 = 0.25$, $\nu_4 = 0.3$, $\kappa_0 = \kappa_3 = 2$, $\kappa_4 = 1$, $\delta_0^4 = \delta_3^4$, $\delta_4^4 = 1$, $2h_1 = 2h_2 = 2h_3 = h_4/2 = c$, $p(x_1) = \sigma_0$, $q(x_1) = 0$.

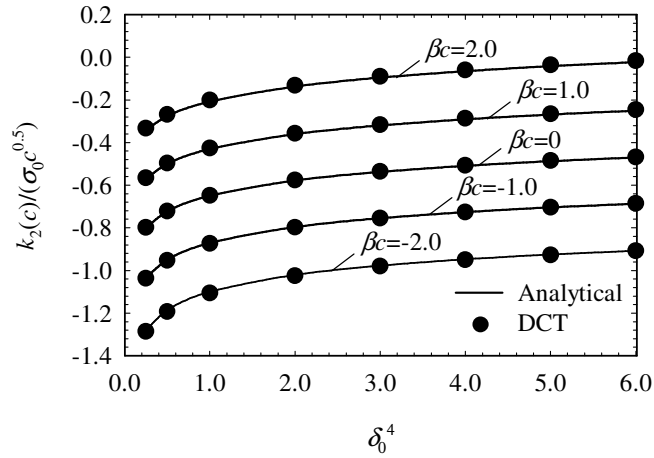


Figure-4.2.1.9 Normalized mode II stress intensity factor versus stiffness ratio δ_0^4 and nonhomogeneity constant βc , $E_0 \exp(-\beta h_2) = E_3 = E_4/1.5$, $\nu_0 = \nu_3 = 0.25$, $\nu_4 = 0.3$, $\kappa_0 = \kappa_3 = 2$, $\kappa_4 = 1$, $\delta_0^4 = \delta_3^4$, $\delta_4^4 = 1$, $2h_1 = 2h_2 = 2h_3 = h_4/2 = c$, $p(x_1) = \sigma_0$, $q(x_1) = 0$.

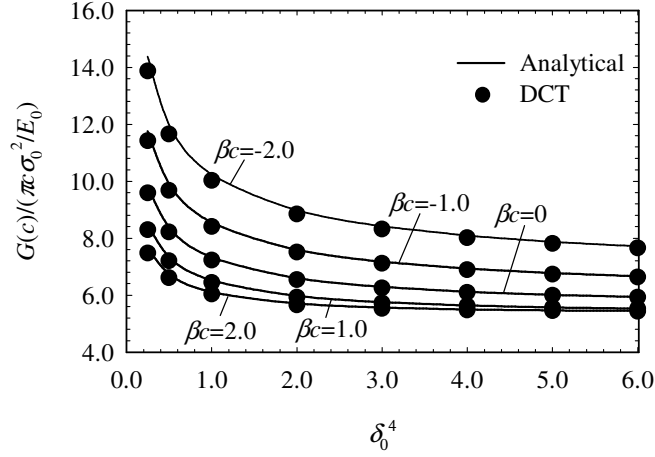


Figure-4.2.1.10 Normalized energy release rate versus stiffness ratio δ_0^4 and nonhomogeneity constant βc , $E_0 \exp(-\beta h_2) = E_3 = E_4/1.5$, $\nu_0 = \nu_3 = 0.25$, $\nu_4 = 0.3$, $\kappa_0 = \kappa_3 = 2$, $\kappa_4 = 1$, $\delta_0^4 = \delta_3^4$, $\delta_4^4 = 1$, $2h_1 = 2h_2 = 2h_3 = h_4/2 = c$, $p(x_1) = \sigma_0$, $q(x_1) = 0$.

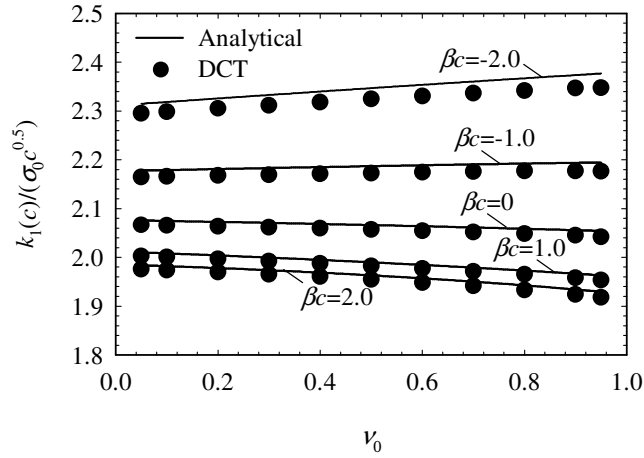


Figure-4.2.1.11 Normalized mode I stress intensity factor versus effective Poisson's ratio ν_0 and nonhomogeneity constant βc , $E_0 \exp(-\beta h_2) = E_3 = E_4/1.5$, $\nu_0 = \nu_3$, $\nu_4 = 0.3$, $\kappa_0 = \kappa_3 = 2$, $\kappa_4 = 1$, $\delta_0^4 = \delta_3^4 = 2$, $\delta_4^4 = 1$, $2h_1 = 2h_2 = 2h_3 = h_4/2 = c$, $p(x_1) = \sigma_0$, $q(x_1) = 0$.

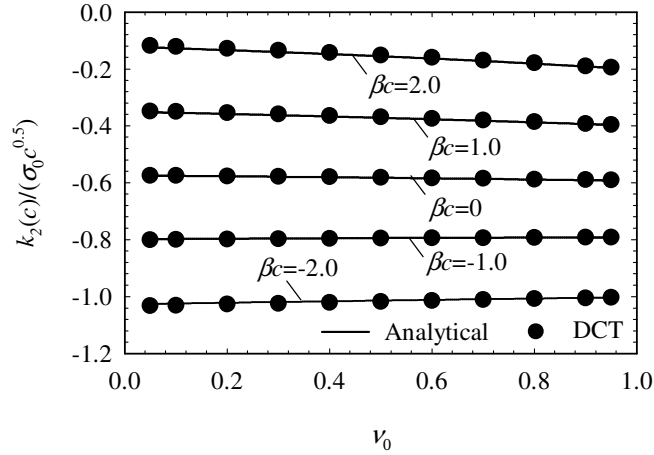


Figure-4.2.1.12 Normalized mode II stress intensity factor versus effective Poisson's ratio ν_0 and nonhomogeneity constant βc , $E_0 \exp(-\beta h_2) = E_3 = E_4/1.5$, $\nu_0 = \nu_3$, $\nu_4 = 0.3$, $\kappa_0 = \kappa_3 = 2$, $\kappa_4 = 1$, $\delta_0^4 = \delta_3^4 = 2$, $\delta_4^4 = 1$, $2h_1 = 2h_2 = 2h_3 = h_4/2 = c$, $p(x_1) = \sigma_0$, $q(x_1) = 0$.

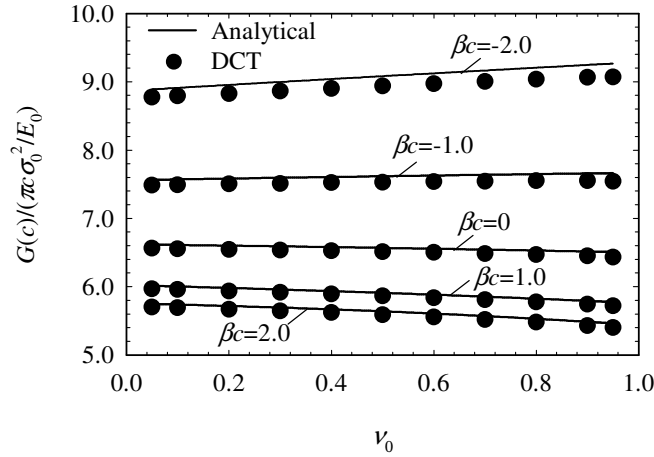


Figure-4.2.1.13 Normalized energy release rate versus effective Poisson's ratio ν_0 and nonhomogeneity constant βc , $E_0 \exp(-\beta h_2) = E_3 = E_4/1.5$, $\nu_0 = \nu_3$, $\nu_4 = 0.3$, $\kappa_0 = \kappa_3 = 2$, $\kappa_4 = 1$, $\delta_0^4 = \delta_3^4 = 2$, $\delta_4^4 = 1$, $2h_1 = 2h_2 = 2h_3 = h_4/2 = c$, $p(x_1) = \sigma_0$, $q(x_1) = 0$.

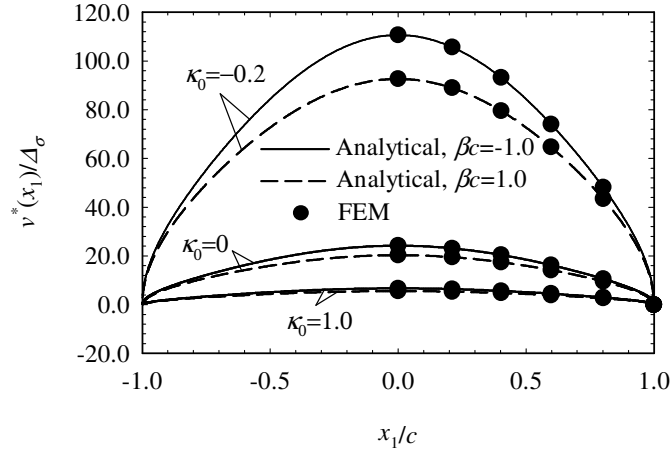


Figure-4.2.1.14 Normalized normal crack opening displacement for various values of shear parameter κ_0 and nonhomogeneity constant βc , $E_0 \exp(-\beta h_2) = E_3 = E_4/1.5$, $\nu_0 = \nu_3 = 0.25$, $\nu_4 = 0.3$, $\kappa_0 = \kappa_3$, $\kappa_4 = 1$, $\delta_0^4 = \delta_3^4 = 2$, $\delta_4^4 = 1$, $2h_1 = 2h_2 = 2h_3 = h_4/2 = c$, $p(x_1) = \sigma_0$, $q(x_1) = 0$.

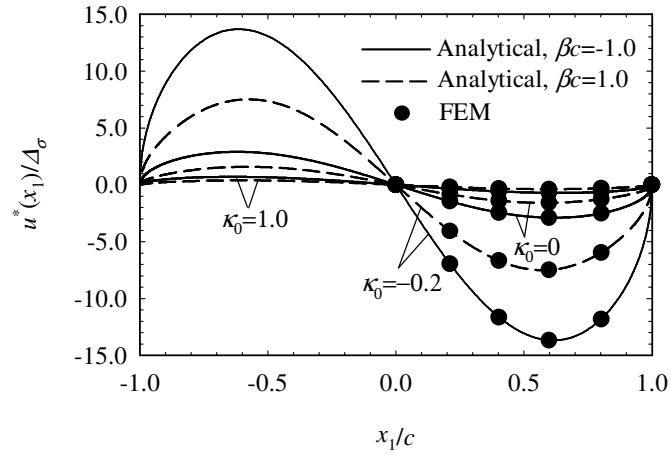


Figure-4.2.1.15 Normalized tangential crack opening displacement for various values of shear parameter κ_0 and nonhomogeneity constant βc , $E_0 \exp(-\beta h_2) = E_3 = E_4/1.5$, $\nu_0 = \nu_3 = 0.25$, $\nu_4 = 0.3$, $\kappa_0 = \kappa_3$, $\kappa_4 = 1$, $\delta_0^4 = \delta_3^4 = 2$, $\delta_4^4 = 1$, $2h_1 = 2h_2 = 2h_3 = h_4/2 = c$, $p(x_1) = \sigma_0$, $q(x_1) = 0$.

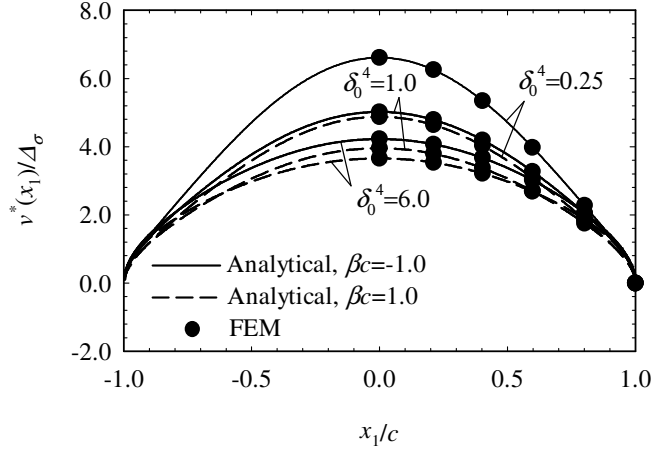


Figure-4.2.1.16 Normalized normal crack opening displacement for various values of stiffness ratio δ_0^4 and nonhomogeneity constant βc , $E_0 \exp(-\beta h_2) = E_3 = E_4/1.5$, $\nu_0 = \nu_3 = 0.25$, $\nu_4 = 0.3$, $\kappa_0 = \kappa_3 = 2$, $\kappa_4 = 1$, $\delta_0^4 = \delta_3^4$, $\delta_4^4 = 1$, $2h_1 = 2h_2 = 2h_3 = h_4/2 = c$, $p(x_1) = \sigma_0$, $q(x_1) = 0$.

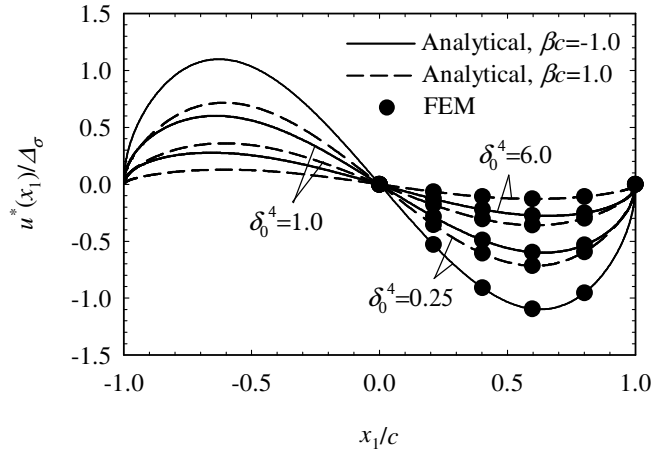


Figure-4.2.1.17 Normalized tangential crack opening displacement for various values of stiffness ratio δ_0^4 and nonhomogeneity constant βc , $E_0 \exp(-\beta h_2) = E_3 = E_4/1.5$, $\nu_0 = \nu_3 = 0.25$, $\nu_4 = 0.3$, $\kappa_0 = \kappa_3 = 2$, $\kappa_4 = 1$, $\delta_0^4 = \delta_3^4$, $\delta_4^4 = 1$, $2h_1 = 2h_2 = 2h_3 = h_4/2 = c$, $p(x_1) = \sigma_0$, $q(x_1) = 0$.

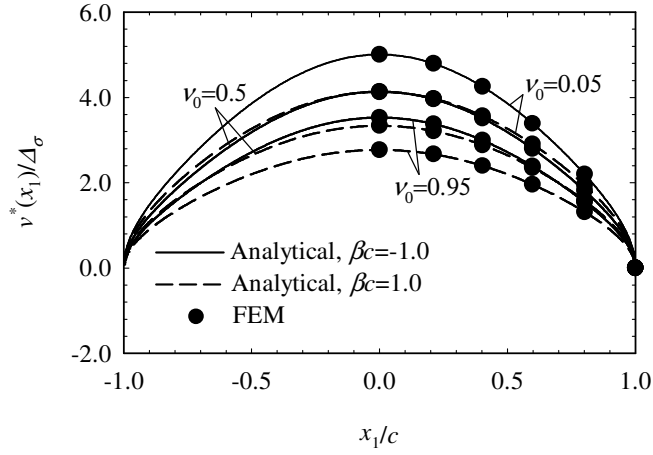


Figure-4.2.1.18 Normalized normal crack opening displacement for various values of effective Poisson's ratio ν_0 and nonhomogeneity constant βc , $E_0 \exp(-\beta h_2) = E_3 = E_4/1.5$, $\nu_0 = \nu_3$, $\nu_4 = 0.3$, $\kappa_0 = \kappa_3 = 2$, $\kappa_4 = 1$, $\delta_0^4 = \delta_3^4 = 2$, $\delta_4^4 = 1$, $2h_1 = 2h_2 = 2h_3 = h_4/2 = c$, $p(x_1) = \sigma_0$, $q(x_1) = 0$.

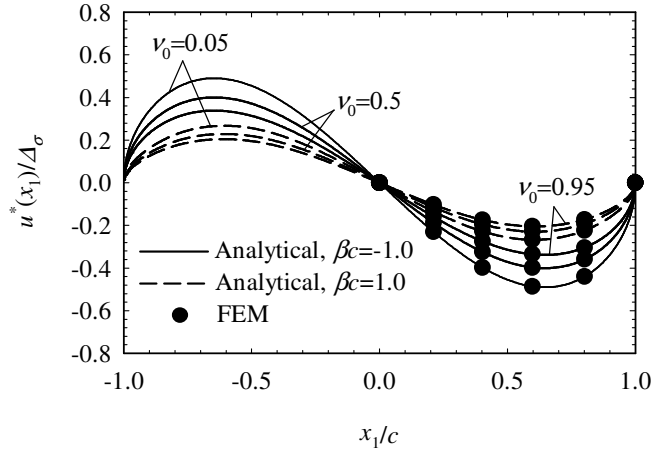


Figure-4.2.1.19 Normalized tangential crack opening displacement for various values of effective Poisson's ratio ν_0 and nonhomogeneity constant βc , $E_0 \exp(-\beta h_2) = E_3 = E_4/1.5$, $\nu_0 = \nu_3$, $\nu_4 = 0.3$, $\kappa_0 = \kappa_3 = 2$, $\kappa_4 = 1$, $\delta_0^4 = \delta_3^4 = 2$, $\delta_4^4 = 1$, $2h_1 = 2h_2 = 2h_3 = h_4/2 = c$, $p(x_1) = \sigma_0$, $q(x_1) = 0$.

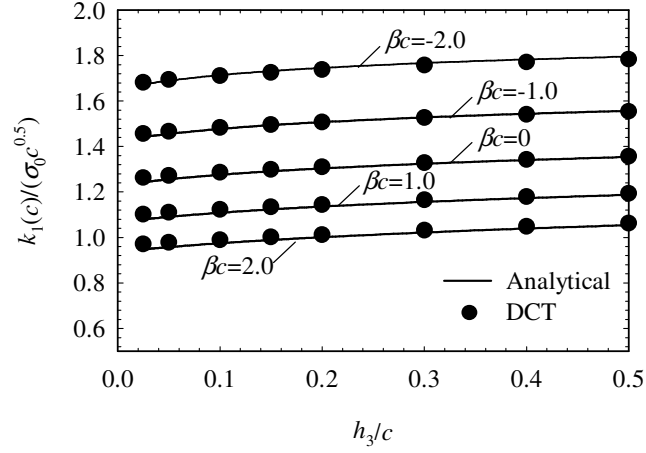


Figure-4.2.1.20 Normalized mode I stress intensity factor versus h_3/c and nonhomogeneity constant βc , $E_0 \exp(-\beta h_2) = E_3 = E_4/3.0$, $\nu_0 = \nu_3 = 0.25$, $\nu_4 = 0.3$, $\kappa_0 = \kappa_3 = 2$, $\kappa_4 = 1$, $\delta_0^4 = \delta_3^4 = 2$, $\delta_4^4 = 1$, $h_1 = 0.95c$, $h_2 = 0.05c$, $h_4 = 2c$, $p(x_1) = \sigma_0$, $q(x_1) = 0$.

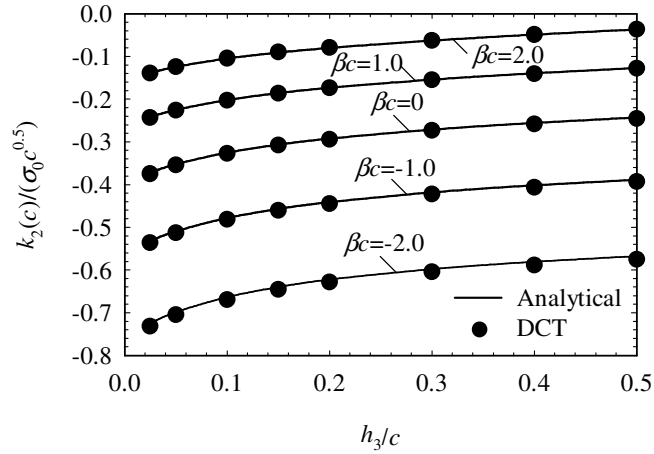


Figure-4.2.1.21 Normalized mode II stress intensity factor versus h_3/c and nonhomogeneity constant βc , $E_0 \exp(-\beta h_2) = E_3 = E_4/3.0$, $\nu_0 = \nu_3 = 0.25$, $\nu_4 = 0.3$, $\kappa_0 = \kappa_3 = 2$, $\kappa_4 = 1$, $\delta_0^4 = \delta_3^4 = 2$, $\delta_4^4 = 1$, $h_1 = 0.95c$, $h_2 = 0.05c$, $h_4 = 2c$, $p(x_1) = \sigma_0$, $q(x_1) = 0$.

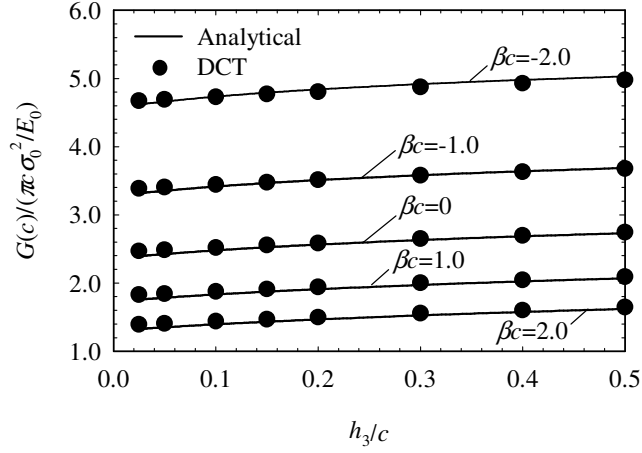


Figure-4.2.1.22 Normalized energy release rate versus h_3/c and nonhomogeneity constant βc , $E_0 \exp(-\beta h_2) = E_3 = E_4/3.0$, $\nu_0 = \nu_3 = 0.25$, $\nu_4 = 0.3$, $\kappa_0 = \kappa_3 = 2$, $\kappa_4 = 1$, $\delta_0^4 = \delta_3^4 = 2$, $\delta_4^4 = 1$, $h_1 = 0.95c$, $h_2 = 0.05c$, $h_4 = 2c$, $p(x_1) = \sigma_0$, $q(x_1) = 0$.

In all of the examined cases, mode I stress intensity factor is numerically larger than the mode II stress intensity factor. It is shown that mode I stress intensity factor and energy release rate are decreasing functions of the material nonhomogeneity constant βc for all considered values of material and geometric parameters when only uniform normal stress acts on crack surfaces. As the material nonhomogeneity constant βc decreases from positive to negative, the effect of its variation on mode I stress intensity factor and the energy release rate becomes more significant. It is also observed that mode II stress intensity factor decreases in absolute values as the material nonhomogeneity constant βc increases from negative to positive for all examined values of (h_3/c) , κ_0 , δ_0^4 , ν_0 and small values of (h_1/c) when crack surfaces are under uniform normal stress. For relatively large values of (h_1/c) , absolute values of mode II stress intensity factors first decrease and then increase as βc increases from negative to positive.

In Figure-4.2.1.2, it is shown that mode I stress intensity factor first decreases and then becomes almost constant with increasing h_1/c for all examined values of material nonhomogeneity constant βc . On the other hand, the effect of variation in βc on mode I stress intensity factor is more significant for large values of h_1/c . This is expected because both the nonhomogeneity parameter and the distance from the crack line affect the effective stiffness of the coating.

In Figure-4.2.1.3, mode II stress intensity factor first changes and then becomes almost constant with increasing h_1/c for all examined values of material nonhomogeneity constant βc .

In Figure-4.2.1.4, the energy release rate first decreases and then becomes almost constant with increasing h_1/c for all considered values of material nonhomogeneity constant βc .

In Figure-4.2.1.5, mode I stress intensity factor first decreases and then increases noticeably with increasing shear parameter κ_0 for some of the examined values of material nonhomogeneity constant βc .

In Figure-4.2.1.6, mode II stress intensity factor first decreases in absolute values with increasing shear parameter κ_0 and then becomes almost insensitive to the variations in κ_0 as βc increases from negative to positive.

In Figure-4.2.1.7, the energy release rate is an increasing function of the shear parameter κ_0 for all examined values of material nonhomogeneity constant βc .

In Figure-4.2.1.8, mode I stress intensity factor is a decreasing function of the stiffness ratio δ_0^4 for all considered values of material nonhomogeneity constant

βc . For relatively small values of stiffness ratio δ_0^4 , the effect of its variation on mode I stress intensity factor seems to be more significant.

In Figure-4.2.1.9, mode II stress intensity factor decreases in absolute values as the stiffness ratio δ_0^4 increases for all examined values of material nonhomogeneity constant βc .

In Figure-4.2.1.10, the energy release rate first decreases and then becomes almost constant with increasing stiffness ratio δ_0^4 for all examined values of material nonhomogeneity constant βc .

In Figure-4.2.1.11 and Figure-4.2.1.12, the influence of variation in effective Poisson's ratio ν_0 on the mode I and II stress intensity factors depends on the degree of material nonhomogeneity. Mode I stress intensity factor decreases with increasing ν_0 for $\beta c = 0, 1, 2$ and increases with increasing ν_0 for $\beta c = -1, -2$. Mode II stress intensity factor decreases in absolute values for $\beta c = -1, -2$ and increases in absolute values for $\beta c = 0, 1, 2$ as the value of effective Poisson's ratio ν_0 increases.

In Figure-4.2.1.13, the effect of the variation in the effective Poisson's ratio ν_0 on the energy release rate is relatively small for all considered values of βc .

In the figures related with the normalized normal and tangential crack opening displacements, the normalized normal crack opening displacements are symmetric and the normalized tangential crack opening displacements are anti-symmetric about x_2 - axis. Normalized normal crack opening displacement and absolute value of the normalized tangential crack opening displacement decrease with increasing values of βc , κ_0 , δ_0^4 and ν_0 .

In Figure-4.2.1.20, Figure-4.2.1.21 and Figure-4.2.1.22, mode I stress intensity factor and energy release rate of the single embedded crack increase and the absolute value of the mode II stress intensity factor decreases slightly with the increasing relative bond-coat thickness h_3/c for all considered values of βc .

When the presented analytical and computational results are compared, it is seen that the computational method agrees very well with the analytical method.

4.2.2 Single Embedded Crack Problem Considering Uniform Shear Stress on Crack Surfaces

In this subsection, some numerical results are presented for the analytical solution of the single embedded crack problem in the orthotropic FGM coating bonded to the homogeneous substrate through the homogeneous bond-coat considering the uniform shear stress on crack surfaces such that $q(x_1) = \tau_0$.

When the crack surfaces are subjected to pure uniform shear traction, it is concluded from Eq.(4.2.1b) that one of the crack tips has always negative mode I stress intensity factor. For the case of a negative mode I stress intensity factor, the formulation of the problem has to be done considering the crack closure condition. However, the results of the current formulation can still be used in superposition problems if the resultant mode I stress intensity factor is not negative at both tips of the crack.

In order to show the effects of nonhomogeneity and material parameters of the orthotropic FGM coating on the fracture behavior, normalized mode I and mode II stress intensity factors are plotted with respect to the shear parameter κ_0 in Figure-4.2.2.1 and Figure-4.2.2.2, with respect to the stiffness ratio δ_0^4 in Figure-4.2.2.3 and Figure-4.2.2.4 and with respect to the effective Poisson's ratio ν_0 in Figure-

4.2.2.5 and Figure-4.2.2.6 for various values of the material nonhomogeneity constant βc . The normalized normal and tangential crack opening displacements are given in Figure-4.2.2.7 and Figure-4.2.2.8 for various values of κ_0 , in Figure-4.2.2.9 and Figure-4.2.2.10 for various values of δ_0^4 and in Figure-4.2.2.11 and Figure-4.2.2.12 for various values of ν_0 , respectively, taking βc as -1 or 1 . For all of the examined cases, $2h_1 = 2h_2 = 2h_3 = h_4/2 = c$ and $E_0 \exp(-\beta h_2) = E_3 = E_4/1.5$.

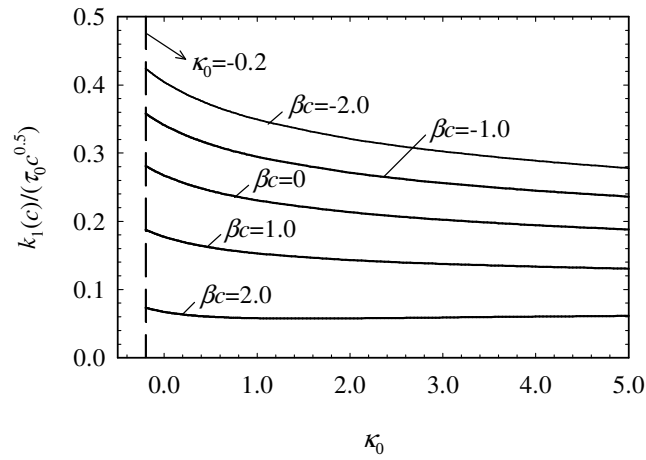


Figure-4.2.2.1 Normalized mode I stress intensity factor versus shear parameter κ_0 and nonhomogeneity constant βc , $E_0 \exp(-\beta h_2) = E_3 = E_4/1.5$, $\nu_0 = \nu_3 = 0.25$, $\nu_4 = 0.3$, $\kappa_0 = \kappa_3$, $\kappa_4 = 1$, $\delta_0^4 = \delta_3^4 = 2$, $\delta_4^4 = 1$, $2h_1 = 2h_2 = 2h_3 = h_4/2 = c$, $p(x_1) = 0$, $q(x_1) = \tau_0$.

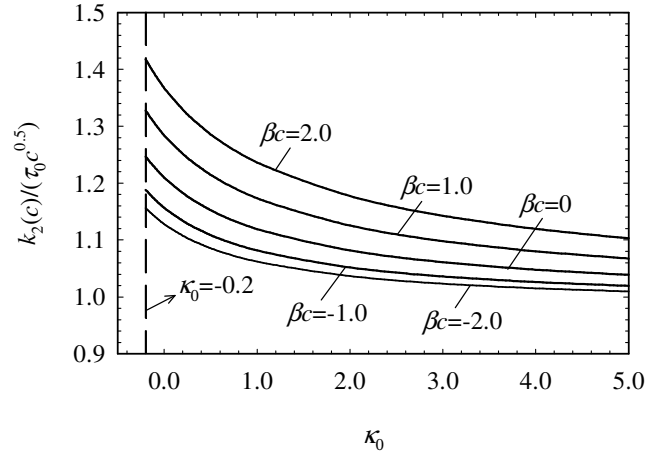


Figure-4.2.2.2 Normalized mode II stress intensity factor versus shear parameter κ_0 and nonhomogeneity constant βc , $E_0 \exp(-\beta h_2) = E_3 = E_4/1.5$, $\nu_0 = \nu_3 = 0.25$, $\nu_4 = 0.3$, $\kappa_0 = \kappa_3$, $\kappa_4 = 1$, $\delta_0^4 = \delta_3^4 = 2$, $\delta_4^4 = 1$, $2h_1 = 2h_2 = 2h_3 = h_4/2 = c$, $p(x_1) = 0$, $q(x_1) = \tau_0$.

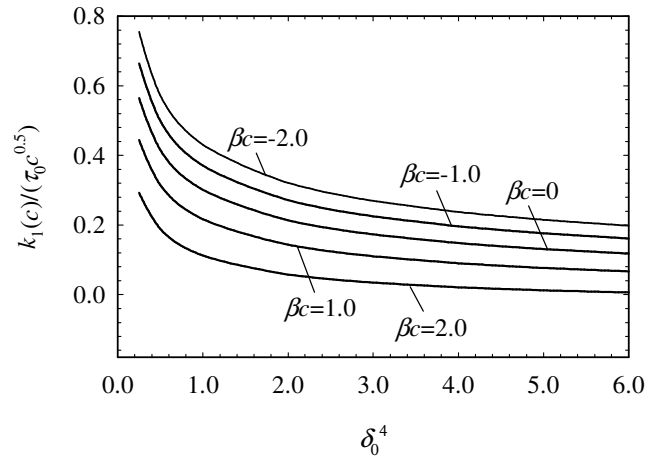


Figure-4.2.2.3 Normalized mode I stress intensity factor versus stiffness ratio δ_0^4 and nonhomogeneity constant βc , $E_0 \exp(-\beta h_2) = E_3 = E_4/1.5$, $\nu_0 = \nu_3 = 0.25$, $\nu_4 = 0.3$, $\kappa_0 = \kappa_3 = 2$, $\kappa_4 = 1$, $\delta_0^4 = \delta_3^4$, $\delta_4^4 = 1$, $2h_1 = 2h_2 = 2h_3 = h_4/2 = c$, $p(x_1) = 0$, $q(x_1) = \tau_0$.

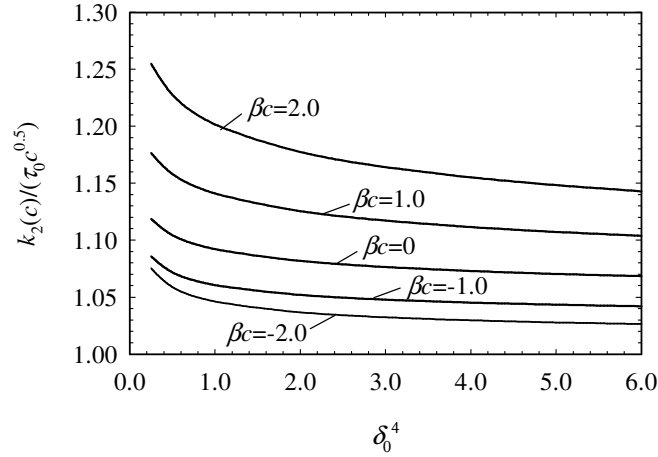


Figure-4.2.2.4 Normalized mode II stress intensity factor versus stiffness ratio δ_0^4 and nonhomogeneity constant βc , $E_0 \exp(-\beta h_2) = E_3 = E_4/1.5$, $\nu_0 = \nu_3 = 0.25$, $\nu_4 = 0.3$, $\kappa_0 = \kappa_3 = 2$, $\kappa_4 = 1$, $\delta_0^4 = \delta_3^4$, $\delta_4^4 = 1$, $2h_1 = 2h_2 = 2h_3 = h_4/2 = c$, $p(x_1) = 0$, $q(x_1) = \tau_0$.

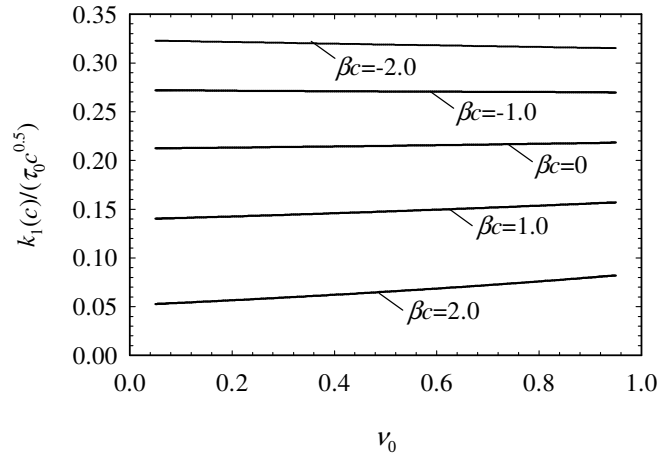


Figure-4.2.2.5 Normalized mode I stress intensity factor versus effective Poisson's ratio ν_0 and nonhomogeneity constant βc , $E_0 \exp(-\beta h_2) = E_3 = E_4/1.5$, $\nu_0 = \nu_3$, $\nu_4 = 0.3$, $\kappa_0 = \kappa_3 = 2$, $\kappa_4 = 1$, $\delta_0^4 = \delta_3^4 = 2$, $\delta_4^4 = 1$, $2h_1 = 2h_2 = 2h_3 = h_4/2 = c$, $p(x_1) = 0$, $q(x_1) = \tau_0$.

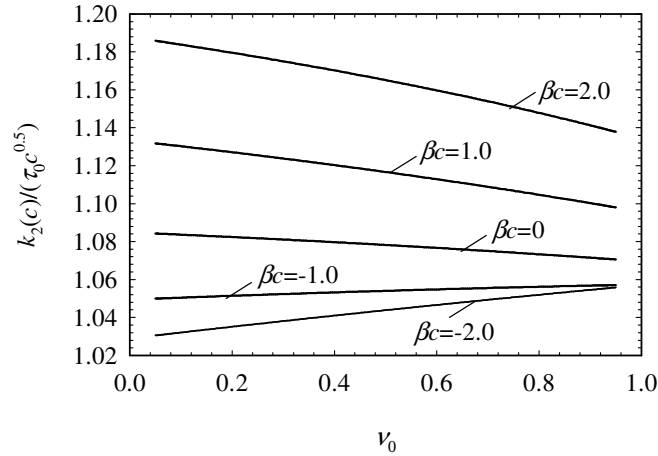


Figure-4.2.2.6 Normalized mode II stress intensity factor versus effective Poisson's ratio ν_0 and nonhomogeneity constant βc , $E_0 \exp(-\beta h_2) = E_3 = E_4/1.5$, $\nu_0 = \nu_3$, $\nu_4 = 0.3$, $\kappa_0 = \kappa_3 = 2$, $\kappa_4 = 1$, $\delta_0^4 = \delta_3^4 = 2$, $\delta_4^4 = 1$, $2h_1 = 2h_2 = 2h_3 = h_4/2 = c$, $p(x_1) = 0$, $q(x_1) = \tau_0$.

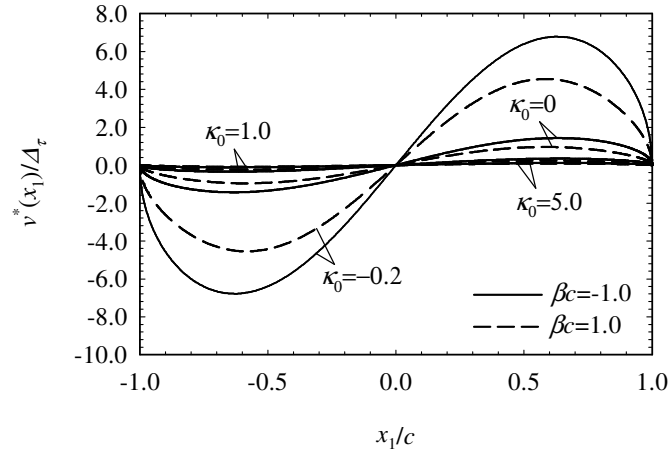


Figure-4.2.2.7 Normalized normal crack opening displacement for various values of shear parameter κ_0 and nonhomogeneity constant βc , $E_0 \exp(-\beta h_2) = E_3 = E_4/1.5$, $\nu_0 = \nu_3 = 0.25$, $\nu_4 = 0.3$, $\kappa_0 = \kappa_3$, $\kappa_4 = 1$, $\delta_0^4 = \delta_3^4 = 2$, $\delta_4^4 = 1$, $2h_1 = 2h_2 = 2h_3 = h_4/2 = c$, $p(x_1) = 0$, $q(x_1) = \tau_0$.

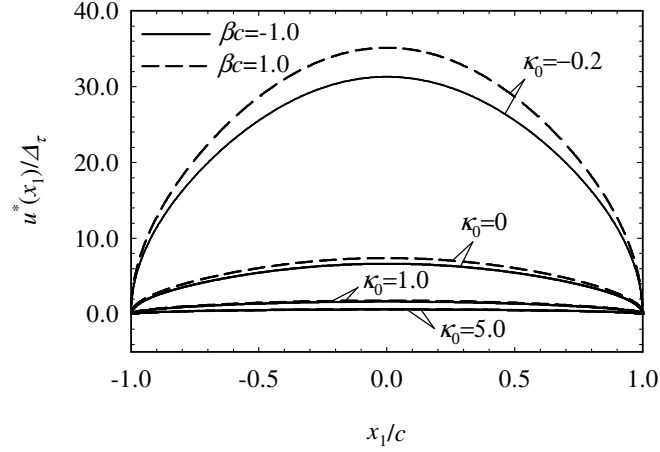


Figure-4.2.2.8 Normalized tangential crack opening displacement for various values of shear parameter κ_0 and nonhomogeneity constant βc , $E_0 \exp(-\beta h_2) = E_3 = E_4/1.5$, $\nu_0 = \nu_3 = 0.25$, $\nu_4 = 0.3$, $\kappa_0 = \kappa_3$, $\kappa_4 = 1$, $\delta_0^4 = \delta_3^4 = 2$, $\delta_4^4 = 1$, $2h_1 = 2h_2 = 2h_3 = h_4/2 = c$, $p(x_1) = 0$, $q(x_1) = \tau_0$.

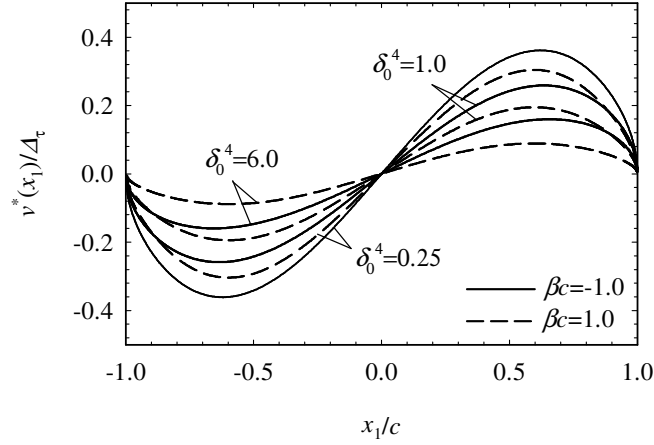


Figure-4.2.2.9 Normalized normal crack opening displacement for various values of stiffness ratio δ_0^4 and nonhomogeneity constant βc , $E_0 \exp(-\beta h_2) = E_3 = E_4/1.5$, $\nu_0 = \nu_3 = 0.25$, $\nu_4 = 0.3$, $\kappa_0 = \kappa_3 = 2$, $\kappa_4 = 1$, $\delta_0^4 = \delta_3^4$, $\delta_4^4 = 1$, $2h_1 = 2h_2 = 2h_3 = h_4/2 = c$, $p(x_1) = 0$, $q(x_1) = \tau_0$.

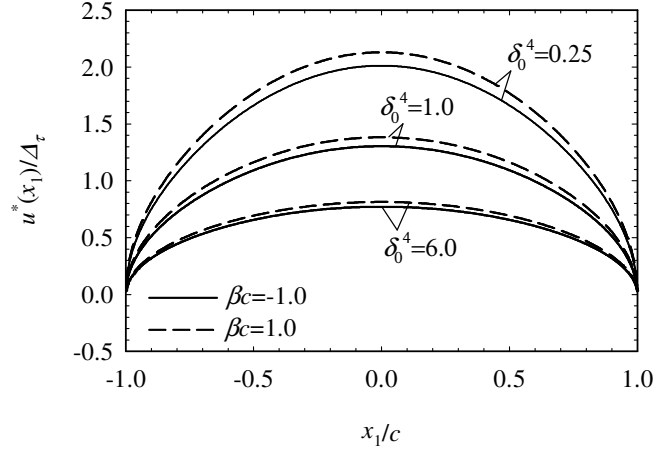


Figure-4.2.2.10 Normalized tangential crack opening displacement for various values of stiffness ratio δ_0^4 and nonhomogeneity constant βc , $E_0 \exp(-\beta h_2) = E_3 = E_4/1.5$, $\nu_0 = \nu_3 = 0.25$, $\nu_4 = 0.3$, $\kappa_0 = \kappa_3 = 2$, $\kappa_4 = 1$, $\delta_0^4 = \delta_3^4$, $\delta_4^4 = 1$, $2h_1 = 2h_2 = 2h_3 = h_4/2 = c$, $p(x_1) = 0$, $q(x_1) = \tau_0$.

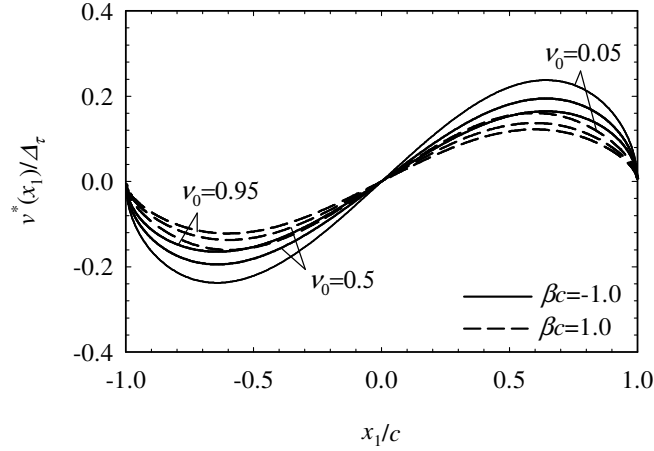


Figure-4.2.2.11 Normalized normal crack opening displacement for various values of effective Poisson's ratio ν_0 and nonhomogeneity constant βc , $E_0 \exp(-\beta h_2) = E_3 = E_4/1.5$, $\nu_0 = \nu_3$, $\nu_4 = 0.3$, $\kappa_0 = \kappa_3 = 2$, $\kappa_4 = 1$, $\delta_0^4 = \delta_3^4 = 2$, $\delta_4^4 = 1$, $2h_1 = 2h_2 = 2h_3 = h_4/2 = c$, $p(x_1) = 0$, $q(x_1) = \tau_0$.

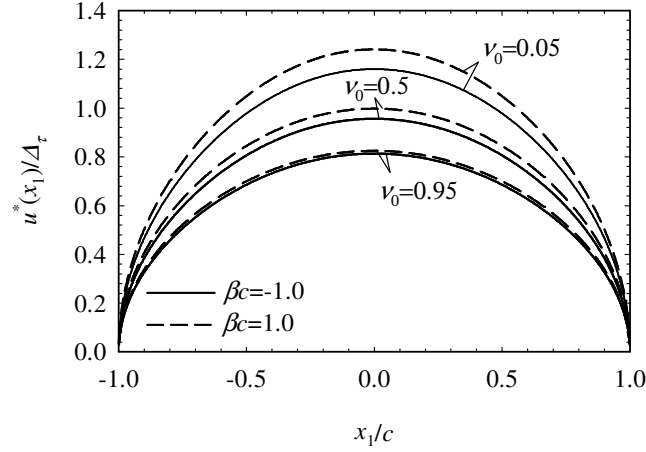


Figure-4.2.2.12 Normalized tangential crack opening displacement for various values of effective Poisson's ratio ν_0 and nonhomogeneity constant βc , $E_0 \exp(-\beta h_2) = E_3 = E_4/1.5$, $\nu_0 = \nu_3$, $\nu_4 = 0.3$, $\kappa_0 = \kappa_3 = 2$, $\kappa_4 = 1$, $\delta_0^4 = \delta_3^4 = 2$, $\delta_4^4 = 1$, $2h_1 = 2h_2 = 2h_3 = h_4/2 = c$, $p(x_1) = 0$, $q(x_1) = \tau_0$.

In all of the examined cases, it is observed that the mode II stress intensity factor is numerically larger than the mode I stress intensity factor. It is shown that mode I stress intensity factor is an absolutely decreasing function of βc and mode II stress intensity factor is an increasing function of βc for all considered values of κ_0 , δ_0^4 and ν_0 when the crack surfaces are under pure uniform shear traction.

In Figure-4.2.2.1, mode I stress intensity factor decreases in absolute values with increasing shear parameter κ_0 for small values of βc and becomes almost independent of κ_0 for large values of βc .

In Figure-4.2.2.2, mode II stress intensity factor decreases with increasing shear parameter κ_0 for all considered values of βc . When κ_0 has small values, the effect of its variation on mode II stress intensity factor is more significant.

In Figure-4.2.2.3, mode I stress intensity factor is an absolutely decreasing function of the stiffness ratio δ_0^4 for all examined values of βc . When δ_0^4 has large values, the effect of its variation on the mode I stress intensity factor becomes less significant.

In Figure-4.2.2.4, mode II stress intensity factor decreases with increasing δ_0^4 for all considered values of βc . The effect of variation in δ_0^4 on mode II stress intensity factor is less noticeable for large values of δ_0^4 .

In Figure-4.2.2.5, mode I stress intensity factor behaves as an absolutely decreasing function of effective Poisson's ratio ν_0 for $\beta c = -1, -2$ and an absolutely increasing function of ν_0 for $\beta c = 0, 1, 2$.

In Figure-4.2.2.6, mode II stress intensity factor increases with increasing effective Poisson's ratio ν_0 for $\beta c = -1, -2$ and decreases with increasing ν_0 for $\beta c = 0, 1, 2$.

In the figures related with the normalized normal and tangential crack opening displacements, normalized normal crack opening displacements are anti-symmetric about x_2 - axis which means that there is crack closure at either tip of the crack for the pure uniform shear loading on crack surfaces. Normalized tangential crack opening displacements are symmetric about x_2 - axis. Normalized normal crack opening displacement decreases in absolute values as βc increases from negative to positive whereas normalized tangential crack opening displacement increases as βc increases from negative to positive for all examined values of κ_0 , δ_0^4 and ν_0 . Normalized tangential crack opening displacement and absolute values of

normalized normal crack opening displacement are decreasing functions of κ_0 , δ_0^4 and ν_0 .

4.2.3 Periodic Embedded Cracking Problem Considering Uniform Normal Stress on Crack Surfaces

In this subsection, the problem described in Chapter 2 is investigated computationally considering embedded periodic cracks in the orthotropic FGM coating rather than the single embedded crack. The illustration of the problem is shown in Figure-4.2.3.1. The orthotropic FGM coating is perfectly bonded to homogeneous substrate through the homogeneous bond-coat. The periodic cracks of length $2c$ and spacing W are located parallel to the boundaries along $x_2 = 0$ line. Distance from the crack line to the upper and lower surfaces of the coating is h_1 and h_2 , respectively. Thickness of the bond-coat is h_3 and thickness of the substrate is h_4 . Principal axes of orthotropy are along x_1 - and x_2 - directions in each medium. The material property distributions of the orthotropic FGM coating, homogeneous bond-coat and homogeneous substrate are as defined by Eq.(2.2.3), Eq.(2.2.4) and Eq.(2.2.5), respectively.

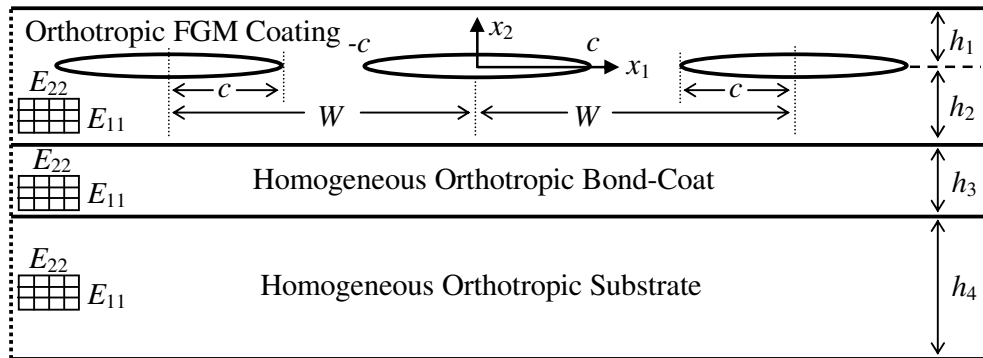


Figure-4.2.3.1 Illustration of the periodic embedded cracking problem.

Assuming that $p(x_1)$ is the normal traction, the surfaces of all the cracks are subjected to the following boundary condition:

$$\sigma_{22}(x_1, 0) = -p(x_1) = -\sigma_0 \quad (4.2.3.1)$$

The finite element model of the problem is created considering a unit cell. The applied symmetry and periodicity conditions [126] are depicted in Figure-4.2.3.2. To satisfy the symmetry about x_2 -axis, the horizontal displacement component u_1 is fixed as zero at $x_1 = 0$. Since the structure is infinitely long in x_1 direction, the lines $x_1 = \pm(n/2)W$, ($n = 1, 2, 3, \dots$), are the symmetry lines and they should be free to undergo both rigid body translation and rotation [126]. Satisfaction of this condition is achieved by using a rigid block in contact with the unit cell at $x_1 = W/2$ and creating a set of coupling between the horizontal displacement components of the coinciding nodes of the unit cell and the rigid block [126].

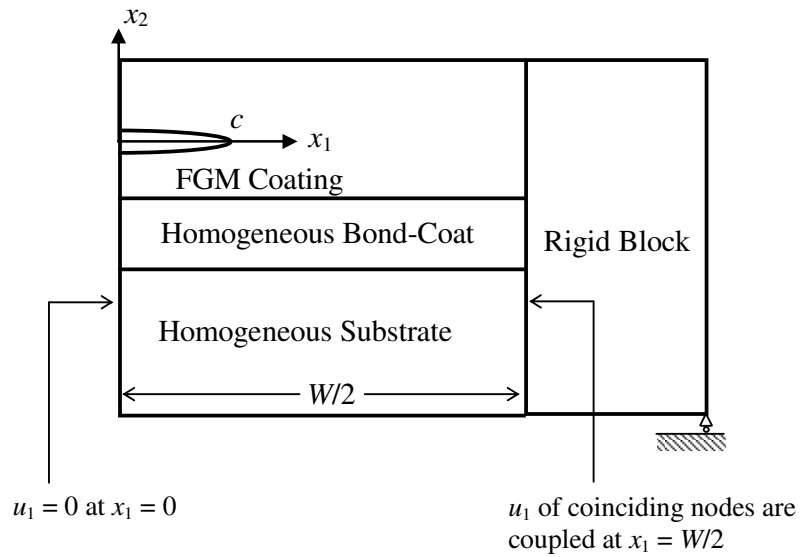


Figure-4.2.3.2 Applied symmetry and periodicity conditions on the unit cell.

Taking $E_0 \exp(-\beta h_2) = E_3 = E_4/1.5$, $\nu_0 = \nu_3 = 0.25$, $\nu_4 = 0.3$, $\kappa_0 = \kappa_3 = 2$, $\kappa_4 = 1$, $\delta_0^4 = \delta_3^4 = 2$, $\delta_4^4 = 1$ and $2h_1 = 2h_2 = 2h_3 = h_4/2 = c$, the effects of the relative crack length c/W on normalized mode I and mode II stress intensity factors and normalized energy release rate are shown in Figure-4.2.3.3, Figure-4.2.3.4 and Figure-4.2.3.5, respectively, for various values of material nonhomogeneity constant. In these figures, examined values of c/W change from 0.02 to 0.45.

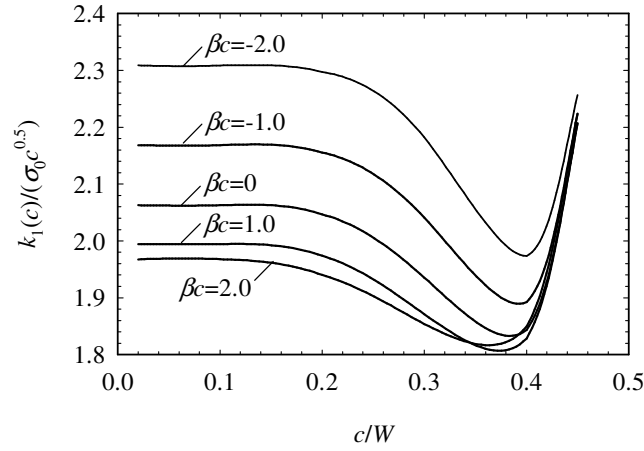


Figure-4.2.3.3 Normalized mode I stress intensity factor versus c/W and nonhomogeneity constant βc , $E_0 \exp(-\beta h_2) = E_3 = E_4/1.5$, $\nu_0 = \nu_3 = 0.25$, $\nu_4 = 0.3$, $\kappa_0 = \kappa_3 = 2$, $\kappa_4 = 1$, $\delta_0^4 = \delta_3^4 = 2$, $\delta_4^4 = 1$, $2h_2 = 2h_3 = h_4/2 = c$, $p(x_1) = \sigma_0$.

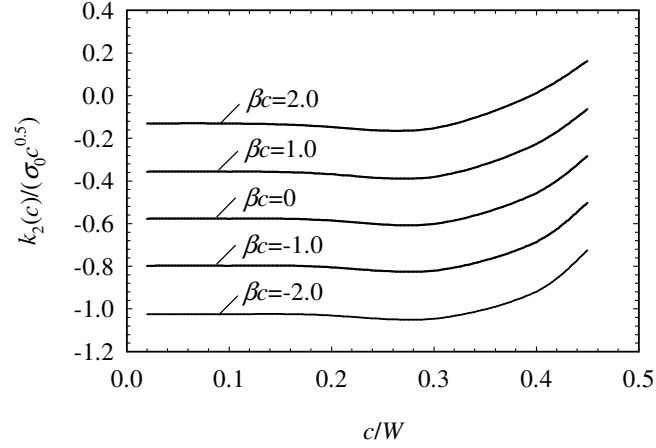


Figure-4.2.3.4 Normalized mode II stress intensity factor versus c/W and nonhomogeneity constant βc , $E_0 \exp(-\beta h_2) = E_3 = E_4/1.5$, $\nu_0 = \nu_3 = 0.25$, $\nu_4 = 0.3$, $\kappa_0 = \kappa_3 = 2$, $\kappa_4 = 1$, $\delta_0^4 = \delta_3^4 = 2$, $\delta_4^4 = 1$, $2h_2 = 2h_3 = h_4/2 = c$, $p(x_1) = \sigma_0$.

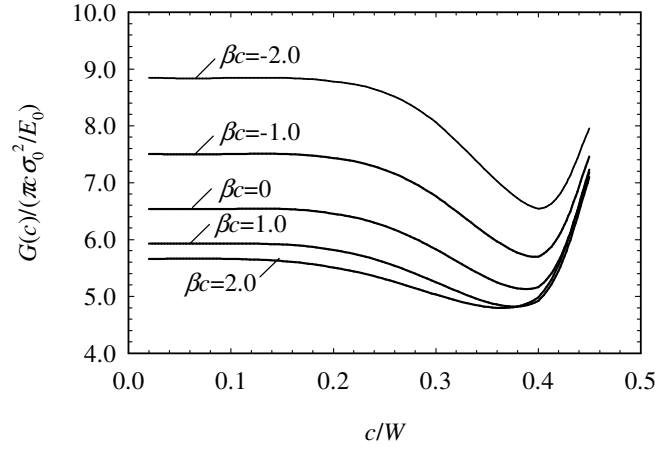


Figure-4.2.3.5 Normalized energy release rate versus c/W and nonhomogeneity constant βc , $E_0 \exp(-\beta h_2) = E_3 = E_4/1.5$, $\nu_0 = \nu_3 = 0.25$, $\nu_4 = 0.3$, $\kappa_0 = \kappa_3 = 2$, $\kappa_4 = 1$, $\delta_0^4 = \delta_3^4 = 2$, $\delta_4^4 = 1$, $2h_2 = 2h_3 = h_4/2 = c$, $p(x_1) = \sigma_0$.

It is seen that mode I and mode II stress intensity factors and energy release rate are almost constant for small values of c/W . As c/W increases further, they first make a minimum and then start increasing significantly. The reason of the reduction in mixed-mode stress intensity factors and energy release rate is the interaction of stress fields developing around the cracks. Similar reductions resulting from the same reason were observed by Cinar and Erdogan [134] for two collinear cracks in an orthotropic homogeneous strip and by Dag et al. [122] for periodic interface cracks between an orthotropic FGM coating and orthotropic homogeneous substrate. It is also seen that the influence of nonhomogeneity constant βc on the mode I stress intensity factor and energy release rate becomes less noticeable for large values of c/W .

The deformed shape of the unit cell is shown in Figure-4.2.3.6 for $c/W = 0.3$ and $\beta c = 1.0$.

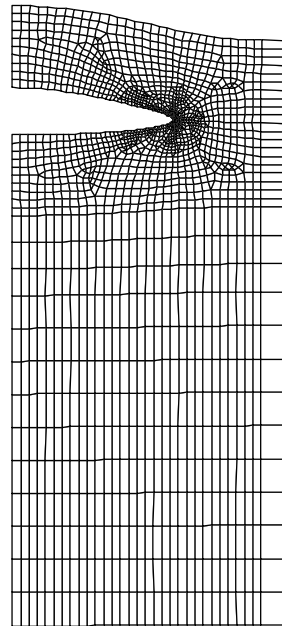


Figure-4.2.3.6 Deformed shape of the unit cell for $c/W = 0.3$ and $\beta c = 1.0$.

CHAPTER 5

COMPUTATIONAL SOLUTION FOR THE EMBEDDED CRACK PROBLEMS IN AN ORTHOTROPIC FGM COATING UNDER THERMAL LOADING

5.1 Description of the Problem

In this chapter, fracture behavior of an orthotropic FGM coating containing a single embedded crack or periodic embedded cracks is analyzed computationally under thermal loading assuming the plane stress state. The problem is illustrated in Figure-5.1.1 for the case of single embedded crack and in Figure-5.1.2 for the case of periodic cracks. The orthotropic FGM coating is perfectly bonded to a homogeneous isotropic substrate through a homogeneous isotropic bond-coat. Principal axes of orthotropy are along x_1 - and x_2 - directions in the FGM coating. The embedded cracks of length $2c$ lie along $x_2 = 0$ line. Distance from the crack line to the upper and lower surfaces of the coating is h_1 and h_2 , respectively. Thickness of the bond-coat is h_3 and thickness of the substrate is h_4 . The structure is infinitely long in x_1 - direction. The crack surfaces are considered to be completely insulated. Top and bottom surfaces of the structure are subjected to uniform constant temperatures T_1 and T_2 , respectively. The reference temperature is denoted by T_0 . The material properties are continuous in each medium. At the interface between the coating and the bond-coat, material properties are taken to be continuous with discontinuous derivatives.

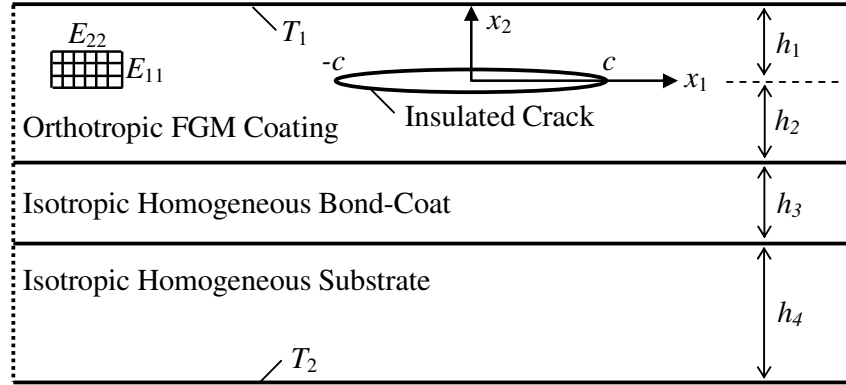


Figure-5.1.1 Illustration of the problem for the single embedded crack.

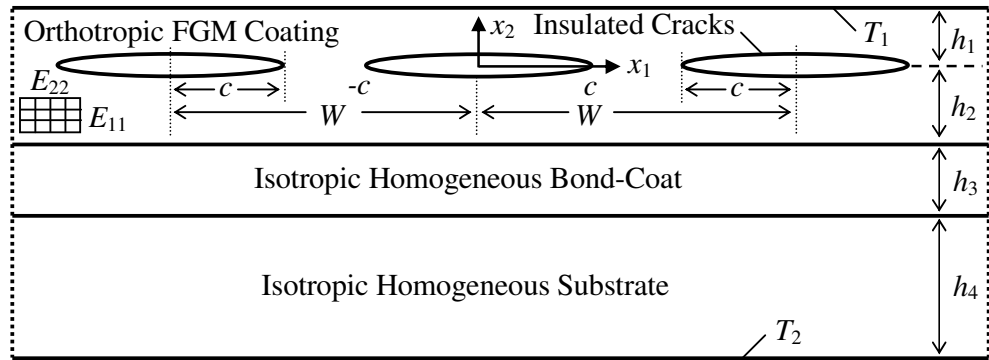


Figure-5.1.2 Illustration of the problem for the periodic embedded cracks.

Material property variation in the FGM coating is in x_2 - direction and defined as follows:

$$\begin{bmatrix} E_{11}(x_2) \\ E_{22}(x_2) \\ G_{12}(x_2) \\ \nu_{12}(x_2) \end{bmatrix} = \begin{bmatrix} E^{BC} \\ E^{BC} \\ G^{BC} \\ \nu^{BC} \end{bmatrix} + \left(\begin{bmatrix} E_{11}^{CTS} \\ E_{22}^{CTS} \\ G_{12}^{CTS} \\ \nu_{12}^{CTS} \end{bmatrix} - \begin{bmatrix} E^{BC} \\ E^{BC} \\ G^{BC} \\ \nu^{BC} \end{bmatrix} \right) \left(\frac{x_2 + h_2}{h_1 + h_2} \right)^p \quad (5.1.1a)$$

$$\begin{bmatrix} \alpha_{11}(x_2) \\ \alpha_{22}(x_2) \end{bmatrix} = \begin{bmatrix} \alpha^{BC} \\ \alpha^{BC} \end{bmatrix} + \left(\begin{bmatrix} \alpha_{11}^{CTS} \\ \alpha_{22}^{CTS} \end{bmatrix} - \begin{bmatrix} \alpha^{BC} \\ \alpha^{BC} \end{bmatrix} \right) \left(\frac{x_2 + h_2}{h_1 + h_2} \right)^q \quad (5.1.1b)$$

$$\begin{bmatrix} k_{11}(x_2) \\ k_{22}(x_2) \end{bmatrix} = \begin{bmatrix} k^{BC} \\ k^{BC} \end{bmatrix} + \left(\begin{bmatrix} k_{11}^{CTS} \\ k_{22}^{CTS} \end{bmatrix} - \begin{bmatrix} k^{BC} \\ k^{BC} \end{bmatrix} \right) \left(\frac{x_2 + h_2}{h_1 + h_2} \right)^r \quad (5.1.1c)$$

where E denotes the modulus of elasticity, G denotes the shear modulus, ν denotes the Poisson's ratio, α denotes the thermal expansion coefficient and k denotes the heat conductivity. Subscripts 11 and 22 denote the directions with respect to x_1 - x_2 coordinate system. Superscripts BC and CTS stand for bond-coat material and coating top surface material, respectively. The nonhomogeneity parameter controlling the elastic properties is denoted by p , the nonhomogeneity parameter controlling the thermal expansion coefficients is denoted by q and the nonhomogeneity parameter controlling the heat conductivities is denoted by r .

5.2 Numerical Results

In this section, numerical results for the fracture parameters are presented considering single and periodic embedded crack problems under thermal loading.

All of the results are obtained assuming that the top surface of the coating is 100% orthotropic alumina, the bond-coat is nickel-chromium-aluminum-zirconium and the substrate is nickel. The elastic properties of alumina are taken as $E_{11} = 90.43$ GPa, $E_{22} = 116.36$ GPa, $G_{12} = 38.21$ GPa and $\nu_{21} = 0.28$ [126, 135]. The heat conductivities of alumina are taken as $k_{11} = 21.25$ W/(m°C) and $k_{22} = 29.82$ W/(m°C) [126, 136]. The thermal expansion coefficients of alumina are assumed to be such that $\alpha_{11} = 8.0 \times 10^{-6}$ (°C)⁻¹ and $\alpha_{22} = 7.5 \times 10^{-6}$ (°C)⁻¹ [126]. The material properties of nickel-chromium-aluminum-zirconium are taken as $E = 137.9$ GPa,

$\nu = 0.27$, $k = 25 \text{ W/(m}^\circ\text{C)}$, $\alpha = 15.16 \times 10^{-6} \text{ (}^\circ\text{C)}^{-1}$ [137]. Finally, the material properties of nickel are taken as $E = 204 \text{ GPa}$, $\nu = 0.31$, $k = 70 \text{ W/(m}^\circ\text{C)}$, $\alpha = 13.3 \times 10^{-6} \text{ (}^\circ\text{C)}^{-1}$ [126, 138].

In all of the examined cases, the top and the bottom surfaces of the structure are subjected to the constant uniform temperatures such that $T(x_1, h_1) = T_1 = 10T_0$ and $T(x_1, -(h_2 + h_3 + h_4)) = T_2 = T_0$ for $|x_1| < \infty$. Geometric dimensions are taken as $2h_1 = 2h_2 = 2h_3 = h_4/2 = c$.

The presented results consist of normalized mixed-mode stress intensity factors. Definitions of normalized mode I and mode II stress intensity factors are given as follows, respectively.

$$k_{1n} = \frac{k_1}{\left(E_{22}^{CTS} \alpha_{22}^{CTS} T_0 \sqrt{\pi c}\right)} \quad (5.2.1a)$$

$$k_{2n} = \frac{k_2}{\left(E_{22}^{CTS} \alpha_{22}^{CTS} T_0 \sqrt{\pi c}\right)} \quad (5.2.1b)$$

5.2.1 Single Embedded Crack Problem under Thermal Loading

In this subsection, the effect of material nonhomogeneity on mixed-mode stress intensity factors is investigated considering a single embedded crack problem under thermal loading.

The finite element model of the problem is created using half of the structure with appropriate symmetry boundary conditions shown in Figure-5.2.1.1. The structure is taken sufficiently long to satisfy the infinite length assumption in x_1 - direction.

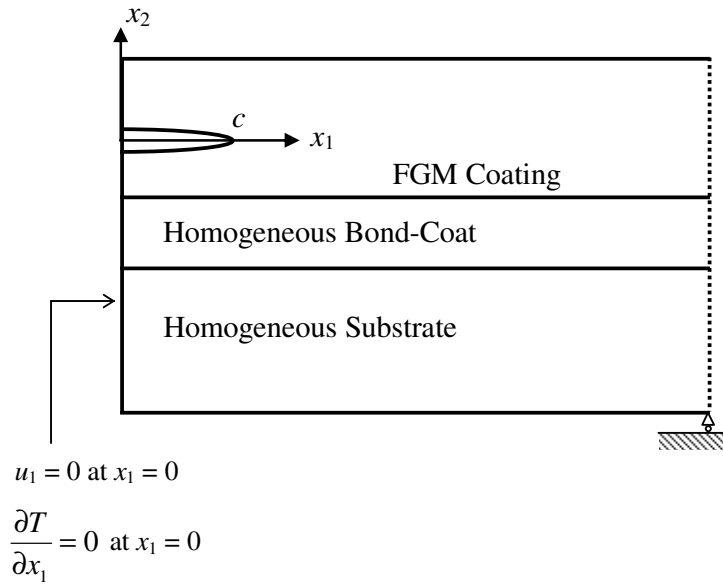


Figure-5.2.1.1 Applied symmetry conditions.

The insulation of the crack surfaces is imposed to the finite element model by fixing the heat flux as zero at the crack surfaces such that:

$$\frac{\partial T}{\partial x_2} = 0, 0 < x_1 < c, x_2 = 0^\pm \quad (5.2.1.1)$$

The constant uniform temperatures at the top and bottom surfaces of the structure $T_1 = 10T_0$ and $T_2 = T_0$, respectively, are applied as the thermal loading.

The normalized mode I and mode II stress intensity factors are plotted with respect to nonhomogeneity parameter p for various values of nonhomogeneity parameter q in Figure-5.2.1.2 and Figure-5.2.1.3 and for various values of nonhomogeneity parameter r in Figure-5.2.1.4 and Figure-5.2.1.5, respectively.

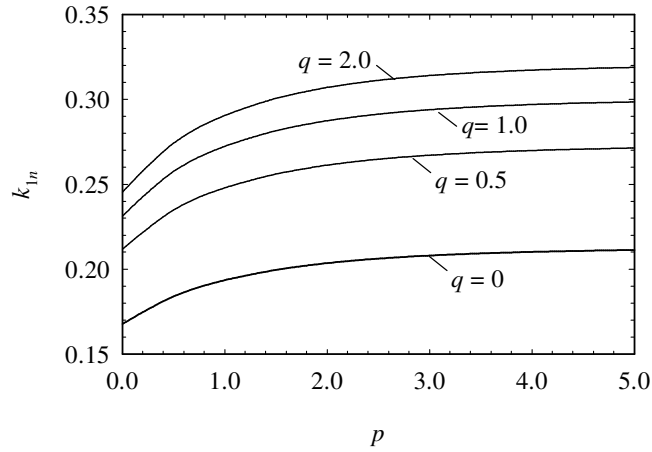


Figure-5.2.1.2 Normalized mode I stress intensity factor versus nonhomogeneity parameters p and q under steady state thermal loading, $r = 1.0$, $2h_1 = 2h_2 = 2h_3 = h_4/2 = c$, $T_1 = 10T_0$ and $T_2 = T_0$.

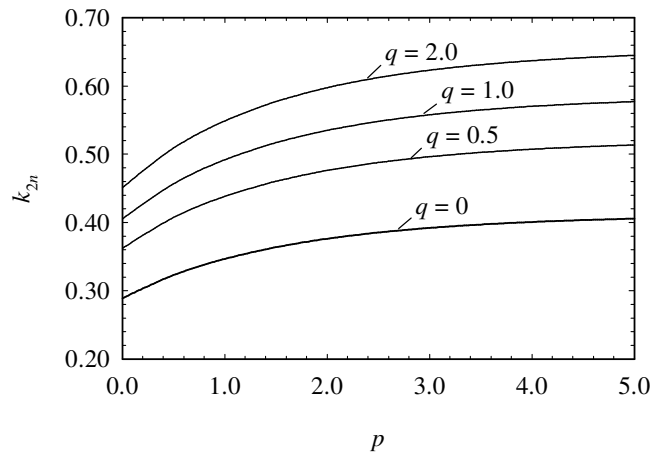


Figure-5.2.1.3 Normalized mode II stress intensity factor versus nonhomogeneity parameters p and q under steady state thermal loading, $r = 1.0$, $2h_1 = 2h_2 = 2h_3 = h_4/2 = c$, $T_1 = 10T_0$ and $T_2 = T_0$.

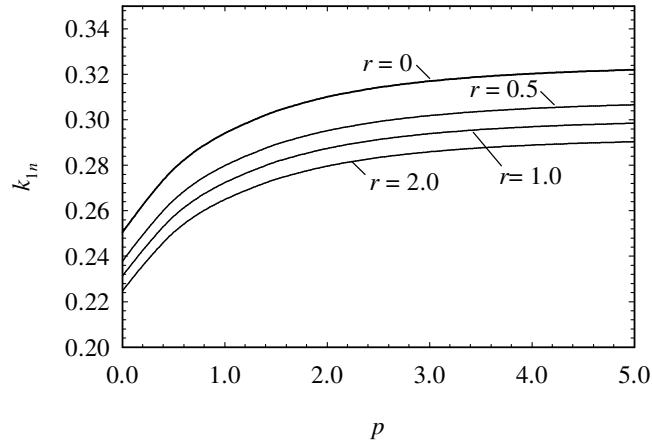


Figure-5.2.1.4 Normalized mode I stress intensity factor versus nonhomogeneity parameters p and r under steady state thermal loading, $q = 1.0$, $2h_1 = 2h_2 = 2h_3 = h_4/2 = c$, $T_1 = 10T_0$ and $T_2 = T_0$.

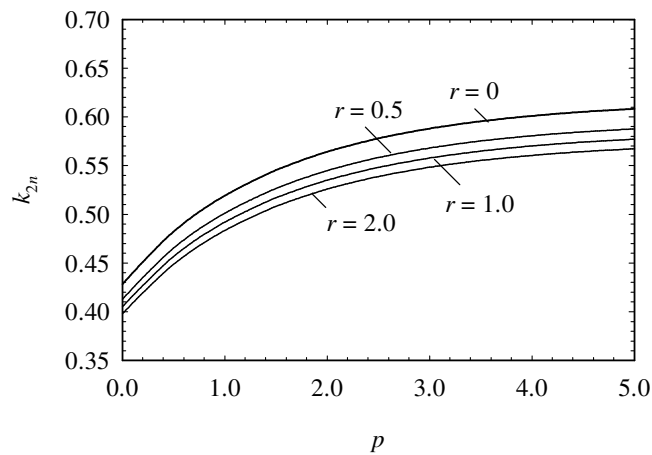


Figure-5.2.1.5 Normalized mode II stress intensity factor versus nonhomogeneity parameters p and r under steady state thermal loading, $q = 1.0$, $2h_1 = 2h_2 = 2h_3 = h_4/2 = c$, $T_1 = 10T_0$ and $T_2 = T_0$.

Under the applied loading condition, the mode II stress intensity factor is found to be numerically larger than the mode I stress intensity factor. It is shown that the

increase in both nonhomogeneity parameters p and q increases the mixed-mode stress intensity factors. It is observed that mode I and mode II stress intensity factors are decreasing functions of nonhomogeneity parameter r for all interested values of p . When p , q and r have small values, the effect of their variation on mixed-mode stress intensity factors is more significant.

The deformed shape of the structure is shown in Figure-5.2.1.6 for $p = q = r = 1.0$.

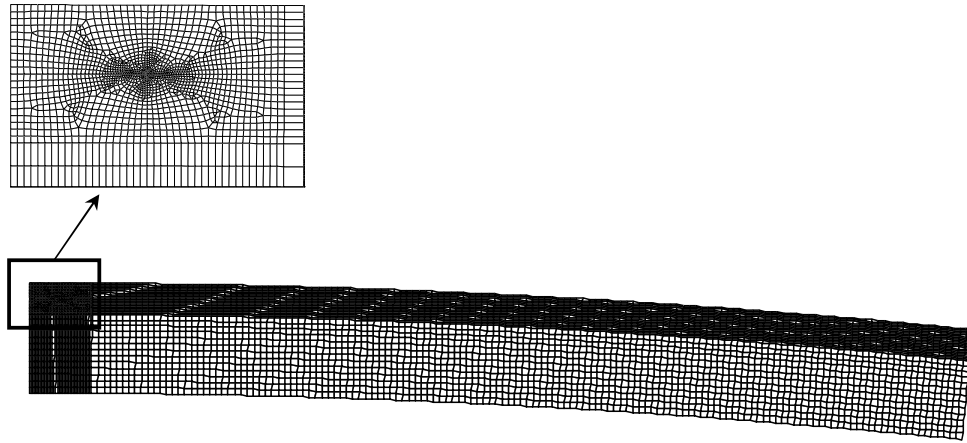


Figure-5.2.1.6 Deformed shape of the structure for $p = q = r = 1.0$.

5.2.2 Periodic Embedded Cracking Problem under Thermal Loading

In this subsection, fracture behavior of the orthotropic FGM coating is investigated considering the periodic embedded cracks of spacing W as shown in Figure-5.1.2.

The finite element model of the problem is created considering a unit cell. The applied symmetry and periodicity conditions [126] are depicted in Figure-5.2.2.1. Since the x_2 - axis is the symmetry axis, the heat flux and the horizontal displacement component u_1 is fixed as zero at $x_1 = 0$ line. Since the structure is

infinitely long in x_1 direction, the lines $x_1 = \pm(n/2)W$, ($n = 1, 2, 3, \dots$), are also symmetry lines [126]. Therefore, the heat flux is fixed as zero at $x_1 = W/2$ line and the structure is allowed to be free to undergo both rigid body translation and rotation at $x_1 = W/2$ [126]. The free rigid body translation and rotation condition is achieved by using a rigid block in contact with the unit cell at $x_1 = W/2$ and creating a set of coupling between the horizontal displacement components of the coinciding nodes of the unit cell and the rigid block [126].

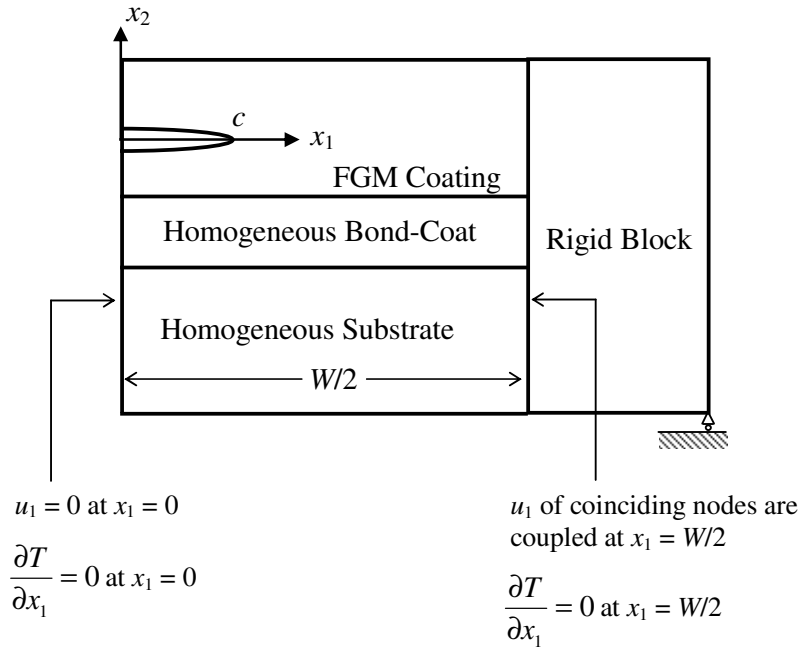


Figure-5.2.2.1 Applied symmetry and periodicity conditions on the unit cell.

The insulation of the crack surfaces is imposed to the finite element model by fixing the heat flux as zero at the crack surfaces such that:

$$\frac{\partial T}{\partial x_2} = 0, \quad 0 < x_1 < c, \quad x_2 = 0^\pm \quad (5.2.2.1)$$

The constant uniform temperatures at the top and bottom surfaces of the structure $T_1 = 10T_0$ and $T_2 = T_0$, respectively, are applied as the thermal loading.

The normalized mode I and mode II stress intensity factors are plotted with respect to the relative crack length c/W for various values of nonhomogeneity parameter p in Figure-5.2.2.2 and Figure-5.2.2.3, for various values of nonhomogeneity parameter q in Figure-5.2.2.4 and Figure-5.2.2.5 and for various values of nonhomogeneity parameter r in Figure-5.2.2.6 and Figure-5.2.2.7, respectively. In these figures, examined values of c/W change from 0.02 to 0.45.

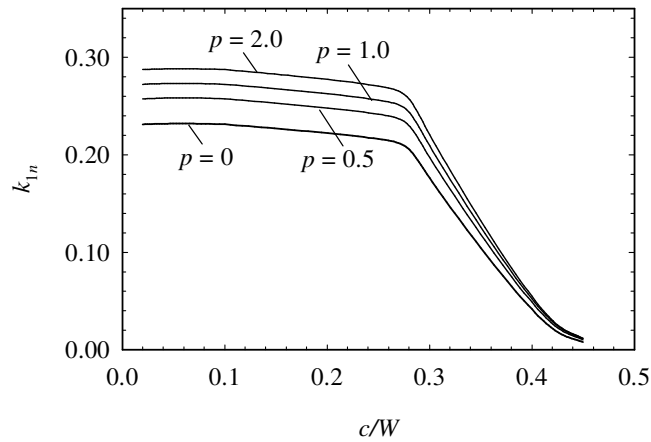


Figure-5.2.2.2 Normalized mode I stress intensity factor versus c/W and the nonhomogeneity parameter p under steady state thermal loading, $q = 1.0$, $r = 1.0$, $2h_1 = 2h_2 = 2h_3 = h_4/2 = c$, $T_1 = 10T_0$ and $T_2 = T_0$.

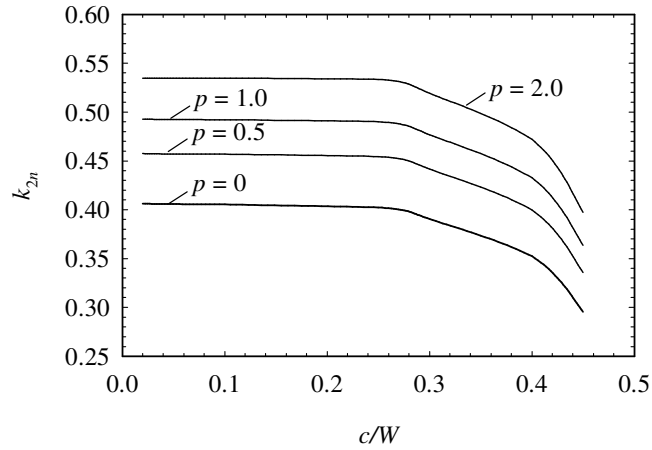


Figure-5.2.2.3 Normalized mode II stress intensity factor versus c/W and the nonhomogeneity parameter p under steady state thermal loading, $q = 1.0$, $r = 1.0$
 $2h_1 = 2h_2 = 2h_3 = h_4/2 = c$, $T_1 = 10T_0$ and $T_2 = T_0$.

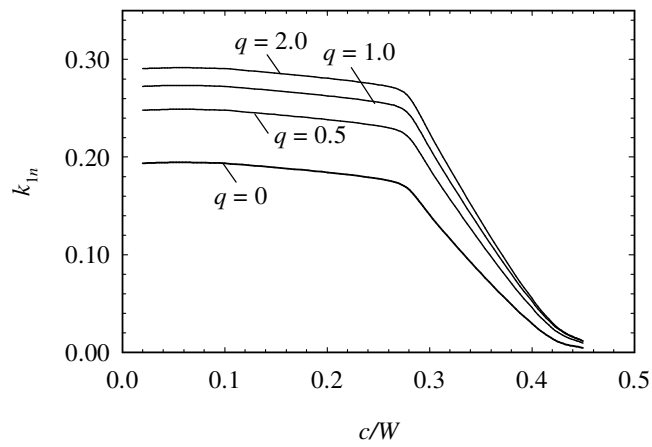


Figure-5.2.2.4 Normalized mode I stress intensity factor versus c/W and the nonhomogeneity parameter q under steady state thermal loading, $p = 1.0$, $r = 1.0$
 $2h_1 = 2h_2 = 2h_3 = h_4/2 = c$, $T_1 = 10T_0$ and $T_2 = T_0$.

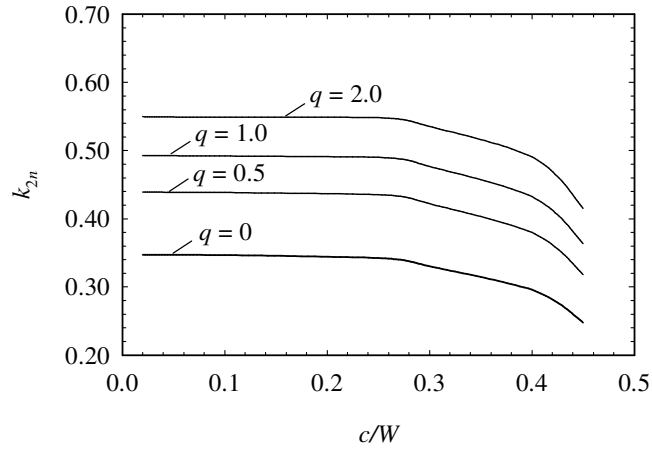


Figure-5.2.2.5 Normalized mode II stress intensity factor versus c/W and the nonhomogeneity parameter q under steady state thermal loading, $p = 1.0$, $r = 1.0$, $2h_1 = 2h_2 = 2h_3 = h_4/2 = c$, $T_1 = 10T_0$ and $T_2 = T_0$.

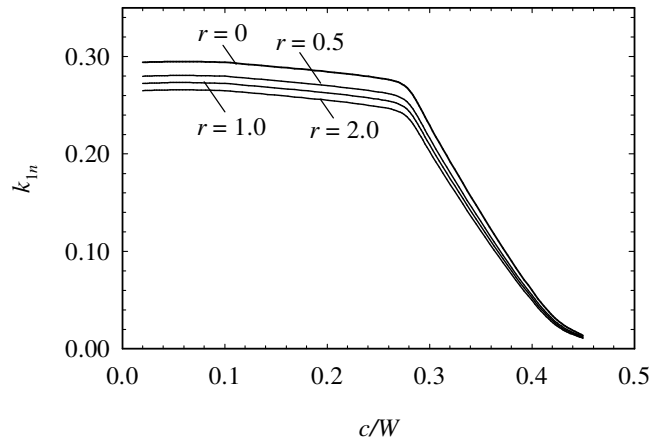


Figure-5.2.2.6 Normalized mode I stress intensity factor versus c/W and the nonhomogeneity parameter r under steady state thermal loading, $p = 1.0$, $q = 1.0$, $2h_1 = 2h_2 = 2h_3 = h_4/2 = c$, $T_1 = 10T_0$ and $T_2 = T_0$.

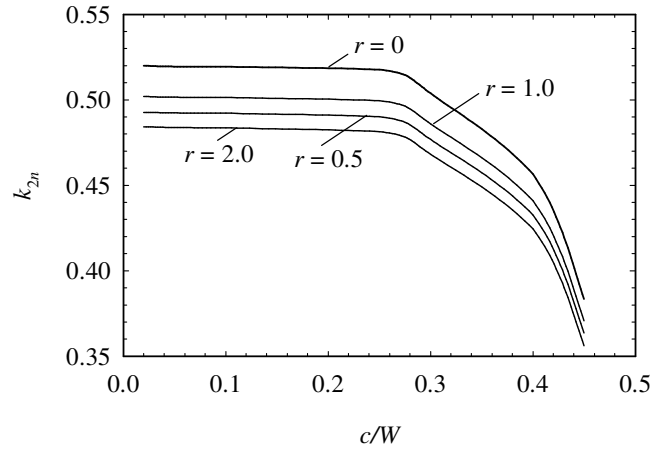


Figure-5.2.2.7 Normalized mode II stress intensity factor versus c/W and the nonhomogeneity parameter r under steady state thermal loading, $p = 1.0$, $q = 1.0$, $2h_1 = 2h_2 = 2h_3 = h_4/2 = c$, $T_1 = 10T_0$ and $T_2 = T_0$.

It is seen that mode I and mode II stress intensity factors vary very little until $c/W \cong 0.28$ and then make sharp decreases with increasing c/W for all examined values of nonhomogeneity parameters p , q and r .

The deformed shape of the unit cell is shown in Figure-5.2.2.8 for $c/W = 0.3$ and $p = q = r = 1.0$.

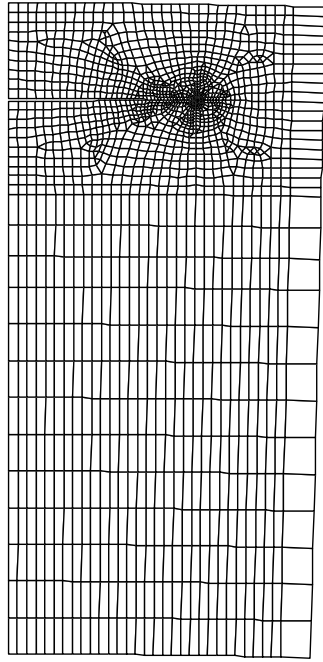


Figure-5.2.2.8 Deformed shape of the unit cell for $c/W = 0.3$ and $p = q = r = 1.0$.

CHAPTER 6

CONCLUSIONS AND FUTURE STUDIES

6.1 Conclusions

In certain applications, thermal barrier coatings designed for high temperature environments are bonded to the substrate through a bond-coat layer that provides oxidation resistance [137].

In this study, it is aimed to investigate the fracture behavior of an orthotropic FGM coating bonded to a homogeneous substrate through a homogeneous bond-coat considering embedded cracking problems under crack surface tractions or steady state thermal loading. Both analytical and computational approaches are utilized to obtain the solutions.

In Chapter 2, a single embedded crack in an orthotropic FGM coating bonded to a homogeneous orthotropic substrate through a homogeneous orthotropic bond-coat is investigated analytically considering the uniform normal or uniform shear stresses on crack surfaces. It is assumed that the length of the structure is infinite. For the FGM coating, the gradation in the thickness direction is represented by the effective stiffness term in an exponential form and effective Poisson's ratio, stiffness ratio and shear parameter is kept constant. The crack lies perpendicular to the thickness direction and principal axes of orthotropy are considered as parallel and perpendicular to the crack line. Governing equations for the coating, bond-coat and substrate are derived using the equilibrium and the stress-displacement equations. Then a homogeneous ordinary differential equation system is obtained

for each medium applying Fourier transformations to the corresponding governing equations. After satisfying the continuity and boundary conditions, a couple of singular integral equations are derived. These singular integral equations are solved using an expansion-collocation technique. Then, the expressions for the mixed-mode stress intensity factors, energy release rate and crack opening displacements are obtained.

In this study, the adopted computational approach employs the finite element method in conjunction with the displacement correlation technique (DCT). In Chapter 3, the used computational approach is described and the displacement correlation technique is reviewed. Utilization of the computational approach provides the solutions for the analytically untractable problems without the restrictive assumptions.

In Chapter 4, after verifying the analytical study performed in Chapter 2, some numerical results based on analytical and/or computational methods are given considering the single or periodic embedded cracking problems under crack surface tractions.

In order to verify the derived analytical formulation, results of the present study is compared with the analytical results given by Cinar and Erdogan [134] for an embedded crack in an orthotropic homogeneous strip and it is observed that the two studies agree with each other quite well.

Then, the numerical results for the single embedded crack problem are presented considering the pure uniform normal stress on crack surfaces. Both analytical and computational solutions are given for this problem to assess the computational method. These results show how the material nonhomogeneity constant of the coating βc , the relative coating thickness above the crack line h_1/c , the relative thickness of the bond-coat h_3/c , shear parameter of the coating κ_0 , stiffness ratio

of the coating δ_0^4 and effective Poisson's ratio of the coating ν_0 affects the fracture related parameters. It is assumed that material properties are continuous at the coating and bond-coat interface with discontinuous derivatives and the homogeneous substrate material is isotropic. While examining the effects of h_1/c and h_3/c on fracture parameters, the dimensions of the structure are taken as $2h_2 = 2h_3 = h_4/2 = c$ and $h_1/0.95 = h_2/0.05 = h_4/2 = c$, respectively. To investigate the effects of κ_0 , δ_0^4 and ν_0 on the fracture behavior of the structure, the geometric dimensions are taken as $2h_1 = 2h_2 = 2h_3 = h_4/2 = c$.

It is observed that mode I stress intensity factor of the single embedded crack is numerically larger than the mode II stress intensity factor when the crack surfaces are under the pure uniform normal stress.

Considering the uniform normal stress on the surfaces of the single embedded crack, the following concluding remarks can be stated:

- Mode I stress intensity factors and energy release rates are decreasing functions of material nonhomogeneity constant βc for all examined values of h_1/c , h_3/c , κ_0 , δ_0^4 and ν_0 . Absolute values of mode II stress intensity factors are also decreasing functions of material nonhomogeneity constant βc for all examined values of h_3/c , κ_0 , δ_0^4 , ν_0 and small values of h_1/c . For larger values of h_1/c , absolute values of mode II stress intensity factors first decrease and then increase with increasing βc from -2.0 to 2.0 . As the material nonhomogeneity constant βc decreases from 2.0 to -2.0 , the effect of its variation on mode I stress intensity factor and energy release rate becomes more significant. The influence of variation in βc on mode I stress intensity factor is more noticeable for large values of h_1/c due to the

dependence of effective stiffness of coating on both the nonhomogeneity parameter and the distance from the crack line.

- Mode I stress intensity factors and energy release rates first decrease and then become almost constant with increasing h_1/c for all considered values of βc . Absolute values of mode II stress intensity factors also show an almost constant behavior for large values of h_1/c .
- Mode I stress intensity factors show first a decreasing and then an increasing trend with increasing κ_0 for the examined small values of βc . Mode II stress intensity factors decrease in absolute values with increasing κ_0 for the negative large values of βc and become almost insensitive to the variation in κ_0 for positive large values of βc . The energy release rates are increasing functions of κ_0 for all considered values of βc .
- Mode I stress intensity factors and absolute values of mode II stress intensity factors are decreasing functions of δ_0^4 for all considered values of βc . As δ_0^4 becomes smaller, the effect of its variation on mode I stress intensity factor seems to be more significant. The energy release rate first decreases and then becomes almost constant with increasing δ_0^4 for all examined values of βc .
- The effect of variation in ν_0 on mode I and mode II stress intensity factors depends on the degree of material nonhomogeneity. Mode I stress intensity factor decreases and absolute value of mode II stress intensity factor increases with increasing ν_0 for the examined positive values of βc . On the other hand, mode I stress intensity factor increases and absolute value of

mode II stress intensity factor decreases with increasing ν_0 for the considered negative values of βc . It is observed that the influence of the variation in ν_0 on the energy release rate is relatively small for all examined values of βc .

- Mode I stress intensity factor and energy release rate increase and the absolute value of the mode II stress intensity factor decreases slightly with increasing relative bond-coat thickness h_3/c for all considered values of βc .
- The normalized normal crack opening displacement and absolute value of the normalized tangential crack opening displacement decrease with increasing examined values of βc , κ_0 , δ_0^4 and ν_0 . The normal crack opening displacement is symmetric and tangential crack opening displacement is anti-symmetric with respect to the center line of the structure at mid-length.

When the presented results of analytical and computational solutions are compared with each other, a good agreement is observed.

Then, the numerical results for the single embedded crack problem are presented based on the analytical method considering the pure uniform shear stress on crack surfaces. These results show the effects of the material nonhomogeneity constant of the coating βc , shear parameter of the coating κ_0 , stiffness ratio of the coating δ_0^4 and effective Poisson's ratio of the coating ν_0 on the fracture parameters. It is assumed that material properties are continuous at the coating and bond-coat interface with discontinuous derivatives and the homogeneous substrate material is

isotropic. For all of the examined cases, geometric dimensions of the structure are taken as $2h_1 = 2h_2 = 2h_3 = h_4/2 = c$.

When the crack surfaces are under the uniform shear traction, it is observed that the crack is always closed at either of its tips which requires the reformulation of the problem by taking into account the crack closure condition. For this reason, results for the mixed-mode stress intensity factors based on present study considering the uniform shear traction on crack surfaces are only applicable in superposition applications if the resultant mode I stress intensity factor is positive at both of the crack tips.

It is also observed that mode II stress intensity factor of the single embedded crack is the numerically larger stress intensity factor when crack surfaces are under the uniform shear stress.

Considering the uniform shear stress on the surfaces of the single embedded crack, the following concluding remarks can be stated:

- Mode I stress intensity factor at the open tip of the crack is decreasing function of βc and mode II stress intensity factor is increasing function of βc for all examined values of κ_0 , δ_0^4 and ν_0 .
- Mode I stress intensity factor at the open tip of the crack decreases considerably with increasing κ_0 for small values of βc and becomes almost independent of κ_0 for large values of βc . Mode II stress intensity factor decreases with increasing κ_0 for all examined values of βc . When κ_0 has small values, the effect of its variation on mode II stress intensity factor is more significant.

- Mode I stress intensity factor obtained at the open tip of the crack and mode II stress intensity factor are decreasing functions of δ_0^4 for all considered values of βc . The effect of variation in δ_0^4 on mode I and mode II stress intensity factors is less significant when δ_0^4 has large values.
- Mode I stress intensity factor obtained at the open tip of the crack behaves as a decreasing function of ν_0 for the considered negative values of βc and an increasing function of ν_0 for the considered positive values of βc . Mode II stress intensity factor shows the opposite trend.
- Normalized normal crack opening displacement is anti-symmetric and normalized tangential crack opening displacement is symmetric with respect to the center line at the mid-length of the structure. The anti-symmetry in normalized normal crack opening displacement means that a crack closure condition is experienced by the structure.

Then, using the computational approach, embedded periodic cracking problem is investigated in the orthotropic FGM coating bonded to a homogeneous isotropic substrate through a homogeneous bond-coat considering uniform normal stress on the crack surfaces. It is assumed that the cracks of length $2c$ are located parallel to the boundaries with spacing W in the structure of infinite length. The directions for the principal axes of orthotropy and material property distribution in each layer are taken the same as the ones for previously investigated single embedded crack problem. The presented numerical results show the effects of crack periodicity and material nonhomogeneity on the fracture parameters. The geometric dimensions of the structure are taken as $2h_1 = 2h_2 = 2h_3 = h_4/2 = c$.

It is observed that mode I and mode II stress intensity factors and energy release rate of the periodic cracks under the uniform normal stress are almost constant if

W is relatively large with respect to c . As W decreases relative to c , mixed-mode stress intensity factors and energy release rate first make a minimum and then start increasing significantly. The reduction in these fracture parameters results from the interaction of stress fields developing around the cracks. Similar behavior due to the same reason was observed also by Cinar and Erdogan [134] for two collinear cracks in an orthotropic homogeneous strip and by Dag et al. [122] for periodic interface cracks between an orthotropic FGM coating and orthotropic homogeneous substrate. In the examined periodic cracking cases, the influence of nonhomogeneity constant βc on the mode I stress intensity factor and energy release rate is insignificant for relatively small values of W with respect to c .

In Chapter 5, single and periodic embedded cracking problems in an orthotropic FGM coating are investigated computationally under steady state thermal loading assuming the plane stress state. The orthotropic FGM coating is bonded to a homogeneous isotropic substrate through a homogeneous isotropic bond-coat considering an infinite length. The embedded cracks of length $2c$ are located parallel to the boundaries in both of the single and periodic cracking problems. In periodic cracking case, the spacing between the cracks is equal to W . The top and the bottom surfaces of the structure are subjected to uniform constant temperatures and crack surfaces are insulated. The material property gradation in the FGM coating is represented in a power function form with separate nonhomogeneity parameters p , q and r for elastic properties, thermal expansion coefficients and heat conductivities, respectively. For the numerical results, the top surface of the coating is taken as 100% orthotropic alumina, the bond-coat is taken as nickel-chromium-aluminum-zirconium and the substrate is taken as nickel. It is assumed that the material properties at the coating and bond-coat interface are continuous with discontinuous derivatives. The geometric dimensions of the structure are taken as $2h_1 = 2h_2 = 2h_3 = h_4/2 = c$.

According to the presented numerical results for the single embedded crack problem under thermal loading, the mode II stress intensity factor is numerically larger than the mode I stress intensity factor. The mixed-mode stress intensity factors are increasing functions of nonhomogeneity parameters p and q and decreasing functions of nonhomogeneity parameter r . When p , q and r have small values, the effects of their variation on mixed-mode stress intensity factors are found to be more significant.

According to the presented numerical results for the periodic embedded cracking problem under thermal loading, the mixed-mode stress intensity factors are almost constant if W is relatively large with respect to c and then make sharp decreases with decreasing W relative to c for all examined values of nonhomogeneity parameters p , q and r .

Using the analytical method developed in this study to examine the fracture behavior of the orthotropic FGM coating bonded to a homogeneous substrate through a homogeneous bond-coat, design optimization of the structure can be made efficiently by applying tractions to the crack surfaces and employing the superposition technique. The adopted computational method is found to agree very well with the analytical method. Using the computational method it is possible to deal with more complex problems related with the orthotropic FGM coatings without restrictive assumptions about the form of gradation profiles and loading condition.

6.2 Future Studies

In this study, the examined embedded cracks in the orthotropic FGM coating are parallel to the boundaries. As a future study, inclined embedded cracks in the orthotropic FGM coating can be investigated.

In this study, the investigated cracks are embedded in the orthotropic FGM coating. The surface cracks in the structure can be considered in the future.

In the future studies, crack propagation analysis of the structure can be performed considering both embedded and surface cracks in the structure.

In this study, the crack closure condition is not taken into account. This condition can be dealt with in the future studies.

The thermal loading condition considered in this study is assumed to be steady state. Transient thermal loading conditions can be studied in the future works using temperature dependent material properties.

REFERENCES

- [1] PINDER, M.-J., ABOUDI, J., GLAESER, A. M. and ARNOLD, S. M., 'Foreword', *Composites Part B: Engineering*, Vol. 28B, pp. iii-v, 1997.
- [2] MORO, A., KURODA, Y. and KUSAKA, K., 'Development Status of the Reusable High-Performance Engines with Functionally Graded Materials', *Acta Astronautica*, Vol. 50, No. 7, pp. 427-432, 2002.
- [3] CETINEL, H., UYULGAN, B., TEKMEK, C., OZDEMIR, I. and CELIK, E., 'Wear Properties of Functionally Gradient Layers on Stainless Steel Substrates for High Temperature Applications', *Surface and Coatings Technology*, Vol. 174-175, pp. 1089-1094, 2003.
- [4] LING, Y.-H., LI, J.-T., GE, C.-C. and BAI, X.-D., 'Fabrication and Evaluation of SiC/Cu Functionally Graded Material Used for Plasma Facing Components in a Fusion Reactor', *Journal of Nuclear Materials*, Vol. 303, pp. 188-195, 2002.
- [5] ERDOGAN, F., 'Fracture Mechanics', *International Journal of Solids and Structures*, Vol. 37, pp. 171-183, 2000.

- [6] SCHULZ, U., PETERS, M., BACH, Fr.-W. and TEGEDER, G., 'Graded Coatings for Thermal, Wear and Corrosion Barriers', *Materials Science and Engineering*, Vol. A362, pp. 61-80, 2003.
- [7] PENDER, D. C., PADTURE, N. P., GIANNAKOPOULOS, A. E. and SURESH, S., 'Gradients in Elastic Modulus for Improved Contact-Damage Resistance. Part I: The Silicon Nitride-Oxynitride Glass System', *Acta Materialia*, Vol. 49, pp. 3255-3262, 2001.
- [8] PENDER, D. C., THOMPSON, S. C., PADTURE, N. P., GIANNAKOPOULOS, A. E. and SURESH, S., 'Gradients in Elastic Modulus for Improved Contact-Damage Resistance. Part II: The Silicon Nitride-Silicon Carbide System', *Acta Materialia*, Vol. 49, pp. 3263-3268, 2001.
- [9] MÜLLER, E., DRAŠAR, Č., SCHILZ, J. and KAYSSER, W., A., 'Functionally Graded Materials for Sensor and Energy Applications', *Materials Science and Engineering*, Vol. A362, pp. 17-39, 2003.
- [10] POMPE, W., WORCH, H., EPPLE, M., FRIESS, W., GELINSKY, M., GREIL, P., HEMPEL, U., SCHARNWEBER, D. and SCHULTE, K., 'Functionally Graded Materials for Biomedical Applications', *Materials Science and Engineering*, Vol. A362, pp. 40-60, 2003.

- [11] KIEBACK, B., NEUBRAND, A. and RIEDEL, H., 'Processing Techniques for Functionally Graded Materials', *Materials Science and Engineering*, Vol. A362, pp. 81-105, 2003.
- [12] KHOR, K. A. and GU, Y. W., 'Thermal Properties of Plasma-Sprayed Functionally Graded Thermal Barrier Coatings', *Thin Solid Films*, Vol. 372, pp. 104-113, 2000.
- [13] KHOR, K. A. and GU, Y. W., 'Effects of Residual Stress on the Performance of Plasma Sprayed Functionally Graded $ZrO_2/NiCoCrAlY$ Coatings', *Materials Science and Engineering*, Vol. A277, pp. 64-76, 2000.
- [14] KHOR, K. A., GU, Y. W., QUEK, C. H. and CHEANG, P., 'Plasma Spraying of Functionally Graded Hydroxyapatite/Ti-6Al-4V Coatings', *Surface and Coatings Technology*, Vol. 168, pp. 195-201, 2003.
- [15] KIM, J. I., KIM, W.-J., CHOI, D. J. and PARK, J. Y., 'Deposition of Compositionally Graded SiC/C Layers on C-C Composites by Low Pressure Chemical Vapor Deposition', *Journal of Nuclear Materials*, Vol. 307-311, pp. 1084-1087, 2002.
- [16] KAWASAKI, A. and WATANABE, R., 'Concept and P/M Fabrication of Functionally Gradient Materials', *Ceramics International*, Vol. 23, pp. 73-83, 1997.

- [17] ZHU, J., LAI, Z., YIN, Z., JEON, J. and LEE, S., 'Fabrication of ZrO₂-NiCr Functionally Graded Material by Powder Metallurgy', *Materials Chemistry and Physics*, Vol. 68, pp. 130-135, 2001.
- [18] RODRÍGUEZ-CASTRO, R., WETHERHOLD, R. C. and KELESTEMUR, M. H., 'Microstructure and Mechanical Behavior of Functionally Graded Al A359/SiC_p Composite', *Materials Science and Engineering*, Vol. A323, pp. 445-456, 2002.
- [19] MOON, J., CABALLERO, A. C., HOZER, L., CHIANG, Y.-M. and CIMA, M. J., 'Fabrication of Functionally Graded Reaction Infiltrated SiC-Si Composite by Three-Dimensional Printing (3DPTM) Process', *Materials Science and Engineering*, Vol. A298, pp. 110-119, 2001.
- [20] DELALE, F. and ERDOGAN, F., 'The Crack Problem for a Nonhomogeneous Plane', *ASME Journal of Applied Mechanics*, Vol. 50, pp. 609-614, 1983.
- [21] KONDA, N. and ERDOGAN, F., 'The Mixed Mode Crack Problem in a Nonhomogeneous Elastic Medium', *Engineering Fracture Mechanics*, Vol. 47, No. 4, pp. 533-545, 1994.

- [22] ERDOGAN, F., 'The Crack Problem for Bonded Nonhomogeneous Materials under Antiplane Shear Loading', *ASME Journal of Applied Mechanics*, Vol. 52, pp. 823-828,1985.
- [23] ERDOGAN, F. and WU, B. H., 'The Surface Crack Problem for a Plate with Functionally Graded Properties', *ASME Journal of Applied Mechanics*, Vol. 64, pp. 449-456,1997.
- [24] OZTURK, M. and ERDOGAN, F., 'The Axisymmetric Crack Problem in a Nonhomogeneous Medium', *ASME Journal of Applied Mechanics*, Vol. 60, pp. 406-413,1993.
- [25] MARUR, P. R. and TIPPUR, H. V., 'Numerical Analysis of Crack-Tip Fields in Functionally Graded Materials with a Crack Normal to the Elastic Gradient', *International Journal of Solids and Structures*, Vol. 37, pp. 5353-5370, 2000.
- [26] CHOI, H. J., 'A Periodic Array of Cracks in a Functionally Graded Nonhomogeneous Medium Loaded under In-Plane Normal and Shear', *International Journal of Fracture*, Vol. 88, pp. 107-128, 1997.
- [27] ERGÜVEN, M. E. and GROSS, D., 'On the Penny-Shaped Crack in Inhomogeneous Elastic Materials under Normal Extension', *International Journal of Solids and Structures*, Vol. 36, pp. 1869-1882, 1999.

- [28] GU, P., DAO, M. and ASARO, R. J., 'A Simplified Method for Calculating the Crack-Tip Field of Functionally Graded Materials Using the Domain Integral', *ASME Journal of Applied Mechanics*, Vol. 66, pp. 101-108, 1999.
- [29] DAG, S. and ERDOGAN, F., 'A Surface Crack in a Graded Medium under General Loading Conditions', *ASME Journal of Applied Mechanics*, Vol. 69, pp. 580-588, 2002.
- [30] WANG, B.-L., MAI, Y.-W. and SUN, Y.-G., 'Anti-Plane Fracture of a Functionally Graded Material Strip', *European Journal of Mechanics A/Solids*, Vol. 22, pp. 357-368, 2003.
- [31] LI, C., ZOU, Z. and DUAN, Z., 'Stress Intensity Factors for Functionally Graded Solid Cylinders', *Engineering Fracture Mechanics*, Vol. 63, pp. 735-749, 1999.
- [32] KADIOĞLU, S., DAĞ, S. and YAHŞI, S., 'Crack Problem for a Functionally Graded Layer on an Elastic Foundation', *International Journal of Fracture*, Vol. 94, pp. 63-77, 1998.
- [33] LI, C. and ZOU, Z., 'Stress Intensity Factors for a Functionally Graded Material Cylinder with an External Circumferential Crack', *Fatigue and Fracture of Engineering Materials and Structures*, Vol. 21, pp. 1447-1457, 1998.

- [34] DAĞ, S., KADIOĞLU, S. and YAŞI, S., 'Circumferential Crack Problem for an FGM Cylinder under Thermal Stresses', *Journal of Thermal Stresses*, Vol. 22, pp. 659-687, 1999.
- [35] CHOI, H. J., 'Effects of Graded Layering on the Tip Behavior of a Vertical Crack in a Substrate under Frictional Hertzian Contact', *Engineering Fracture Mechanics*, Vol. 68, pp. 1033-1059, 2001.
- [36] DAG, S. and ERDOGAN, F., 'A Surface Crack in a Graded Medium Loaded by a Sliding Rigid Stamp', *Engineering Fracture Mechanics*, Vol. 69, pp.1729-1751, 2002.
- [37] KOLEDNIK, O., 'The Yield Stress Gradient Effect in Inhomogeneous Materials', *International Journal of Solids and Structures*, Vol. 37, pp. 781-808, 2000.
- [38] JIN, Z.-H. and DODDS JR., R. H., 'Crack Growth Resistance Behavior of a Functionally Graded Material: Computational Studies', *Engineering Fracture Mechanics*, Vol. 71, pp. 1651-1672, 2004.
- [39] SHBEEB, N. I., BINIENDA, W. K. and KREIDER, K. L., 'Analysis of the Driving Forces for Multiple Cracks in an Infinite Nonhomogeneous Plate, Part I: Theoretical Analysis', *ASME Journal of Applied Mechanics*, Vol. 66, pp. 492-500, 1999.

- [40] SHBEEB, N. I., BINIENDA, W. K. and KREIDER, K. L., 'Analysis of the Driving Forces for Multiple Cracks in an Infinite Nonhomogeneous Plate, Part II: Numerical Solutions', *ASME Journal of Applied Mechanics*, Vol. 66, pp. 501-506, 1999.
- [41] JIN, Z.-H. and BATRA, R. C., 'R-Curve and Strength Behavior of a Functionally Graded Material', *Materials Science and Engineering*, Vol. A242, pp. 70-76, 1998.
- [42] JIN, Z.-H., PAULINO, G. H. and DODDS JR., R. H., 'Cohesive Fracture Modeling of Elastic-Plastic Crack Growth in Functionally Graded Materials', *Engineering Fracture Mechanics*, Vol. 70, pp. 1885-1912, 2003.
- [43] CAI, H. and BAO, G., 'Crack Bridging in Functionally Graded Coatings', *International Journal of Solids and Structures*, Vol. 35, No. 7-8, pp. 701-717, 1998.
- [44] ABANTO-BUENO, J. and LAMBROS, J., 'Investigation of Crack Growth in Functionally Graded Materials Using Digital Image Correlation', *Engineering Fracture Mechanics*, Vol. 69, pp.1695-1711, 2002.
- [45] MOON, R. J., HOFFMAN, M., HILDEN, J., BOWMAN, K. J., TRUMBLE, K. P. and RÖDEL, J. 'R-Curve Behavior in Alumina-Zirconia

Composites with Repeating Graded Layers’, *Engineering Fracture Mechanics*, Vol. 69, pp.1647-1665, 2002.

- [46] FORTH, S. C., FAVROW, L. H., KEAT, W. D. and NEWMAN, J. A., ‘Three-Dimensional Mixed-Mode Fatigue Crack Growth in a Functionally Graded Titanium Alloy’, *Engineering Fracture Mechanics*, Vol. 70, pp.2175-2185, 2003.
- [47] BECKER JR., T. L., CANNON, R. M. and RITCHIE, R. O., ‘Statistical Fracture Modeling: Crack Path and Fracture Criteria with Application to Homogeneous and Functionally Graded Materials’, *Engineering Fracture Mechanics*, Vol. 69, pp.1521-1555, 2002.
- [48] AMADA, S. and UNTAO, S., ‘Fracture Properties of Bamboo’, *Composites Part B: Engineering*, Vol. 32, pp. 451-459, 2001.
- [49] QIAN, G., NAKAMURA, T., BERNDT, C. C. and LEIGH, S. H., ‘Tensile Toughness Test and High Temperature Fracture Analysis of Thermal Barrier Coatings’, *Acta Materialia*, Vol. 45, No. 4, pp. 1767-1784, 1997.
- [50] GU, P. and ASARO, R. J., ‘Crack Deflection in Functionally Graded Materials’, *International Journal of Solids and Structures*, Vol. 34, No. 24, pp. 3085-3098, 1997.

- [51] UEDA, S. and SHINDO, Y., 'Crack Kinking in Functionally Graded Materials due to an Initial Strain Resulting from Stress Relaxation', *Journal of Thermal Stresses*, Vol. 23, pp. 285-290, 2000.
- [52] KIM, J.-H. and PAULINO, G. H., 'T-Stress, Mixed-Mode Stress Intensity Factors, and Crack Initiation Angles in Functionally Graded Materials: A Unified Approach Using the Interaction Integral Method', *Computer Methods in Applied Mechanics and Engineering*, Vol. 192, pp. 1463-1494, 2003.
- [53] AFSAR, A. M. and SEKINE, H., 'Optimum Material Distributions for Prescribed Apparent Fracture Toughness in Thick-Walled FGM Circular Pipes', *International Journal of Pressure Vessels and Piping*, Vol. 78, pp. 471-484, 2001.
- [54] AFSAR, A. M. and SEKINE, H., 'Inverse Problems of Material Distributions for Prescribed Apparent Fracture Toughness in FGM Coatings around a Circular Hole in Infinite Elastic Media', *Composites Science and Technology*, Vol. 62, pp. 1063-1077, 2002.
- [55] CHEN, J., WU, L. and DU, S., 'A Modified J Integral for Functionally Graded Materials', *Mechanics Research Communications*, Vol. 27, No. 3, pp. 301-306, 2000.

- [56] DELALE, F. and ERDOGAN, F., 'Interface Crack in a Nonhomogeneous Elastic Medium', *International Journal of Engineering Science*, Vol. 26, No. 6, pp. 559-568, 1988.
- [57] DELALE, F. and ERDOGAN, F., 'On the Mechanical Modeling of the Interfacial Region in Bonded Half-Planes', *ASME Journal of Applied Mechanics*, Vol. 55, pp. 317-324, 1988.
- [58] ERDOGAN, F. and OZTURK, M., 'Diffusion Problems in Bonded Nonhomogeneous Materials with an Interface Cut', *International Journal of Engineering Science*, Vol. 30, No. 10, pp. 1507-1523, 1992.
- [59] OZTURK, M. and ERDOGAN, F., 'Antiplane Shear Crack Problem in Bonded Materials with a Graded Interfacial Zone', *International Journal of Engineering Science*, Vol. 31, No. 12, pp. 1641-1657, 1993.
- [60] ERDOGAN, F. and OZTURK, M., 'Periodic Cracking of Functionally Graded Coatings', *International Journal of Engineering Science*, Vol. 33, No. 15, pp. 2179-2195, 1995.
- [61] OZTURK, M. and ERDOGAN, F., 'Axisymmetric Crack Problem in Bonded Materials with a Graded Interfacial Region', *International Journal of Solids and Structures*, Vol. 33, No. 2, pp. 193-219, 1996.

- [62] CHEN, Y. F. and ERDOGAN, F., 'The Interface Crack Problem for a Nonhomogeneous Coating Bonded to a Homogeneous Substrate', *Journal of the Mechanics and Physics of Solids*, Vol. 44, No. 5, pp. 771-787, 1996.
- [63] GUO, L.-C., WU, L. Z. and MA, L., 'The Interface Crack Problem under a Concentrated Load for a Functionally Graded Coating-Substrate Composite System', *Composite Structures*, Vol. 63, pp. 397-406, 2004.
- [64] JIN, Z.-H. and BATRA, R. C., 'Interface Cracking between Functionally Graded Coatings and a Substrate under Antiplane Shear', *International Journal of Engineering Science*, Vol. 34, No. 15, pp. 1705-1716, 1996.
- [65] CHOI, H. J., LEE, K. Y. and JIN, T. E., 'Collinear Cracks in a Layered Half-Plane with a Graded Nonhomogeneous Interfacial Zone - Part I: Mechanical Response', *International Journal of Fracture*, Vol. 94, pp. 103-122, 1998.
- [66] SHBEEB, N. I. and BINIENDA, W. K. 'Analysis of an Interface Crack for a Functionally Graded Strip Sandwiched between Two Homogeneous Layers of Finite Thickness', *Engineering Fracture Mechanics*, Vol. 64, pp. 693-720, 1999.

- [67] HUANG, G.-Y., WANG, Y.-S. and GROSS, D., 'Fracture Analysis of Functionally Graded Coatings: Antiplane Deformation', *European Journal of Mechanics A/Solids*, Vol. 21, pp. 391-400, 2002.
- [68] HUANG, G.-Y., WANG, Y.-S. and GROSS, D., 'Fracture Analysis of Functionally Graded Coatings: Plane Deformation', *European Journal of Mechanics A/Solids*, Vol. 22, pp. 535-544, 2003.
- [69] HUANG, G.-Y., WANG, Y.-S. and YU, S.-W., 'Fracture Analysis of a Functionally Graded Interfacial Zone under Plane Deformation', *International Journal of Solids and Structures*, Vol. 41, pp. 731-743, 2004.
- [70] YUE, Z. Q., XIAO, H. T. and THAM, L. G., 'Boundary Element Analysis of Crack Problems in Functionally Graded Materials', *International Journal of Solids and Structures*, Vol. 40, pp. 3273-3291, 2003.
- [71] CHOI, H. J., 'The Problem for Bonded Half-Planes Containing a Crack at an Arbitrary Angle to the Graded Interfacial Zone', *International Journal of Solids and Structures*, Vol. 38, pp. 6559-6588, 2001.
- [72] CHI, S.-H. and CHUNG, Y.-L., 'Cracking in Coating-Substrate Composites with Multi-Layered and FGM Coatings', *Engineering Fracture Mechanics*, Vol. 70, pp. 1227-1243, 2003.

- [73] CHIU, T.-C. and ERDOGAN, F., 'Debonding of Graded Coatings under In-Plane Compression', *International Journal of Solids and Structures*, Vol. 40, pp. 7155-7179, 2003.
- [74] LEE, Y.-D. and ERDOGAN, F., 'Residual/Thermal Stresses in FGM and Laminated Thermal Barrier Coatings', *International Journal of Fracture*, Vol. 69, pp. 145-165, 1994/1995.
- [75] DAO, M., GU, P., MAEWAL, A. and ASARO, R. J., 'A Micromechanical Study of Residual Stresses in Functionally Graded Materials', *Acta Materialia*, Vol. 45, No. 8, pp. 3265-3276, 1997.
- [76] QIANJUN, X., SHOUWEN, Y. and YILAN, K., 'Residual Stress Analysis of Functionally Gradient Materials', *Mechanics Research Communications*, Vol. 26, No.1, pp. 55-60, 1999.
- [77] BRUCK, H. A. and GERSHON, A. L., 'Three-Dimensional Effects near the Interface in a Functionally Graded Ni-Al₂O₃ Plate Specimen', *International Journal of Solids and Structures*, Vol. 39, pp. 547-557, 2002.
- [78] DRAKE, J. T., WILLIAMSON, R. L. and RABIN, B. H., 'Finite Element Analysis of Thermal Residual Stresses at Graded Ceramic-Metal Interfaces. Part II. Interface Optimization for Residual Stress Reduction', *Journal of Applied Physics*, Vol. 74, pp. 1321-1326, 1993.

- [79] GRUJICIC, M. and ZHAO, H., 'Optimization of 316 Stainless Steel/Alumina Functionally Graded Material for Reduction of Damage Induced by Thermal Residual Stresses', *Materials Science and Engineering*, Vol. A252, pp. 117-132, 1998.
- [80] SHABANA, Y. M. and NODA, N., 'Thermo-Elasto-Plastic Stresses in Functionally Graded Materials Subjected to Thermal Loading Taking Residual Stresses of the Fabrication Process into Consideration', *Composites: Part B*, Vol. 32, pp. 111-121, 2001.
- [81] NODA, N. and JIN, Z.-H., 'Thermal Stress Intensity Factors for a Crack in a Strip of a Functionally Gradient Material', *International Journal of Solids and Structures*, Vol. 30, No. 8, pp. 1039-1056, 1993.
- [82] JIN, Z.-H. and NODA, N., 'An Internal Crack Parallel to the Boundary of a Nonhomogeneous Half Plane under Thermal Loading', *International Journal of Engineering Science*, Vol. 31, No. 5, pp. 793-806, 1993.
- [83] NODA, N. and JIN, Z.-H., 'Steady Thermal Stresses in an Infinite Nonhomogeneous Elastic Solid Containing a Crack', *Journal of Thermal Stresses*, Vol. 16, pp. 181-196, 1993.

- [84] BAO, G. and WANG, L., 'Multiple Cracking in Functionally Graded Ceramic/Metal Coatings', *International Journal of Solids and Structures*, Vol. 32, No. 19, pp. 2853-2871, 1995.
- [85] NEMAT-ALLA, M. and NODA, N., 'Edge Crack Problem in a Semi-Infinite FGM Plate with a Bi-Directional Coefficient of Thermal Expansion under Two-Dimensional Thermal Loading', *Acta Mechanica*, Vol. 144, pp. 211-229, 2000.
- [86] BAO, G. and CAI, H., 'Delamination Cracking in Functionally Graded Coating/Metal Substrate Systems', *Acta Materialia*, Vol. 45, No. 3, pp. 1055-1066, 1997.
- [87] LEE, Y.-D. and ERDOGAN, F., 'Interface Cracking of FGM Coatings under Steady-State Heat Flow', *Engineering Fracture Mechanics*, Vol. 59, No.3, pp. 361-380, 1998.
- [88] YANG, Y. Y., 'Stress Analysis in a Joint with a Functionally Graded Material under a Thermal Loading by Using the Mellin Transform Method', *International Journal of Solids and Structures*, Vol. 35, No. 12, pp. 1261-1287, 1998.
- [89] NODA, N., 'Thermal Stresses in Functionally Graded Materials', *Journal of Thermal Stresses*, Vol. 22, pp. 477-512, 1999.

- [90] WANG, B. L. and NODA, N., 'Thermally Induced Fracture of a Smart Functionally Graded Composite Structure', *Theoretical and Applied Fracture Mechanics*, Vol. 35, pp. 93-109, 2001.
- [91] WANG, B. L. and NODA, N., 'Thermally Loaded Functionally Graded Materials with Embedded Defects', *Journal of Thermal Stresses*, Vol. 26, pp. 25-39, 2003.
- [92] EL-BORGI, S., ERDOGAN, F. and HIDRI, L., 'A Partially Insulated Embedded Crack in an Infinite Functionally Graded Medium under Thermo-Mechanical Loading', *International Journal of Engineering Science*, Vol. 42, pp. 371-393, 2004.
- [93] EL-BORGI, S., ERDOGAN, F. and HATIRA, F. B., 'Stress Intensity Factors for an Interface Crack between a Functionally Graded Coating and a Homogeneous Substrate', *International Journal of Fracture*, Vol. 123, pp. 139-162, 2003.
- [94] ITOU, S., 'Thermal Stresses around a Crack in the Nonhomogeneous Interfacial Layer between Two Dissimilar Elastic Half-Planes', *International Journal of Solids and Structures*, Vol. 41, pp. 923-945, 2004.
- [95] YILDIRIM, B., ERDOGAN, F., 'Edge Crack Problems in Homogeneous and Functionally Graded Material Thermal Barrier Coatings under Uniform

Thermal Loading', *Journal of Thermal Stresses*, Vol. 27, pp. 311-329, 2004.

- [96] DAG, S., 'Mixed-Mode Fracture Analysis of Functionally Graded Materials under Thermal Stresses: A New Approach Using Jk-Integral', *Journal of Thermal Stresses*, Vol. 30, pp. 269-296, 2007.
- [97] JIN, Z.-H. and NODA, N., 'Transient Thermal Stress Intensity Factors for a Crack in a Semi-Infinite Plate of a Functionally Gradient Material', *International Journal of Solids and Structures*, Vol. 31, No. 2, pp. 203-218, 1994.
- [98] JIN, Z.-H., 'Effect of Thermal Property Gradients on the Edge Cracking in a Functionally Graded Coating', *Surface and Coatings Technology*, Vol. 179, pp. 210-214, 2004.
- [99] KAWASAKI, A. and WATANABE, R., 'Thermal Fracture Behavior of Metal/Ceramic Functionally Graded Materials', *Engineering Fracture Mechanics*, Vol. 69, pp. 1713-1728, 2002.
- [100] RANGARAJ, S. and KOKINI, K., 'Multiple Surface Cracking and Its Effect on Interface Cracks in Functionally Graded Thermal Barrier Coatings under Thermal Shock', *ASME Journal of Applied Mechanics*, Vol. 70, pp. 234-245, 2003.

- [101] UEDA, S., 'Thermal Shock Fracture in a W-Cu Divertor Plate with a Functionally Graded Nonhomogeneous Interface', *Journal of Thermal Stresses*, Vol. 24, pp. 1021-1041, 2001.
- [102] UEDA, S., 'Transient Thermal Singular Stresses of Multiple Cracking in a W-Cu Functionally Graded Divertor Plate', *Journal of Thermal Stresses*, Vol. 25, pp. 83-95, 2002.
- [103] KAWASAKI, A. and WATANABE, R., 'Evaluation of Thermomechanical Performance for Thermal Barrier Type of Sintered Functionally Graded Materials', *Composites Part B*, Vol. 28B, pp. 29-35, 1997.
- [104] ZHANG, L. M., HIRAI, T., KUMAKAWA, A. and YUAN, R. Z., 'Cyclic Thermal Shock Resistance of TiC/Ni₃Al FGMs', *Composites Part B*, Vol. 28B, pp. 21-27, 1997.
- [105] KOKINI, K., DEJONGE, J., RANGARAJ, S. and BEARDSLEY, B., 'Thermal Shock of Functionally Graded Thermal Barrier Coatings with Similar Thermal Resistance', *Surface and Coatings Technology*, Vol. 154, pp. 223-231, 2002.
- [106] RANGARAJ, S. and KOKINI, K., 'Estimating the Fracture Resistance of Functionally Graded Thermal Barrier Coatings from Thermal Shock Tests', *Surface and Coatings Technology*, Vol. 173, pp. 201-212, 2003.

- [107] LI, J. Q., ZENG, X. R., TANG, J. N. and XIAO, P., 'Fabrication and Thermal Properties of a YSZ-NiCr Joint with an Interlayer of YSZ-NiCr Functionally Graded Material', *Journal of the European Ceramic Society*, Vol. 23, pp. 1847-1853, 2003.
- [108] WANG, B. L., HAN, J. C. and DU, S. Y., 'Crack Problems for Functionally Graded Materials under Transient Thermal Loading', *Journal of Thermal Stresses*, Vol. 23, pp. 143-168, 2000.
- [109] NODA, N. and WANG, B. L., 'Transient Thermoelastic Responses of Functionally Graded Materials Containing Collinear Cracks', *Engineering Fracture Mechanics*, Vol. 69, pp. 1791-1809, 2002.
- [110] RANGARAJ, S. and KOKINI, K., 'Interface Thermal Fracture in Functionally Graded Zirconia-Mullite-Bond Coat Alloy Thermal Barrier Coatings', *Acta Materialia*, Vol. 51, pp. 251-267, 2003.
- [111] FUJIMOTO, T. and NODA, N., 'Two Crack Growths in a Functionally Graded Plate under Thermal Shock', *Journal of Thermal Stresses*, Vol. 24, pp. 847-862, 2001.
- [112] NODA, N., 'Thermal Stresses Intensity Factor for Functionally Gradient Plate with an Edge Crack', *Journal of Thermal Stresses*, Vol. 20, pp. 373-387, 1997.

- [113] YILDIRIM, B., DAG, S. and ERDOGAN, F., 'Three Dimensional Fracture Analysis of FGM Coatings under Thermomechanical Loading', *International Journal of Fracture*, Vol. 132, pp. 369-395, 2005.
- [114] INAN, O., DAG, S. and ERDOGAN, F., 'Three Dimensional Fracture Analysis of FGM Coatings', *Material Science Forum*, Vol. 492-493, pp. 373-378, 2005.
- [115] OZTURK, M. and ERDOGAN, F., 'The Mixed Mode Crack Problem in an Inhomogeneous Orthotropic Medium', *International Journal of Fracture*, Vol. 98, pp. 243-261, 1999.
- [116] GU, P. and ASARO, R. J., 'Cracks in Functionally Graded Materials', *International Journal of Solids and Structures*, Vol. 34, No. 1, pp.1-17, 1997.
- [117] OZTURK, M. and ERDOGAN, F., 'Mode I Crack Problem in an Inhomogeneous Orthotropic Medium', *International Journal of Engineering Science*, Vol. 35, No. 9, pp. 869-883, 1997.
- [118] KIM, J.-H. and PAULINO, G. H., 'Isoparametric Graded Finite Elements for Nonhomogeneous Isotropic and Orthotropic Materials', *ASME Journal of Applied Mechanics*, Vol. 69, pp. 502-514, 2002.
- [119] KIM, J.-H. and PAULINO, G. H., 'Mixed-Mode J-Integral Formulation and Implementation Using Graded Elements for Fracture Analysis of

Nonhomogeneous Orthotropic Materials’, *Mechanics of Materials*, Vol. 35, pp. 107-128, 2003.

[120] KIM, J.-H. and PAULINO, G. H., ‘Mixed-Mode Fracture of Orthotropic Functionally Graded Materials Using Finite Elements and the Modified Crack Closure Method’, *Engineering Fracture Mechanics*, Vol. 69, pp. 1557-1586, 2002.

[121] KIM, J.-H. and PAULINO, G. H., ‘The Interaction Integral for Fracture of Orthotropic Functionally Graded Materials: Evaluation of Stress Intensity Factors’, *International Journal of Solids and Structures*, Vol. 40, pp. 3967-4001, 2003.

[122] DAG, S., YILDIRIM, B. and ERDOGAN, F., ‘Interface Crack Problems in Graded Orthotropic Media: Analytical and Computational Approaches’, *International Journal of Fracture*, Vol. 130, pp. 471-496, 2004.

[123] YILDIRIM, B., DAG, S. and ERDOGAN, F., ‘Steady State Heat Conduction in Orthotropic Functionally Graded Materials Containing Cracks: Analytical and Computational Techniques’, *Proceedings of the 6th International Congress on Thermal Stresses*, Vol. 2, pp. 517-520,

[124] CHEN, J., ‘Determination of Thermal Stress Intensity Factors for an Interface Crack in a Graded Orthotropic Coating-Substrate Structure’, *International Journal of Fracture*, Vol. 133, pp. 303-328, 2005.

- [125] DAG, S., 'Thermal Fracture Analysis of Orthotropic Functionally Graded Materials Using an Equivalent Domain Integral Approach', *Engineering Fracture Mechanics*, Vol. 73, pp. 2802-2828, 2006.
- [126] DAG, S., YILDIRIM, B. and SARIKAYA, D., 'Mixed-Mode Fracture Analysis of Orthotropic Functionally Graded Materials under Thermomechanical Loading', accepted for publication, *International Journal of Solids and Structures*, 2007.
- [127] BARSOUM, R. S., 'Application of Quadratic Isoparametric Finite Elements in Linear Fracture Mechanics', *International Journal of Fracture*, Vol. 10, pp. 603-605, 1974.
- [128] SHIH, C. F., DELORENZI, H. G. and GERMAN, M. D., 'Crack Extension Modeling with Singular Quadratic Isoparametric Elements', *International Journal of Fracture*, Vol. 12, pp. 647-651, 1976.
- [129] INGRAFFEA, A. R. and MANU, C., 'Stress-Intensity Factor Computation in Three Dimensions with Quarter-Point Elements', *International Journal for Numerical Methods in Engineering*, Vol. 15, pp. 1427-1445, 1980.
- [130] SAOUMA, V. E. and SIKIOTIS, E. S., 'Stress Intensity Factors in Anisotropic Bodies Using Singular Isoparametric Elements', *Engineering Fracture Mechanics*, Vol. 25, No. 1, pp. 115-121, 1986.
- [131] BOONE, T. J., WAWRZYNEK, P. A. and INGRAFFEA, A. R., 'Finite Element Modeling of Fracture Propagation in Orthotropic Materials', *Engineering Fracture Mechanics*, Vol. 26, No. 2, pp. 185-201, 1987.

- [132] KRENK, S., 'On the Elastic Constants of Plane Orthotropic Elasticity', *Journal of Composite Materials*, Vol. 13, pp. 108-116, 1979.
- [133] OWEN, D. R. J. and FAWKES, A. J., *Engineering Fracture Mechanics: Numerical Methods and Applications*, Pineridge Press Ltd., Swansea, U.K., 1983.
- [134] CINAR, A. and ERDOGAN, F., 'The Crack and Wedging Problem for an Orthotropic Strip', *International Journal of Fracture*, Vol. 19, pp. 83-102, 1983.
- [135] PARTHASARATHI, S., TITTMAN, B. R., SAMPATH, K. and ONESTO, E. J., 'Ultrasonic Characterization of Elastic Anisotropy in Plasma Sprayed Alumina Coatings', *Journal of Thermal Spray Technology*, Vol. 4, pp. 367-373, 1995.
- [136] SEVOSTIANOV, I. and KACHANOV, M., 'Plasma-Sprayed Ceramic Coatings: Anisotropic Elastic and Conductive Properties in Relation to the Microstructure; Cross-Property Correlations', *Material Science and Engineering*, Vol. A297, pp. 235-243, 2001.
- [137] NUSIER, S. and NEWAZ, G., 'Analysis of Interfacial Cracks in a TBC/ Superalloy System under Thermal Loading', *Engineering Fracture Mechanics*, Vol.60, No. 5-6, pp. 577-581, 1998.
- [138] CALLISTER, W. D., *Materials Science and Engineering: An Introduction*, New York: John Wiley and Sons, Inc., 2000.

- [139] ERDOGAN, F., 'Mixed Boundary-Value Problems in Mechanics', *Mechanics Today*, Vol. 4, edited by NEMAT-NASSER, S., Pergamon Press, New York, U.S.A, pp. 1-84, 1978.

APPENDIX A

DETERMINATION OF UNKNOWN FUNCTIONS

The functions $Y_j(\omega)$, $Z_j(\omega)$, $V_j(\omega)$, $W_j(\omega)$, $X_j(\omega)$, $L_j(\omega)$, $P_j(\omega)$ and $Q_j(\omega)$, ($j = 1, 2, 3, 4$), are found from the following equations.

$$\begin{bmatrix} m_{1,1} & m_{1,2} & \cdot & \cdot & \cdot & m_{1,16} \\ m_{2,1} & m_{2,2} & \cdot & \cdot & \cdot & m_{2,16} \\ \cdot & \cdot & \cdot & \cdot & \cdot & \cdot \\ \cdot & \cdot & \cdot & \cdot & \cdot & \cdot \\ m_{16,1} & m_{16,2} & \cdot & \cdot & \cdot & m_{16,16} \end{bmatrix} \begin{bmatrix} Y_1(\omega) \\ Y_2(\omega) \\ Y_3(\omega) \\ Y_4(\omega) \\ V_1(\omega) \\ V_2(\omega) \\ V_3(\omega) \\ V_4(\omega) \\ X_1(\omega) \\ X_2(\omega) \\ X_3(\omega) \\ X_4(\omega) \\ P_1(\omega) \\ P_2(\omega) \\ P_3(\omega) \\ P_4(\omega) \end{bmatrix} = \begin{bmatrix} 0 \\ 0 \\ 1 \\ 0 \\ 0 \\ 0 \\ 0 \\ 0 \\ 0 \\ 0 \\ 0 \\ 0 \\ 0 \\ 0 \\ 0 \\ 0 \end{bmatrix} \tag{A.1a}$$

$$\begin{bmatrix} m_{1,1} & m_{1,2} & \cdot & \cdot & \cdot & m_{1,16} \\ m_{2,1} & m_{2,2} & \cdot & \cdot & \cdot & m_{2,16} \\ \cdot & \cdot & \cdot & \cdot & \cdot & \cdot \\ \cdot & \cdot & \cdot & \cdot & \cdot & \cdot \\ \cdot & \cdot & \cdot & \cdot & \cdot & \cdot \\ m_{16,1} & m_{16,2} & \cdot & \cdot & \cdot & m_{16,16} \end{bmatrix} \begin{bmatrix} Z_1(\omega) \\ Z_2(\omega) \\ Z_3(\omega) \\ Z_4(\omega) \\ W_1(\omega) \\ W_2(\omega) \\ W_3(\omega) \\ W_4(\omega) \\ L_1(\omega) \\ L_2(\omega) \\ L_3(\omega) \\ L_4(\omega) \\ Q_1(\omega) \\ Q_2(\omega) \\ Q_3(\omega) \\ Q_4(\omega) \end{bmatrix} = \begin{bmatrix} 0 \\ 0 \\ 0 \\ 1 \\ 0 \\ 0 \\ 0 \\ 0 \\ 0 \\ 0 \\ 0 \\ 0 \\ 0 \\ 0 \\ 0 \\ 0 \end{bmatrix} \quad (\text{A.1b})$$

where

$$m_{1,j} = N_j(\omega)s_j(\omega) + \nu_0 i \omega, \quad (j = 1, 2, 3, 4) \quad (\text{A.2})$$

$$m_{1,j} = -(N_j(\omega)s_j(\omega) + \nu_0 i \omega), \quad (j = 5, 6, 7, 8) \quad (\text{A.3})$$

$$m_{1,j} = 0, \quad (j = 9, 10, \dots, 16) \quad (\text{A.4})$$

$$m_{2,j} = s_j(\omega) + N_j(\omega)i\omega, \quad (j = 1, 2, 3, 4) \quad (\text{A.5})$$

$$m_{2,j} = -(s_j(\omega) + N_j(\omega)i\omega), \quad (j = 5, 6, 7, 8) \quad (\text{A.6})$$

$$m_{2,j} = 0, \quad (j = 9, 10, \dots, 16) \quad (\text{A.7})$$

$$m_{3,j} = i\omega N_j(\omega), \quad (j = 1, 2, 3, 4) \quad (\text{A.8})$$

$$m_{3,j} = -i\omega N_j(\omega), \quad (j = 5, 6, 7, 8) \quad (\text{A.9})$$

$$m_{3,j} = 0, \quad (j = 9, 10, \dots, 16) \quad (\text{A.10})$$

$$m_{4,j} = i\omega, \quad (j = 1, 2, 3, 4) \quad (\text{A.11})$$

$$m_{4,j} = -i\omega, \quad (j = 5, 6, 7, 8) \quad (\text{A.12})$$

$$m_{4,j} = 0, \quad (j = 9, 10, \dots, 16) \quad (\text{A.13})$$

$$m_{5,j} = (N_j(\omega)s_j(\omega) + v_0 i\omega) \exp(s_j(\omega)h_1\sqrt{\delta_0}), \quad (j = 1, 2, 3, 4) \quad (\text{A.14})$$

$$m_{5,j} = 0, \quad (j = 5, 6, \dots, 16) \quad (\text{A.15})$$

$$m_{6,j} = (s_j(\omega) + N_j(\omega)i\omega) \exp(s_j(\omega)h_1\sqrt{\delta_0}), \quad (j = 1, 2, 3, 4) \quad (\text{A.16})$$

$$m_{6,j} = 0, \quad (j = 5, 6, \dots, 16) \quad (\text{A.17})$$

$$m_{7,j} = 0, \quad (j = 1, 2, 3, 4) \quad (\text{A.18})$$

$$m_{7,j} = \frac{E_0 \exp(-\mathcal{H}_2\sqrt{\delta_0})}{1-v_0^2} (v_0 i\omega + N_j(\omega)s_j(\omega)) \exp(-s_j(\omega)h_2\sqrt{\delta_0}), \quad (j = 5, 6, 7, 8) \quad (\text{A.19})$$

$$m_{7,j} = -\frac{E_3}{1-\nu_3^2} \left(\nu_3 i \omega + \left(\frac{\delta_0}{\delta_3} \right)^2 B_j(\omega) r_j(\omega) \right) \exp(-r_j(\omega) h_2 \sqrt{\delta_0}), \quad (j = 9, 10, 11, 12) \quad (\text{A.20})$$

$$m_{7,j} = 0, \quad (j = 13, 14, 15, 16) \quad (\text{A.21})$$

$$m_{8,j} = 0, \quad (j = 1, 2, 3, 4) \quad (\text{A.22})$$

$$m_{8,j} = \frac{E_0 \exp(-\mathcal{H}_2 \sqrt{\delta_0})}{2(\kappa_0 + \nu_0)} (s_j(\omega) + N_j(\omega) i \omega) \exp(-s_j(\omega) h_2 \sqrt{\delta_0}), \quad (j = 5, 6, 7, 8) \quad (\text{A.23})$$

$$m_{8,j} = -\frac{E_3}{2(\kappa_3 + \nu_3)} i(-r_j(\omega) i + \omega B_j(\omega)) \exp(-r_j(\omega) h_2 \sqrt{\delta_0}), \quad (j = 9, 10, 11, 12) \quad (\text{A.24})$$

$$m_{8,j} = 0, \quad (j = 13, 14, 15, 16) \quad (\text{A.25})$$

$$m_{9,j} = 0, \quad (j = 1, 2, 3, 4) \quad (\text{A.26})$$

$$m_{9,j} = \exp(-s_j(\omega) h_2 \sqrt{\delta_0}), \quad (j = 5, 6, 7, 8) \quad (\text{A.27})$$

$$m_{9,j} = -\exp(-r_j(\omega) h_2 \sqrt{\delta_0}), \quad (j = 9, 10, 11, 12) \quad (\text{A.28})$$

$$m_{9,j} = 0, \quad (j = 13, 14, 15, 16) \quad (\text{A.29})$$

$$m_{10,j} = 0, \quad (j = 1, 2, 3, 4) \quad (\text{A.30})$$

$$m_{10,j} = N_j(\omega) \exp(-s_j(\omega)h_2\sqrt{\delta_0}), \quad (j = 5, 6, 7, 8) \quad (\text{A.31})$$

$$m_{10,j} = -B_j(\omega) \exp(-r_j(\omega)h_2\sqrt{\delta_0}), \quad (j = 9, 10, 11, 12) \quad (\text{A.32})$$

$$m_{10,j} = 0, \quad (j = 13, 14, 15, 16) \quad (\text{A.33})$$

$$m_{11,j} = 0, \quad (j = 1, 2, \dots, 8) \quad (\text{A.34})$$

$$m_{11,j} = \frac{E_3}{1-\nu_3^2} \left(\nu_3 i \omega + \left(\frac{\delta_0}{\delta_3} \right)^2 B_j(\omega) r_j(\omega) \right) \exp(-r_j(\omega)(h_3 + h_2)\sqrt{\delta_0}), \quad (j = 9, 10, 11, 12) \quad (\text{A.35})$$

$$m_{11,j} = -\frac{E_4}{1-\nu_4^2} \left(\nu_4 i \omega + \left(\frac{\delta_0}{\delta_4} \right)^2 D_j(\omega) n_j(\omega) \right) \exp(-n_j(\omega)(h_3 + h_2)\sqrt{\delta_0}), \quad (j = 13, 14, 15, 16) \quad (\text{A.36})$$

$$m_{12,j} = 0, \quad (j = 1, 2, \dots, 8) \quad (\text{A.37})$$

$$m_{12,j} = \frac{E_3}{2(\kappa_3 + \nu_3)} i(-r_j(\omega)i + \omega B_j(\omega)) \exp(-r_j(\omega)(h_3 + h_2)\sqrt{\delta_0}), \quad (j = 9, 10, 11, 12) \quad (\text{A.38})$$

$$m_{12,j} = -\frac{E_4}{2(\kappa_4 + \nu_4)} i(-n_j(\omega)i + \omega D_j(\omega)) \exp(-n_j(\omega)(h_3 + h_2)\sqrt{\delta_0}), \quad (j = 13, 14, 15, 16) \quad (\text{A.39})$$

$$m_{13,j} = 0, \quad (j = 1, 2, \dots, 8) \quad (\text{A.40})$$

$$m_{13,j} = \exp(-r_j(\omega)(h_3 + h_2)\sqrt{\delta_0}), \quad (j = 9, 10, 11, 12) \quad (\text{A.41})$$

$$m_{13,j} = -\exp(-n_j(\omega)(h_3 + h_2)\sqrt{\delta_0}), \quad (j = 13, 14, 15, 16) \quad (\text{A.42})$$

$$m_{14,j} = 0, \quad (j = 1, 2, \dots, 8) \quad (\text{A.43})$$

$$m_{14,j} = B_j(\omega)\exp(-r_j(\omega)(h_3 + h_2)\sqrt{\delta_0}), \quad (j = 9, 10, 11, 12) \quad (\text{A.44})$$

$$m_{14,j} = -D_j(\omega)\exp(-n_j(\omega)(h_3 + h_2)\sqrt{\delta_0}), \quad (j = 13, 14, 15, 16) \quad (\text{A.45})$$

$$m_{15,j} = 0, \quad (j = 1, 2, \dots, 12) \quad (\text{A.46})$$

$$m_{15,j} = \left(i\omega v_4 + \left(\frac{\delta_0}{\delta_4} \right)^2 n_j(\omega) D_j(\omega) \right) \exp(-n_j(\omega)(h_4 + h_3 + h_2)\sqrt{\delta_0}),$$

$$(j = 13, 14, 15, 16) \quad (\text{A.47})$$

$$m_{16,j} = 0, \quad (j = 1, 2, \dots, 12) \quad (\text{A.48})$$

$$m_{16,j} = i(-n_j(\omega)i + \omega D_j(\omega))\exp(-n_j(\omega)(h_4 + h_3 + h_2)\sqrt{\delta_0}), \quad (j = 13, 14, 15, 16)$$

$$(\text{A.49})$$

APPENDIX B

ASYMPTOTIC BEHAVIORS OF THE INTEGRANDS

To determine the asymptotic behaviors of the integrands $F_{11}(\omega,0)$, $F_{11}(-\omega,0)$, $F_{12}(\omega,0)$, $F_{12}(-\omega,0)$, $D_{11}(\omega,0)$, $D_{11}(-\omega,0)$, $D_{12}(\omega,0)$ and $D_{12}(-\omega,0)$ as ω approaches infinity, two orthotropic FGM half planes are considered instead of the orthotropic FGM coating of finite thickness as shown in Figure-B.1.

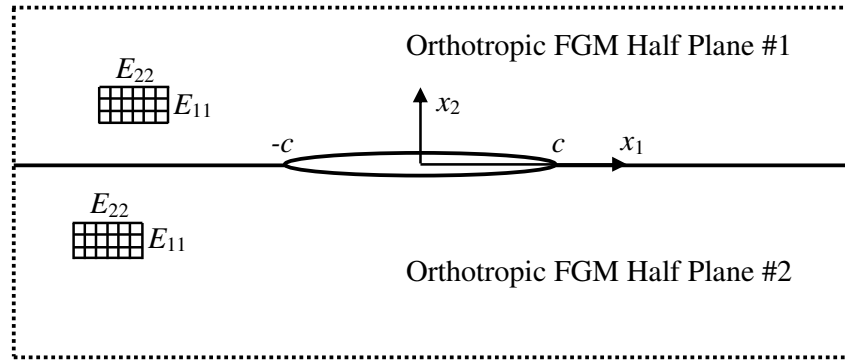


Figure-B.1 Illustration of the two orthotropic FGM half planes.

In a similar way described in Section 2.2, governing equations for the orthotropic FGM half planes can be obtained as [115]:

$$\frac{\partial^2 u^{(i)}}{\partial y^2} + \beta_1 \frac{\partial^2 u^{(i)}}{\partial x^2} + \beta_2 \frac{\partial^2 v^{(i)}}{\partial x \partial y} + \gamma \left(\frac{\partial u^{(i)}}{\partial y} + \frac{\partial v^{(i)}}{\partial x} \right) = 0 \quad (\text{B.1a})$$

$$\frac{\partial^2 v^{(i)}}{\partial x^2} + \beta_1 \frac{\partial^2 v^{(i)}}{\partial y^2} + \beta_2 \frac{\partial^2 u^{(i)}}{\partial x \partial y} + \beta_1 \gamma \left(\frac{\partial v^{(i)}}{\partial y} + \nu_0 \frac{\partial u^{(i)}}{\partial x} \right) = 0 \quad (\text{B.1b})$$

where the superscript (i) is (1) for the orthotropic FGM half plane #1 where $y > 0$ and (2) for the orthotropic FGM half plane #2 where $y < 0$. β_1 and β_2 are given in Eq.(2.2.17).

In a similar way described in Section 2.2, the displacement and stress components for the orthotropic FGM half plane #1 can be obtained as given in Eq.(B.2) and Eq.(B.3), respectively.

$$u^{(i)}(x, y) = \frac{1}{2\pi} \int_{-\infty}^{\infty} \sum_{j=1}^2 \hat{M}_j(\omega) \exp(s_j(\omega)y + i\omega x) d\omega \quad (\text{B.2a})$$

$$v^{(i)}(x, y) = \frac{1}{2\pi} \int_{-\infty}^{\infty} \sum_{j=1}^2 \hat{M}_j(\omega) N_j(\omega) \exp(s_j(\omega)y + i\omega x) d\omega \quad (\text{B.2b})$$

$$\sigma_{yy}^{(i)}(x, y) = \frac{E_0 \exp(\gamma y)}{1 - \nu_0^2} \left\{ \frac{1}{2\pi} \int_{-\infty}^{\infty} \sum_{j=1}^2 \hat{M}_j(\omega) (\nu_0 i\omega + N_j(\omega) s_j(\omega)) \exp(s_j(\omega)y + i\omega x) d\omega \right\} \quad (\text{B.3a})$$

$$\sigma_{xy}^{(i)}(x, y) = \frac{E_0 \exp(\gamma y)}{2(\kappa_0 + \nu_0)} \left\{ \frac{1}{2\pi} \int_{-\infty}^{\infty} \sum_{j=1}^2 \hat{M}_j(\omega) (N_j(\omega) i\omega + s_j(\omega)) \exp(s_j(\omega)y + i\omega x) d\omega \right\} \quad (\text{B.3b})$$

where $\hat{M}_j(\omega)$, ($j = 1, 2$), are unknown functions of ω . $s_j(\omega)$ and $N_j(\omega)$, ($j = 1, 2$), are given in Eq.(2.2.25) and Eq.(2.2.26), respectively.

In a similar way described in Section 2.2, the displacement and stress components for the orthotropic FGM half plane #2 can be obtained as given in Eq.(B.4) and Eq.(B.5), respectively.

$$u^{(2)}(x, y) = \frac{1}{2\pi} \int \sum_{-\infty}^{\infty} \hat{M}_j(\omega) \exp(s_j(\omega)y + i\omega x) d\omega \quad (\text{B.4a})$$

$$v^{(2)}(x, y) = \frac{1}{2\pi} \int \sum_{-\infty}^{\infty} \hat{M}_j(\omega) N_j(\omega) \exp(s_j(\omega)y + i\omega x) d\omega \quad (\text{B.4b})$$

$$\sigma_{xy}^{(2)}(x, y) = \frac{E_0 \exp(\gamma y)}{1 - \nu_0^2} \left\{ \frac{1}{2\pi} \int \sum_{-\infty}^{\infty} \hat{M}_j(\omega) (\nu_0 i\omega + N_j(\omega) s_j(\omega)) \exp(s_j(\omega)y + i\omega x) d\omega \right\} \quad (\text{B.5a})$$

$$\sigma_{yy}^{(2)}(x, y) = \frac{E_0 \exp(\gamma y)}{2(\kappa_0 + \nu_0)} \left\{ \frac{1}{2\pi} \int \sum_{-\infty}^{\infty} \hat{M}_j(\omega) (N_j(\omega) i\omega + s_j(\omega)) \exp(s_j(\omega)y + i\omega x) d\omega \right\} \quad (\text{B.5b})$$

where $\hat{M}_j(\omega)$, ($j = 3, 4$), are unknown functions of ω . $s_j(\omega)$ and $N_j(\omega)$, ($j = 3, 4$), are given in Eq.(2.2.25) and Eq.(2.2.26), respectively.

In order to determine the unknown functions $\hat{M}_j(\omega)$, ($j = 1, 2, 3, 4$), the following boundary and continuity conditions have to be satisfied.

$$\sigma_{22}^{(1)}(x_1, 0) = \sigma_{22}^{(2)}(x_1, 0), \quad |x_1| < \infty \quad (\text{B.6a})$$

$$\sigma_{12}^{(1)}(x_1, 0) = \sigma_{12}^{(2)}(x_1, 0), \quad |x_1| < \infty \quad (\text{B.6b})$$

$$\frac{\partial}{\partial x_1} (u_2^{(1)}(x_1, 0) - u_2^{(2)}(x_1, 0)) = \begin{cases} \hat{f}_1(x_1), & |x_1| < c \\ 0, & |x_1| > c \end{cases} \quad (\text{B.6c})$$

$$\frac{\partial}{\partial x_1} (u_1^{(1)}(x_1, 0) - u_1^{(2)}(x_1, 0)) = \begin{cases} \hat{f}_2(x_1), & |x_1| < c \\ 0, & |x_1| > c \end{cases} \quad (\text{B.6d})$$

where $\hat{f}_1(x_1)$ and $\hat{f}_2(x_1)$ are the primary unknown functions of the problem. Expressing Eq.(B.6) in the transformed coordinate system and applying Fourier transformations to them, the following system of equations is obtained:

$$\sum_{j=1}^2 \hat{M}_j(\omega) (v_0 i\omega + N_j(\omega) s_j(\omega)) - \sum_{j=3}^4 \hat{M}_j(\omega) (v_0 i\omega + N_j(\omega) s_j(\omega)) = 0 \quad (\text{B.7a})$$

$$\sum_{j=1}^2 \hat{M}_j(\omega) (N_j(\omega) i\omega + s_j(\omega)) - \sum_{j=3}^4 \hat{M}_j(\omega) (N_j(\omega) i\omega + s_j(\omega)) = 0 \quad (\text{B.7b})$$

$$i\omega \left(\sum_{j=1}^2 \hat{M}_j(\omega) N_j(\omega) - \sum_{j=3}^4 \hat{M}_j(\omega) N_j(\omega) \right) = \int_{-c/\sqrt{\delta_0}}^{c/\sqrt{\delta_0}} \hat{\phi}_1(t) \exp(-i\omega t) dt \quad (\text{B.7c})$$

$$i\omega \left(\sum_{j=1}^2 \hat{M}_j(\omega) - \sum_{j=3}^4 \hat{M}_j(\omega) \right) = \int_{-c/\sqrt{\delta_0}}^{c/\sqrt{\delta_0}} \hat{\phi}_2(t) \exp(-i\omega t) dt \quad (\text{B.7d})$$

where $\hat{\phi}_1(t) = \hat{f}_1(\sqrt{\delta_0} t)$ and $\hat{\phi}_2(t) = \delta_0 \hat{f}_2(\sqrt{\delta_0} t)$. From Eq.(B.7), the unknown functions $\hat{M}_j(\omega)$, ($j = 1, 2, 3, 4$), can be determined in the following form.

$$\hat{M}_j(\omega) = \hat{Y}_j(\omega) \int_{-c/\sqrt{\delta_0}}^{c/\sqrt{\delta_0}} \hat{\phi}_1(t) \exp(-i\omega t) dt + \hat{Z}_j(\omega) \int_{-c/\sqrt{\delta_0}}^{c/\sqrt{\delta_0}} \hat{\phi}_2(t) \exp(-i\omega t) dt, \quad (j = 1, 2) \quad (\text{B.8a})$$

$$\hat{M}_j(\omega) = \hat{V}_j(\omega) \int_{-c/\sqrt{\delta_0}}^{c/\sqrt{\delta_0}} \hat{\phi}_1(t) \exp(-i\omega t) dt + \hat{W}_j(\omega) \int_{-c/\sqrt{\delta_0}}^{c/\sqrt{\delta_0}} \hat{\phi}_2(t) \exp(-i\omega t) dt, \quad (j = 3, 4) \quad (\text{B.8b})$$

Assuming that $p(x_1)$ is the normal traction and $q(x_1)$ is the shear traction at the crack surfaces, the problem is reduced to two singular integral equations using the following boundary conditions.

$$\sigma_{22}(x_1, 0) = -p(x_1), \quad |x_1| < c \quad (\text{B.9a})$$

$$\sigma_{12}(x_1, 0) = -q(x_1), \quad |x_1| < c \quad (\text{B.9b})$$

In a similar way described in Section 2.2, the singular integral equations are obtained as follows.

$$\begin{aligned} \lim_{y \rightarrow 0^+} & \left\{ \int_{-c/\sqrt{\delta_0}}^{c/\sqrt{\delta_0}} \hat{\phi}_1(t) dt \frac{1}{2\pi} \int_0^\infty \hat{F}_{11}(\omega, y) \cos(\omega(x-t)) d\omega \right. \\ & + \int_{-c/\sqrt{\delta_0}}^{c/\sqrt{\delta_0}} \hat{\phi}_1(t) dt \frac{1}{2\pi} \int_0^\infty \hat{F}_{11}(-\omega, y) \cos(\omega(x-t)) d\omega \\ & + \int_{-c/\sqrt{\delta_0}}^{c/\sqrt{\delta_0}} \hat{\phi}_1(t) dt \frac{1}{2\pi} \int_0^\infty i\hat{F}_{11}(\omega, y) \sin(\omega(x-t)) d\omega \\ & + \int_{-c/\sqrt{\delta_0}}^{c/\sqrt{\delta_0}} \hat{\phi}_1(t) dt \frac{1}{2\pi} \int_0^\infty -i\hat{F}_{11}(-\omega, y) \sin(\omega(x-t)) d\omega \\ & + \int_{-c/\sqrt{\delta_0}}^{c/\sqrt{\delta_0}} \hat{\phi}_2(t) dt \frac{1}{2\pi} \int_0^\infty \hat{F}_{12}(\omega, y) \cos(\omega(x-t)) d\omega \\ & + \int_{-c/\sqrt{\delta_0}}^{c/\sqrt{\delta_0}} \hat{\phi}_2(t) dt \frac{1}{2\pi} \int_0^\infty \hat{F}_{12}(-\omega, y) \cos(\omega(x-t)) d\omega \\ & + \int_{-c/\sqrt{\delta_0}}^{c/\sqrt{\delta_0}} \hat{\phi}_2(t) dt \frac{1}{2\pi} \int_0^\infty i\hat{F}_{12}(\omega, y) \sin(\omega(x-t)) d\omega \\ & \left. + \int_{-c/\sqrt{\delta_0}}^{c/\sqrt{\delta_0}} \hat{\phi}_2(t) dt \frac{1}{2\pi} \int_0^\infty -i\hat{F}_{12}(-\omega, y) \sin(\omega(x-t)) d\omega \right\} = -\frac{1-\nu_0^2}{E_0} \delta_0 p(\sqrt{\delta_0} x) \quad (\text{B.10a}) \end{aligned}$$

$$\begin{aligned}
\lim_{y \rightarrow 0^+} & \left\{ \int_{-c/\sqrt{\delta_0}}^{c/\sqrt{\delta_0}} \hat{\phi}_1(t) dt \frac{1}{2\pi} \int_0^\infty \hat{D}_{11}(\omega, y) \cos(\omega(x-t)) d\omega \right. \\
& + \int_{-c/\sqrt{\delta_0}}^{c/\sqrt{\delta_0}} \hat{\phi}_1(t) dt \frac{1}{2\pi} \int_0^\infty \hat{D}_{11}(-\omega, y) \cos(\omega(x-t)) d\omega \\
& + \int_{-c/\sqrt{\delta_0}}^{c/\sqrt{\delta_0}} \hat{\phi}_1(t) dt \frac{1}{2\pi} \int_0^\infty i\hat{D}_{11}(\omega, y) \sin(\omega(x-t)) d\omega \\
& + \int_{-c/\sqrt{\delta_0}}^{c/\sqrt{\delta_0}} \hat{\phi}_1(t) dt \frac{1}{2\pi} \int_0^\infty -i\hat{D}_{11}(-\omega, y) \sin(\omega(x-t)) d\omega \\
& + \int_{-c/\sqrt{\delta_0}}^{c/\sqrt{\delta_0}} \hat{\phi}_2(t) dt \frac{1}{2\pi} \int_0^\infty \hat{D}_{12}(\omega, y) \cos(\omega(x-t)) d\omega \\
& + \int_{-c/\sqrt{\delta_0}}^{c/\sqrt{\delta_0}} \hat{\phi}_2(t) dt \frac{1}{2\pi} \int_0^\infty \hat{D}_{12}(-\omega, y) \cos(\omega(x-t)) d\omega \\
& + \int_{-c/\sqrt{\delta_0}}^{c/\sqrt{\delta_0}} \hat{\phi}_2(t) dt \frac{1}{2\pi} \int_0^\infty i\hat{D}_{12}(\omega, y) \sin(\omega(x-t)) d\omega \\
& \left. + \int_{-c/\sqrt{\delta_0}}^{c/\sqrt{\delta_0}} \hat{\phi}_2(t) dt \frac{1}{2\pi} \int_0^\infty -i\hat{D}_{12}(-\omega, y) \sin(\omega(x-t)) d\omega \right\} = -\frac{2(\kappa_0 + \nu_0)}{E_0} q(\sqrt{\delta_0} x) \quad (\text{B.10b})
\end{aligned}$$

where $|x| < c/\sqrt{\delta_0}$ and,

$$\hat{F}_{11}(\omega, y) = \sum_{j=1}^2 (i\omega \nu_0 + N_j(\omega) s_j(\omega)) \hat{Y}_j(\omega) \exp(s_j(\omega) y) \quad (\text{B.11a})$$

$$\hat{F}_{12}(\omega, y) = \sum_{j=1}^2 (i\omega \nu_0 + N_j(\omega) s_j(\omega)) \hat{Z}_j(\omega) \exp(s_j(\omega) y) \quad (\text{B.11b})$$

$$\hat{D}_{11}(\omega, y) = \sum_{j=1}^2 (s_j(\omega) + N_j(\omega) i\omega) \hat{Y}_j(\omega) \exp(s_j(\omega) y) \quad (\text{B.11c})$$

$$\hat{D}_{12}(\omega, y) = \sum_{j=1}^2 (s_j(\omega) + N_j(\omega)i\omega) \hat{Z}_j(\omega) \exp(s_j(\omega)y) \quad (\text{B.11d})$$

Asymptotic expansions of the integrands $\hat{F}_{11}(\omega, y)$, $\hat{F}_{11}(-\omega, y)$, $\hat{F}_{12}(\omega, y)$, $\hat{F}_{12}(-\omega, y)$, $\hat{D}_{11}(\omega, y)$, $\hat{D}_{11}(-\omega, y)$, $\hat{D}_{12}(\omega, y)$ and $\hat{D}_{12}(-\omega, y)$ are expressed in the following form as ω approaches infinity.

$$\hat{F}_{11}^{\infty}(\omega, y) = \hat{F}_{111}^{\infty}(\omega) \exp(s_1(\omega)y) + \hat{F}_{112}^{\infty}(\omega) \exp(s_2(\omega)y) \quad (\text{B.12a})$$

$$\hat{F}_{11}^{\infty}(-\omega, y) = \hat{F}_{111}^{\infty}(-\omega) \exp(s_1(-\omega)y) + \hat{F}_{112}^{\infty}(-\omega) \exp(s_2(-\omega)y) \quad (\text{B.12b})$$

$$\hat{F}_{12}^{\infty}(\omega, y) = \hat{F}_{121}^{\infty}(\omega) \exp(s_1(\omega)y) + \hat{F}_{122}^{\infty}(\omega) \exp(s_2(\omega)y) \quad (\text{B.12c})$$

$$\hat{F}_{12}^{\infty}(-\omega, y) = \hat{F}_{121}^{\infty}(-\omega) \exp(s_1(-\omega)y) + \hat{F}_{122}^{\infty}(-\omega) \exp(s_2(-\omega)y) \quad (\text{B.12d})$$

$$\hat{D}_{11}^{\infty}(\omega, y) = \hat{D}_{111}^{\infty}(\omega) \exp(s_1(\omega)y) + \hat{D}_{112}^{\infty}(\omega) \exp(s_2(\omega)y) \quad (\text{B.12e})$$

$$\hat{D}_{11}^{\infty}(-\omega, y) = \hat{D}_{111}^{\infty}(-\omega) \exp(s_1(-\omega)y) + \hat{D}_{112}^{\infty}(-\omega) \exp(s_2(-\omega)y) \quad (\text{B.12f})$$

$$\hat{D}_{12}^{\infty}(\omega, y) = \hat{D}_{121}^{\infty}(\omega) \exp(s_1(\omega)y) + \hat{D}_{122}^{\infty}(\omega) \exp(s_2(\omega)y) \quad (\text{B.12g})$$

$$\hat{D}_{12}^{\infty}(-\omega, y) = \hat{D}_{121}^{\infty}(-\omega) \exp(s_1(-\omega)y) + \hat{D}_{122}^{\infty}(-\omega) \exp(s_2(-\omega)y) \quad (\text{B.12h})$$

where

$$\hat{F}_{111}^{\infty}(\omega) = a_0 + \frac{a_2}{\omega^2} \quad (\text{B.13a})$$

$$\hat{F}_{112}^{\infty}(\omega) = b_0 + \frac{b_2}{\omega^2} \quad (\text{B.13b})$$

$$\hat{F}_{111}^{\infty}(-\omega) = c_0 + \frac{c_2}{\omega^2} \quad (\text{B.13c})$$

$$\hat{F}_{112}^{\infty}(-\omega) = d_0 + \frac{d_2}{\omega^2} \quad (\text{B.13d})$$

$$\hat{F}_{121}^{\infty}(\omega) = e_0 + \frac{e_1}{\omega} + \frac{e_2}{\omega^2} \quad (\text{B.13e})$$

$$\hat{F}_{122}^{\infty}(\omega) = f_0 + \frac{f_1}{\omega} + \frac{f_2}{\omega^2} \quad (\text{B.13f})$$

$$\hat{F}_{121}^{\infty}(-\omega) = g_0 + \frac{g_1}{\omega} + \frac{g_2}{\omega^2} \quad (\text{B.13g})$$

$$\hat{F}_{122}^{\infty}(-\omega) = h_0 + \frac{h_1}{\omega} + \frac{h_2}{\omega^2} \quad (\text{B.13h})$$

$$\hat{D}_{111}^{\infty}(\omega) = a_{10} + \frac{a_{11}}{\omega} + \frac{a_{12}}{\omega^2} + \frac{a_{13}}{\omega^3} \quad (\text{B.13i})$$

$$\hat{D}_{112}^{\infty}(\omega) = b_{10} + \frac{b_{11}}{\omega} + \frac{b_{12}}{\omega^2} + \frac{b_{13}}{\omega^3} \quad (\text{B.13j})$$

$$\hat{D}_{111}^{\infty}(-\omega) = c_{10} + \frac{c_{11}}{\omega} + \frac{c_{12}}{\omega^2} + \frac{c_{13}}{\omega^3} \quad (\text{B.13k})$$

$$\hat{D}_{112}^{\infty}(-\omega) = d_{10} + \frac{d_{11}}{\omega} + \frac{d_{12}}{\omega^2} + \frac{d_{13}}{\omega^3} \quad (\text{B.13l})$$

$$\hat{D}_{121}^{\infty}(\omega) = e_{10} + \frac{e_{12}}{\omega^2} \quad (\text{B.13m})$$

$$\hat{D}_{122}^{\infty}(\omega) = f_{10} + \frac{f_{12}}{\omega^2} \quad (\text{B.13n})$$

$$\hat{D}_{121}^{\infty}(-\omega) = g_{10} + \frac{g_{12}}{\omega^2} \quad (\text{B.13p})$$

$$\hat{D}_{122}^{\infty}(-\omega) = h_{10} + \frac{h_{12}}{\omega^2} \quad (\text{B.13r})$$

where $a_0, a_2, b_0, b_2, c_0, c_2, d_0, d_2, e_0, e_1, e_2, f_0, f_1, f_2, g_0, g_1, g_2, h_0, h_1, h_2, a_{10}, a_{11}, a_{12}, a_{13}, b_{10}, b_{11}, b_{12}, b_{13}, c_{10}, c_{11}, c_{12}, c_{13}, d_{10}, d_{11}, d_{12}, d_{13}, e_{10}, e_{12}, f_{10}, f_{12}, g_{10}, g_{12}, h_{10}, h_{12}$ are determined using symbolic manipulator MAPLE as follows:

$$a_0 = (1/4)i\sqrt{\kappa_0 + \sqrt{\kappa_0^2 - 1}} \left(-\nu_0 \kappa_0 - 1 + \nu_0 \sqrt{\kappa_0^2 - 1} \right) \left(\nu_0 - \nu_0^3 - \kappa_0 \nu_0^2 + \kappa_0 + \sqrt{\kappa_0^2 - 1} \nu_0^2 - \sqrt{\kappa_0^2 - 1} \right) \left((1 + \nu_0^2 + 2\nu_0 \kappa_0) \sqrt{\kappa_0^2 - 1} \right)^{-1} \quad (\text{B.14})$$

$$a_2 = -(1/32)i\gamma^2 \left(-2\nu_0^2 \kappa_0^4 + 2\kappa_0^4 - 4\nu_0^3 \kappa_0^3 + 2\kappa_0^3 \sqrt{\kappa_0^2 - 1} \nu_0^2 + 4\nu_0 \kappa_0^3 - 2\kappa_0^3 \sqrt{\kappa_0^2 - 1} + 4\sqrt{\kappa_0^2 - 1} \nu_0^3 \kappa_0^2 + 3\nu_0^2 \kappa_0^2 - 4\kappa_0^2 \sqrt{\kappa_0^2 - 1} \nu_0 - 3\kappa_0^2 + 8\nu_0^3 \kappa_0 - 2\sqrt{\kappa_0^2 - 1} \nu_0^2 \kappa_0 - 8\nu_0 \kappa_0 + 2\kappa_0 \sqrt{\kappa_0^2 - 1} - 6\sqrt{\kappa_0^2 - 1} \nu_0^3 - \nu_0^2 + 6\nu_0 \sqrt{\kappa_0^2 - 1} + 1 \right) \left(-\kappa_0 + \sqrt{\kappa_0^2 - 1} \right)^3 \left(\kappa_0 + \sqrt{\kappa_0^2 - 1} \right)^{-5/2} \left(\kappa_0^2 - 1 \right)^{-3/2} \quad (\text{B.15})$$

$$\begin{aligned}
b_0 = & -(1/4)i\sqrt{\kappa_0 - \sqrt{\kappa_0^2 - 1}} \left(\nu_0 \kappa_0 + 1 + \nu_0 \sqrt{\kappa_0^2 - 1} \right) \left(-\nu_0 + \nu_0^3 + \kappa_0 \nu_0^2 - \kappa_0 \right. \\
& \left. + \sqrt{\kappa_0^2 - 1} \nu_0^2 - \sqrt{\kappa_0^2 - 1} \right) \left((1 + \nu_0^2 + 2\nu_0 \kappa_0) \sqrt{\kappa_0^2 - 1} \right)^{-1} \quad (\text{B.16})
\end{aligned}$$

$$\begin{aligned}
b_2 = & (1/32)i\gamma^2 \left(2\nu_0^2 \kappa_0^4 - 2\kappa_0^4 + 4\nu_0^3 \kappa_0^3 + 2\kappa_0^3 \sqrt{\kappa_0^2 - 1} \nu_0^2 - 4\nu_0 \kappa_0^3 - 2\kappa_0^3 \sqrt{\kappa_0^2 - 1} \right. \\
& + 4\sqrt{\kappa_0^2 - 1} \nu_0^3 \kappa_0^2 - 3\nu_0^2 \kappa_0^2 - 4\kappa_0^2 \sqrt{\kappa_0^2 - 1} \nu_0 + 3\kappa_0^2 - 8\nu_0^3 \kappa_0 - 2\sqrt{\kappa_0^2 - 1} \nu_0^2 \kappa_0 \\
& \left. + 8\nu_0 \kappa_0 + 2\kappa_0 \sqrt{\kappa_0^2 - 1} - 6\sqrt{\kappa_0^2 - 1} \nu_0^3 + \nu_0^2 + 6\nu_0 \sqrt{\kappa_0^2 - 1} - 1 \right) \\
& (\kappa_0^2 - 1)^{-3/2} (\kappa_0 - \sqrt{\kappa_0^2 - 1})^{-5/2} (\kappa_0 + \sqrt{\kappa_0^2 - 1})^{-3} \quad (\text{B.17})
\end{aligned}$$

$$\begin{aligned}
c_0 = & (1/4)i\sqrt{\kappa_0 - \sqrt{\kappa_0^2 - 1}} \left(\nu_0 \kappa_0 + 1 + \nu_0 \sqrt{\kappa_0^2 - 1} \right) \left(-\nu_0 + \nu_0^3 + \kappa_0 \nu_0^2 - \kappa_0 \right. \\
& \left. + \sqrt{\kappa_0^2 - 1} \nu_0^2 - \sqrt{\kappa_0^2 - 1} \right) \left((1 + \nu_0^2 + 2\nu_0 \kappa_0) \sqrt{\kappa_0^2 - 1} \right)^{-1} \quad (\text{B.18})
\end{aligned}$$

$$\begin{aligned}
c_2 = & -(1/32)i\gamma^2 \left(2\nu_0^2 \kappa_0^4 - 2\kappa_0^4 + 4\nu_0^3 \kappa_0^3 + 2\kappa_0^3 \sqrt{\kappa_0^2 - 1} \nu_0^2 - 4\nu_0 \kappa_0^3 - 2\kappa_0^3 \sqrt{\kappa_0^2 - 1} \right. \\
& + 4\sqrt{\kappa_0^2 - 1} \nu_0^3 \kappa_0^2 - 3\nu_0^2 \kappa_0^2 - 4\kappa_0^2 \sqrt{\kappa_0^2 - 1} \nu_0 + 3\kappa_0^2 - 8\nu_0^3 \kappa_0 - 2\sqrt{\kappa_0^2 - 1} \nu_0^2 \kappa_0 \\
& \left. + 8\nu_0 \kappa_0 + 2\kappa_0 \sqrt{\kappa_0^2 - 1} - 6\sqrt{\kappa_0^2 - 1} \nu_0^3 + \nu_0^2 + 6\nu_0 \sqrt{\kappa_0^2 - 1} - 1 \right) \\
& (\kappa_0^2 - 1)^{-3/2} (\kappa_0 - \sqrt{\kappa_0^2 - 1})^{-5/2} (\kappa_0 + \sqrt{\kappa_0^2 - 1})^{-3} \quad (\text{B.19})
\end{aligned}$$

$$\begin{aligned}
d_0 = & -(1/4)i(\nu_0^2 - 1) \sqrt{\kappa_0 + \sqrt{\kappa_0^2 - 1}} \left(\nu_0 \kappa_0 + 1 - \nu_0 \sqrt{\kappa_0^2 - 1} \right) \left(\nu_0 + \kappa_0 - \sqrt{\kappa_0^2 - 1} \right) \\
& \left((1 + \nu_0^2 + 2\nu_0 \kappa_0) \sqrt{\kappa_0^2 - 1} \right)^{-1} \quad (\text{B.20})
\end{aligned}$$

$$\begin{aligned}
d_2 = & (1/32)i\gamma^2 \left(2\nu_0^2 \kappa_0^4 - 2\kappa_0^4 + 4\nu_0^3 \kappa_0^3 - 2\kappa_0^3 \sqrt{\kappa_0^2 - 1} \nu_0^2 - 4\nu_0 \kappa_0^3 + 2\kappa_0^3 \sqrt{\kappa_0^2 - 1} \right. \\
& - 4\sqrt{\kappa_0^2 - 1} \nu_0^3 \kappa_0^2 - 3\nu_0^2 \kappa_0^2 + 4\kappa_0^2 \sqrt{\kappa_0^2 - 1} \nu_0 + 3\kappa_0^2 - 8\nu_0^3 \kappa_0 + 2\sqrt{\kappa_0^2 - 1} \nu_0^2 \kappa_0 \\
& \left. + 8\nu_0 \kappa_0 - 2\kappa_0 \sqrt{\kappa_0^2 - 1} + 6\sqrt{\kappa_0^2 - 1} \nu_0^3 + \nu_0^2 - 6\nu_0 \sqrt{\kappa_0^2 - 1} - 1 \right)
\end{aligned}$$

$$\left(\kappa_0 - \sqrt{\kappa_0^2 - 1}\right)^{-3} \left(\kappa_0 + \sqrt{\kappa_0^2 - 1}\right)^{-5/2} (\kappa_0^2 - 1)^{-3/2} \quad (\text{B.21})$$

$$e_0 = \left(-\nu_0 + \nu_0^3 + \kappa_0 \nu_0^2 - \kappa_0 - \sqrt{\kappa_0^2 - 1} \nu_0^2 + \sqrt{\kappa_0^2 - 1}\right) \left(\nu_0 + \kappa_0 + \sqrt{\kappa_0^2 - 1}\right) \\ \left(4(1 + \nu_0^2 + 2\nu_0 \kappa_0) \sqrt{\kappa_0^2 - 1}\right)^{-1} \quad (\text{B.22})$$

$$e_1 = \gamma \left(2\nu_0^2 \kappa_0^2 - 2\kappa_0^2 - 2\sqrt{\kappa_0^2 - 1} \nu_0^2 \kappa_0 + 2\kappa_0 \sqrt{\kappa_0^2 - 1} + 1 - \nu_0^2\right) \\ \left(8\left(\kappa_0 - \sqrt{\kappa_0^2 - 1}\right)^2 \sqrt{\kappa_0 + \sqrt{\kappa_0^2 - 1}} \sqrt{\kappa_0^2 - 1}\right)^{-1} \quad (\text{B.23})$$

$$e_2 = (1/8) \gamma^2 \nu_0 (\nu_0^2 - 1) (\kappa_0^2 - 1)^{-3/2} \left(\kappa_0 + \sqrt{\kappa_0^2 - 1}\right)^{-3} \left(\kappa_0 - \sqrt{\kappa_0^2 - 1}\right)^3 \quad (\text{B.24})$$

$$f_0 = -\left(-\nu_0 + \nu_0^3 + \kappa_0 \nu_0^2 - \kappa_0 + \sqrt{\kappa_0^2 - 1} \nu_0^2 - \sqrt{\kappa_0^2 - 1}\right) \left(\nu_0 + \kappa_0 - \sqrt{\kappa_0^2 - 1}\right) \\ \left(4(1 + \nu_0^2 + 2\nu_0 \kappa_0) \sqrt{\kappa_0^2 - 1}\right)^{-1} \quad (\text{B.25})$$

$$f_1 = -\gamma \left(2\nu_0^2 \kappa_0^2 - 2\kappa_0^2 + 2\sqrt{\kappa_0^2 - 1} \nu_0^2 \kappa_0 - 2\kappa_0 \sqrt{\kappa_0^2 - 1} + 1 - \nu_0^2\right) \\ \left(8\sqrt{\kappa_0 - \sqrt{\kappa_0^2 - 1}} \left(\kappa_0 + \sqrt{\kappa_0^2 - 1}\right)^2 \sqrt{\kappa_0^2 - 1}\right)^{-1} \quad (\text{B.26})$$

$$f_2 = -(1/8) \gamma^2 \nu_0 (\nu_0^2 - 1) (\kappa_0^2 - 1)^{-3/2} \left(\kappa_0 + \sqrt{\kappa_0^2 - 1}\right)^{-3} \left(\kappa_0 - \sqrt{\kappa_0^2 - 1}\right)^3 \quad (\text{B.27})$$

$$g_0 = -\left(-\nu_0 + \nu_0^3 + \kappa_0 \nu_0^2 - \kappa_0 + \sqrt{\kappa_0^2 - 1} \nu_0^2 - \sqrt{\kappa_0^2 - 1}\right) \left(\nu_0 + \kappa_0 - \sqrt{\kappa_0^2 - 1}\right) \\ \left(4(1 + \nu_0^2 + 2\nu_0 \kappa_0) \sqrt{\kappa_0^2 - 1}\right)^{-1} \quad (\text{B.28})$$

$$g_1 = -\gamma(2\nu_0^2\kappa_0^2 - 2\kappa_0^2 + 2\sqrt{\kappa_0^2 - 1}\nu_0^2\kappa_0 - 2\kappa_0\sqrt{\kappa_0^2 - 1} + 1 - \nu_0^2) \left(8\sqrt{\kappa_0 - \sqrt{\kappa_0^2 - 1}}(\kappa_0 + \sqrt{\kappa_0^2 - 1})^2\sqrt{\kappa_0^2 - 1}\right)^{-1} \quad (\text{B.29})$$

$$g_2 = (1/8)\gamma^2\nu_0(\nu_0^2 - 1)(\kappa_0^2 - 1)^{-3/2}(\kappa_0 + \sqrt{\kappa_0^2 - 1})^3(-\kappa_0 + \sqrt{\kappa_0^2 - 1})^{-3} \quad (\text{B.30})$$

$$h_0 = (-\nu_0 + \nu_0^3 + \kappa_0\nu_0^2 - \kappa_0 - \sqrt{\kappa_0^2 - 1}\nu_0^2 + \sqrt{\kappa_0^2 - 1})(\nu_0 + \kappa_0 + \sqrt{\kappa_0^2 - 1}) \left(4(1 + \nu_0^2 + 2\nu_0\kappa_0)\sqrt{\kappa_0^2 - 1}\right)^{-1} \quad (\text{B.31})$$

$$h_1 = \gamma(2\nu_0^2\kappa_0^2 - 2\kappa_0^2 - 2\sqrt{\kappa_0^2 - 1}\nu_0^2\kappa_0 + 2\kappa_0\sqrt{\kappa_0^2 - 1} + 1 - \nu_0^2) \left(8(\kappa_0 - \sqrt{\kappa_0^2 - 1})^2\sqrt{\kappa_0 + \sqrt{\kappa_0^2 - 1}}\sqrt{\kappa_0^2 - 1}\right)^{-1} \quad (\text{B.32})$$

$$h_2 = (1/8)\gamma^2\nu_0(\nu_0^2 - 1)(\kappa_0^2 - 1)^{-3/2}(\kappa_0 + \sqrt{\kappa_0^2 - 1})^3(\kappa_0 - \sqrt{\kappa_0^2 - 1})^{-3} \quad (\text{B.33})$$

$$a_{10} = -(\kappa_0\nu_0^2 + \kappa_0 - \sqrt{\kappa_0^2 - 1}\nu_0^2 + \nu_0 + \nu_0\kappa_0^2 - \sqrt{\kappa_0^2 - 1}\nu_0\kappa_0)(\nu_0\kappa_0 + 1 + \nu_0\sqrt{\kappa_0^2 - 1}) \left(2(1 + \nu_0^2 + 2\nu_0\kappa_0)\sqrt{\kappa_0^2 - 1}\right)^{-1} \quad (\text{B.34})$$

$$a_{11} = \gamma(\kappa_0 + \nu_0) \left(4\sqrt{\kappa_0^2 - 1}\sqrt{\kappa_0 + \sqrt{\kappa_0^2 - 1}}\right)^{-1} \quad (\text{B.35})$$

$$a_{12} = -(1/4)(\kappa_0 + \nu_0)\gamma^2\nu_0(\kappa_0^2 - 1)^{-3/2}(\kappa_0 - \sqrt{\kappa_0^2 - 1})^3(\kappa_0 + \sqrt{\kappa_0^2 - 1})^{-3} \quad (\text{B.36})$$

$$\begin{aligned}
a_{13} = & -\left(\kappa_0^4 + 3\nu_0\kappa_0^3 - \kappa_0^3\sqrt{\kappa_0^2 - 1} + 2\nu_0^2\kappa_0^2 - 3\kappa_0^2\sqrt{\kappa_0^2 - 1}\nu_0 - \kappa_0^2 - 2\sqrt{\kappa_0^2 - 1}\nu_0^2\kappa_0 \right. \\
& \left. - 7\nu_0\kappa_0 + \kappa_0\sqrt{\kappa_0^2 - 1} - 6\nu_0^2 + \nu_0\sqrt{\kappa_0^2 - 1}\right)\gamma^3\left(32(\kappa_0^2 - 1)^{3/2}\left(\kappa_0 + \sqrt{\kappa_0^2 - 1}\right)^{13/2}\right. \\
& \left.\left(\kappa_0 - \sqrt{\kappa_0^2 - 1}\right)^6\right)^{-1} \quad (\text{B.37})
\end{aligned}$$

$$\begin{aligned}
b_{10} = & \left(\kappa_0\nu_0^2 + \kappa_0 + \sqrt{\kappa_0^2 - 1}\nu_0^2 + \nu_0 + \nu_0\kappa_0^2 + \sqrt{\kappa_0^2 - 1}\nu_0\kappa_0\right)\left(\nu_0\kappa_0 + 1 - \nu_0\sqrt{\kappa_0^2 - 1}\right) \\
& \left(2(1 + \nu_0^2 + 2\nu_0\kappa_0)\sqrt{\kappa_0^2 - 1}\right)^{-1} \quad (\text{B.38})
\end{aligned}$$

$$b_{11} = -\gamma(\kappa_0 + \nu_0)\left(4\sqrt{\kappa_0^2 - 1}\sqrt{\kappa_0 - \sqrt{\kappa_0^2 - 1}}\right)^{-1} \quad (\text{B.39})$$

$$b_{12} = -(1/4)\nu_0(\kappa_0 + \nu_0)\gamma^2(\kappa_0^2 - 1)^{-3/2}\left(\kappa_0 + \sqrt{\kappa_0^2 - 1}\right)^{-3}\left(-\kappa_0 + \sqrt{\kappa_0^2 - 1}\right)^{-3} \quad (\text{B.40})$$

$$\begin{aligned}
b_{13} = & \left(\kappa_0^4 + 3\nu_0\kappa_0^3 + \kappa_0^3\sqrt{\kappa_0^2 - 1} + 2\nu_0^2\kappa_0^2 + 3\kappa_0^2\sqrt{\kappa_0^2 - 1}\nu_0 - \kappa_0^2 + 2\sqrt{\kappa_0^2 - 1}\nu_0^2\kappa_0 \right. \\
& \left. - 7\nu_0\kappa_0 - \kappa_0\sqrt{\kappa_0^2 - 1} - 6\nu_0^2 - \nu_0\sqrt{\kappa_0^2 - 1}\right)\gamma^3\left(32(\kappa_0^2 - 1)^{3/2}\left(\kappa_0 + \sqrt{\kappa_0^2 - 1}\right)^6\right. \\
& \left.\left(\kappa_0 - \sqrt{\kappa_0^2 - 1}\right)^{13/2}\right)^{-1} \quad (\text{B.41})
\end{aligned}$$

$$\begin{aligned}
c_{10} = & \left(\kappa_0\nu_0^2 + \kappa_0 + \sqrt{\kappa_0^2 - 1}\nu_0^2 + \nu_0 + \nu_0\kappa_0^2 + \sqrt{\kappa_0^2 - 1}\nu_0\kappa_0\right)\left(\nu_0\kappa_0 + 1 - \nu_0\sqrt{\kappa_0^2 - 1}\right) \\
& \left(2(1 + \nu_0^2 + 2\nu_0\kappa_0)\sqrt{\kappa_0^2 - 1}\right)^{-1} \quad (\text{B.42})
\end{aligned}$$

$$c_{11} = -\gamma(\kappa_0 + \nu_0)\left(4\sqrt{\kappa_0^2 - 1}\sqrt{\kappa_0 - \sqrt{\kappa_0^2 - 1}}\right)^{-1} \quad (\text{B.43})$$

$$c_{12} = -(1/4)\nu_0(\kappa_0 + \nu_0)\gamma^2(\kappa_0^2 - 1)^{-3/2}(\kappa_0 + \sqrt{\kappa_0^2 - 1})^3(-\kappa_0 + \sqrt{\kappa_0^2 - 1})^{-3} \quad (\text{B.44})$$

$$c_{13} = \left(\kappa_0^4 + 3\nu_0\kappa_0^3 + \kappa_0^3\sqrt{\kappa_0^2 - 1} + 2\nu_0^2\kappa_0^2 + 3\kappa_0^2\sqrt{\kappa_0^2 - 1}\nu_0 - \kappa_0^2 + 2\sqrt{\kappa_0^2 - 1}\nu_0^2\kappa_0 \right. \\ \left. - 7\nu_0\kappa_0 - \kappa_0\sqrt{\kappa_0^2 - 1} - 6\nu_0^2 - \nu_0\sqrt{\kappa_0^2 - 1} \right) \gamma^3 \left(32(\kappa_0^2 - 1)^{3/2}(\kappa_0 + \sqrt{\kappa_0^2 - 1})^6 \right. \\ \left. (\kappa_0 - \sqrt{\kappa_0^2 - 1})^{13/2} \right)^{-1} \quad (\text{B.45})$$

$$d_{10} = -\left(\kappa_0\nu_0^2 + \kappa_0 - \sqrt{\kappa_0^2 - 1}\nu_0^2 + \nu_0 + \nu_0\kappa_0^2 - \sqrt{\kappa_0^2 - 1}\nu_0\kappa_0 \right) \left(\nu_0\kappa_0 + 1 + \nu_0\sqrt{\kappa_0^2 - 1} \right) \\ \left(2(1 + \nu_0^2 + 2\nu_0\kappa_0)\sqrt{\kappa_0^2 - 1} \right)^{-1} \quad (\text{B.46})$$

$$d_{11} = \gamma(\kappa_0 + \nu_0) \left(4\sqrt{\kappa_0^2 - 1}\sqrt{\kappa_0 + \sqrt{\kappa_0^2 - 1}} \right)^{-1} \quad (\text{B.47})$$

$$d_{12} = (1/4)\nu_0(\kappa_0 + \nu_0)\gamma^2(\kappa_0^2 - 1)^{-3/2}(\kappa_0 + \sqrt{\kappa_0^2 - 1})^3(-\kappa_0 + \sqrt{\kappa_0^2 - 1})^{-3} \quad (\text{B.48})$$

$$d_{13} = \left(-\kappa_0^4 - 3\nu_0\kappa_0^3 + \kappa_0^3\sqrt{\kappa_0^2 - 1} - 2\nu_0^2\kappa_0^2 + 3\kappa_0^2\sqrt{\kappa_0^2 - 1}\nu_0 + \kappa_0^2 + 2\sqrt{\kappa_0^2 - 1}\nu_0^2\kappa_0 \right. \\ \left. + 7\nu_0\kappa_0 - \kappa_0\sqrt{\kappa_0^2 - 1} + 6\nu_0^2 - \nu_0\sqrt{\kappa_0^2 - 1} \right) \gamma^3 \left(32(\kappa_0^2 - 1)^{3/2}(-\kappa_0 + \sqrt{\kappa_0^2 - 1})^6 \right. \\ \left. (\kappa_0 + \sqrt{\kappa_0^2 - 1})^{13/2} \right)^{-1} \quad (\text{B.49})$$

$$e_{10} = (1/2)i\left(\nu_0 + \kappa_0 + \sqrt{\kappa_0^2 - 1} \right) \left(\kappa_0\nu_0^2 + \kappa_0 + \sqrt{\kappa_0^2 - 1}\nu_0^2 + \nu_0 + \nu_0\kappa_0^2 + \sqrt{\kappa_0^2 - 1}\nu_0\kappa_0 \right) \\ \left(\sqrt{\kappa_0 + \sqrt{\kappa_0^2 - 1}}(1 + \nu_0^2 + 2\nu_0\kappa_0)\sqrt{\kappa_0^2 - 1} \right)^{-1} \quad (\text{B.50})$$

$$\begin{aligned}
e_{12} = & -(1/16)i\gamma^2 \left(\kappa_0^4 - \nu_0 \kappa_0^3 - \kappa_0^3 \sqrt{\kappa_0^2 - 1} - 2\nu_0^2 \kappa_0^2 + \kappa_0^2 \sqrt{\kappa_0^2 - 1} \nu_0 - \kappa_0^2 \right. \\
& \left. + 2\sqrt{\kappa_0^2 - 1} \nu_0^2 \kappa_0 - 3\nu_0 \kappa_0 + \kappa_0 \sqrt{\kappa_0^2 - 1} - 2\nu_0^2 + \nu_0 \sqrt{\kappa_0^2 - 1} \right) \\
& \left((\kappa_0^2 - 1)^{3/2} (\kappa_0 + \sqrt{\kappa_0^2 - 1})^{7/2} (\kappa_0 - \sqrt{\kappa_0^2 - 1})^4 \right)^{-1} \quad (\text{B.51})
\end{aligned}$$

$$\begin{aligned}
f_{10} = & -(1/2)i \left(\kappa_0 \nu_0^2 + \kappa_0 - \sqrt{\kappa_0^2 - 1} \nu_0^2 + \nu_0 + \nu_0 \kappa_0^2 - \sqrt{\kappa_0^2 - 1} \nu_0 \kappa_0 \right) \left(\nu_0 + \kappa_0 - \sqrt{\kappa_0^2 - 1} \right) \\
& \left(\sqrt{\kappa_0 - \sqrt{\kappa_0^2 - 1}} (1 + \nu_0^2 + 2\nu_0 \kappa_0) \sqrt{\kappa_0^2 - 1} \right)^{-1} \quad (\text{B.52})
\end{aligned}$$

$$\begin{aligned}
f_{12} = & (1/16)i\gamma^2 \left(\kappa_0^4 - \nu_0 \kappa_0^3 + \kappa_0^3 \sqrt{\kappa_0^2 - 1} - 2\nu_0^2 \kappa_0^2 - \kappa_0^2 - \kappa_0^2 \sqrt{\kappa_0^2 - 1} \nu_0 \right. \\
& \left. - 2\sqrt{\kappa_0^2 - 1} \nu_0^2 \kappa_0 - 3\nu_0 \kappa_0 - \kappa_0 \sqrt{\kappa_0^2 - 1} - 2\nu_0^2 - \nu_0 \sqrt{\kappa_0^2 - 1} \right) \\
& \left((\kappa_0^2 - 1)^{3/2} (\kappa_0 - \sqrt{\kappa_0^2 - 1})^{7/2} (\kappa_0 + \sqrt{\kappa_0^2 - 1})^4 \right)^{-1} \quad (\text{B.53})
\end{aligned}$$

$$\begin{aligned}
g_{10} = & (1/2)i \left(\kappa_0 \nu_0^2 + \kappa_0 - \sqrt{\kappa_0^2 - 1} \nu_0^2 + \nu_0 + \nu_0 \kappa_0^2 - \sqrt{\kappa_0^2 - 1} \nu_0 \kappa_0 \right) \left(\nu_0 + \kappa_0 - \sqrt{\kappa_0^2 - 1} \right) \\
& \left(\sqrt{\kappa_0 - \sqrt{\kappa_0^2 - 1}} (1 + \nu_0^2 + 2\nu_0 \kappa_0) \sqrt{\kappa_0^2 - 1} \right)^{-1} \quad (\text{B.54})
\end{aligned}$$

$$\begin{aligned}
g_{12} = & -(1/16)i\gamma^2 \left(\kappa_0^4 - \nu_0 \kappa_0^3 + \kappa_0^3 \sqrt{\kappa_0^2 - 1} - 2\nu_0^2 \kappa_0^2 - \kappa_0^2 - \kappa_0^2 \sqrt{\kappa_0^2 - 1} \nu_0 \right. \\
& \left. - 2\sqrt{\kappa_0^2 - 1} \nu_0^2 \kappa_0 - 3\nu_0 \kappa_0 - \kappa_0 \sqrt{\kappa_0^2 - 1} - 2\nu_0^2 - \nu_0 \sqrt{\kappa_0^2 - 1} \right) \\
& \left((\kappa_0^2 - 1)^{3/2} (\kappa_0 - \sqrt{\kappa_0^2 - 1})^{7/2} (\kappa_0 + \sqrt{\kappa_0^2 - 1})^4 \right)^{-1} \quad (\text{B.55})
\end{aligned}$$

$$\begin{aligned}
h_{10} = & -(1/2)i \left(\nu_0 + \kappa_0 + \sqrt{\kappa_0^2 - 1} \right) \left(\kappa_0 \nu_0^2 + \kappa_0 + \sqrt{\kappa_0^2 - 1} \nu_0^2 + \nu_0 + \nu_0 \kappa_0^2 + \sqrt{\kappa_0^2 - 1} \nu_0 \kappa_0 \right) \\
& \left(\sqrt{\kappa_0 + \sqrt{\kappa_0^2 - 1}} (1 + \nu_0^2 + 2\nu_0 \kappa_0) \sqrt{\kappa_0^2 - 1} \right)^{-1} \quad (\text{B.56})
\end{aligned}$$

$$\begin{aligned}
h_{12} = & -(1/16)i\gamma^2 \left(-\kappa_0^4 + \kappa_0^3 \sqrt{\kappa_0^2 - 1} + \nu_0 \kappa_0^3 + 2\nu_0^2 \kappa_0^2 - \kappa_0^2 \sqrt{\kappa_0^2 - 1} \nu_0 + \kappa_0^2 \right. \\
& \left. + 3\nu_0 \kappa_0 - \kappa_0 \sqrt{\kappa_0^2 - 1} - 2\sqrt{\kappa_0^2 - 1} \nu_0^2 \kappa_0 + 2\nu_0^2 - \nu_0 \sqrt{\kappa_0^2 - 1} \right) \\
& \left((\kappa_0^2 - 1)^{3/2} (\kappa_0 + \sqrt{\kappa_0^2 - 1})^{7/2} (-\kappa_0 + \sqrt{\kappa_0^2 - 1})^4 \right)^{-1} \quad (\text{B.57})
\end{aligned}$$

Then, the asymptotic expansions of the integrands $F_{11}(\omega, y)$, $F_{11}(-\omega, y)$, $F_{12}(\omega, y)$, $F_{12}(-\omega, y)$, $D_{11}(\omega, y)$, $D_{11}(-\omega, y)$, $D_{12}(\omega, y)$ and $D_{12}(-\omega, y)$ are taken as equal to the asymptotic expansions of the integrands $\hat{F}_{11}(\omega, y)$, $\hat{F}_{11}(-\omega, y)$, $\hat{F}_{12}(\omega, y)$, $\hat{F}_{12}(-\omega, y)$, $\hat{D}_{11}(\omega, y)$, $\hat{D}_{11}(-\omega, y)$, $\hat{D}_{12}(\omega, y)$ and $\hat{D}_{12}(-\omega, y)$, respectively, as ω approaches infinity. Expressions for $F_{11}^\infty(\omega, 0)$, $F_{11}^\infty(-\omega, 0)$, $F_{12}^\infty(\omega, 0)$, $F_{12}^\infty(-\omega, 0)$, $D_{11}^\infty(\omega, 0)$, $D_{11}^\infty(-\omega, 0)$, $D_{12}^\infty(\omega, 0)$ and $D_{12}^\infty(-\omega, 0)$ are given in Eq.(2.2.56).

APPENDIX C

DEFINITIONS OF FUNCTIONS APPEARING IN THE INTEGRAL EQUATIONS

Definitions of $H_{ij}(x, t)$, ($i = 1, 2$ and $j = 1, 2, \dots, 8$), are given as follows:

$$\begin{aligned}
 H_{11}(x, t) = & \frac{1}{2\pi} \left\{ \int_0^{A_{11}} [F_{11}(\omega, 0) - (a_0 + b_0)] \cos(\omega(x-t)) d\omega \right. \\
 & \left. + \int_{A_{11}}^{\infty} \left[F_{11}(\omega, 0) - (a_0 + b_0) - \frac{a_2 + b_2}{\omega^2} \right] \cos(\omega(x-t)) d\omega + \int_{A_{11}}^{\infty} \frac{a_2 + b_2}{\omega^2} \cos(\omega(x-t)) d\omega \right\}
 \end{aligned}
 \tag{C.1a}$$

$$\begin{aligned}
 H_{12}(x, t) = & \frac{1}{2\pi} \left\{ \int_0^{A_{12}} [F_{11}(-\omega, 0) - (c_0 + d_0)] \cos(\omega(x-t)) d\omega \right. \\
 & \left. + \int_{A_{12}}^{\infty} \left[F_{11}(-\omega, 0) - (c_0 + d_0) - \frac{c_2 + d_2}{\omega^2} \right] \cos(\omega(x-t)) d\omega + \int_{A_{12}}^{\infty} \frac{c_2 + d_2}{\omega^2} \cos(\omega(x-t)) d\omega \right\}
 \end{aligned}
 \tag{C.1b}$$

$$\begin{aligned}
 H_{13}(x, t) = & \frac{1}{2\pi} i \left\{ \int_0^{A_{13}} [F_{11}(\omega, 0) - (a_0 + b_0)] \sin(\omega(x-t)) d\omega \right. \\
 & \left. + \int_{A_{13}}^{\infty} \left[F_{11}(\omega, 0) - (a_0 + b_0) - \frac{a_2 + b_2}{\omega^2} \right] \sin(\omega(x-t)) d\omega + \int_{A_{13}}^{\infty} \frac{a_2 + b_2}{\omega^2} \sin(\omega(x-t)) d\omega \right\}
 \end{aligned}
 \tag{C.1c}$$

$$\begin{aligned}
H_{14}(x,t) &= \frac{1}{2\pi} i \left\{ \int_0^{A_{14}} [F_{11}(-\omega,0) - (c_0 + d_0)] \sin(\omega(x-t)) d\omega \right. \\
&+ \left. \int_{A_{14}}^{\infty} \left[F_{11}(-\omega,0) - (c_0 + d_0) - \frac{c_2 + d_2}{\omega^2} \right] \sin(\omega(x-t)) d\omega + \int_{A_{14}}^{\infty} \frac{c_2 + d_2}{\omega^2} \sin(\omega(x-t)) d\omega \right\} \\
\end{aligned} \tag{C.1d}$$

$$\begin{aligned}
H_{15}(x,t) &= \frac{1}{2\pi} \left\{ \int_0^{A_{15}} [F_{12}(\omega,0) - (e_0 + f_0)] \cos(\omega(x-t)) d\omega \right. \\
&+ \int_{A_{15}}^{\infty} \left[F_{12}(\omega,0) - (e_0 + f_0) - \frac{e_1 + f_1}{\omega} - \frac{e_2 + f_2}{\omega^2} \right] \cos(\omega(x-t)) d\omega \\
&- (e_1 + f_1) \left[\gamma_0 + \int_0^{A_{15}|x-t|} \frac{\cos \alpha - 1}{\alpha} d\alpha \right] + \int_{A_{15}}^{\infty} \frac{e_2 + f_2}{\omega^2} \cos(\omega(x-t)) d\omega \left. \right\} \\
\end{aligned} \tag{C.1e}$$

$$\begin{aligned}
H_{16}(x,t) &= \frac{1}{2\pi} \left\{ \int_0^{A_{16}} [F_{12}(-\omega,0) - (g_0 + h_0)] \cos(\omega(x-t)) d\omega \right. \\
&+ \int_{A_{16}}^{\infty} \left[F_{12}(-\omega,0) - (g_0 + h_0) - \frac{g_1 + h_1}{\omega} - \frac{g_2 + h_2}{\omega^2} \right] \cos(\omega(x-t)) d\omega \\
&- (g_1 + h_1) \left[\gamma_0 + \int_0^{A_{16}|x-t|} \frac{\cos \alpha - 1}{\alpha} d\alpha \right] + \int_{A_{16}}^{\infty} \frac{g_2 + h_2}{\omega^2} \cos(\omega(x-t)) d\omega \left. \right\} \\
\end{aligned} \tag{C.1f}$$

$$\begin{aligned}
H_{17}(x,t) &= \frac{1}{2\pi} i \left\{ \int_0^{A_{17}} \left[F_{12}(\omega,0) - (e_0 + f_0) - \frac{e_1 + f_1}{\omega} \right] \sin(\omega(x-t)) d\omega \right. \\
&+ \int_{A_{17}}^{\infty} \left[F_{12}(\omega,0) - (e_0 + f_0) - \frac{e_1 + f_1}{\omega} - \frac{e_2 + f_2}{\omega^2} \right] \sin(\omega(x-t)) d\omega \\
&+ \left. \int_{A_{17}}^{\infty} \frac{e_2 + f_2}{\omega^2} \sin(\omega(x-t)) d\omega \right\} \\
\end{aligned} \tag{C.1g}$$

$$\begin{aligned}
H_{18}(x,t) &= \frac{1}{2\pi} i \left\{ \int_0^{A_{18}} \left[F_{12}(-\omega,0) - (g_0 + h_0) - \frac{g_1 + h_1}{\omega} \right] \sin(\omega(x-t)) d\omega \right. \\
&+ \int_{A_{18}}^{\infty} \left[F_{12}(-\omega,0) - (g_0 + h_0) - \frac{g_1 + h_1}{\omega} - \frac{g_2 + h_2}{\omega^2} \right] \sin(\omega(x-t)) d\omega \\
&\left. + \int_{A_{18}}^{\infty} \frac{g_2 + h_2}{\omega^2} \sin(\omega(x-t)) d\omega \right\} \tag{C.1h}
\end{aligned}$$

$$\begin{aligned}
H_{21}(x,t) &= \frac{1}{2\pi} \left\{ \int_0^{A_{21}} [D_{11}(\omega,0) - (a_{10} + b_{10})] \cos(\omega(x-t)) d\omega \right. \\
&+ \int_{A_{21}}^{\infty} \left[D_{11}(\omega,0) - (a_{10} + b_{10}) - \frac{a_{11} + b_{11}}{\omega} - \frac{a_{12} + b_{12}}{\omega^2} - \frac{a_{13} + b_{13}}{\omega^3} \right] \cos(\omega(x-t)) d\omega \\
&\left. - (a_{11} + b_{11}) \left[\gamma_0 + \int_0^{A_{21}|x-t|} \frac{\cos \alpha - 1}{\alpha} d\alpha \right] + \int_{A_{21}}^{\infty} \left(\frac{a_{12} + b_{12}}{\omega^2} - \frac{a_{13} + b_{13}}{\omega^3} \right) \cos(\omega(x-t)) d\omega \right\} \tag{C.1i}
\end{aligned}$$

$$\begin{aligned}
H_{22}(x,t) &= \frac{1}{2\pi} \left\{ \int_0^{A_{22}} [D_{11}(-\omega,0) - (c_{10} + d_{10})] \cos(\omega(x-t)) d\omega \right. \\
&+ \int_{A_{22}}^{\infty} \left[D_{11}(-\omega,0) - (c_{10} + d_{10}) - \frac{c_{11} + d_{11}}{\omega} - \frac{c_{12} + d_{12}}{\omega^2} - \frac{c_{13} + d_{13}}{\omega^3} \right] \cos(\omega(x-t)) d\omega \\
&\left. - (c_{11} + d_{11}) \left[\gamma_0 + \int_0^{A_{22}|x-t|} \frac{\cos \alpha - 1}{\alpha} d\alpha \right] + \int_{A_{22}}^{\infty} \left(\frac{c_{12} + d_{12}}{\omega^2} + \frac{c_{13} + d_{13}}{\omega^3} \right) \cos(\omega(x-t)) d\omega \right\} \tag{C.1j}
\end{aligned}$$

$$\begin{aligned}
H_{23}(x,t) &= \frac{1}{2\pi} i \left\{ \int_0^{A_{23}} \left[D_{11}(\omega,0) - (a_{10} + b_{10}) - \frac{a_{11} + b_{11}}{\omega} \right] \sin(\omega(x-t)) d\omega \right. \\
&+ \int_{A_{23}}^{\infty} \left[D_{11}(\omega,0) - (a_{10} + b_{10}) - \frac{a_{11} + b_{11}}{\omega} - \frac{a_{12} + b_{12}}{\omega^2} - \frac{a_{13} + b_{13}}{\omega^3} \right] \sin(\omega(x-t)) d\omega \\
&\left. + \int_{A_{23}}^{\infty} \left(\frac{a_{12} + b_{12}}{\omega^2} + \frac{a_{13} + b_{13}}{\omega^3} \right) \sin(\omega(x-t)) d\omega \right\} \quad (C.1k)
\end{aligned}$$

$$\begin{aligned}
H_{24}(x,t) &= \frac{1}{2\pi} i \left\{ \int_0^{A_{24}} \left[D_{11}(-\omega,0) - (c_{10} + d_{10}) - \frac{c_{11} + d_{11}}{\omega} \right] \sin(\omega(x-t)) d\omega \right. \\
&+ \int_{A_{24}}^{\infty} \left[D_{11}(-\omega,0) - (c_{10} + d_{10}) - \frac{c_{11} + d_{11}}{\omega} - \frac{c_{12} + d_{12}}{\omega^2} - \frac{c_{13} + d_{13}}{\omega^3} \right] \sin(\omega(x-t)) d\omega \\
&\left. + \int_{A_{24}}^{\infty} \left(\frac{c_{12} + d_{12}}{\omega^2} + \frac{c_{13} + d_{13}}{\omega^3} \right) \sin(\omega(x-t)) d\omega \right\} \quad (C.1l)
\end{aligned}$$

$$\begin{aligned}
H_{25}(x,t) &= \frac{1}{2\pi} \left\{ \int_0^{A_{25}} [D_{12}(\omega,0) - (e_{10} + f_{10})] \cos(\omega(x-t)) d\omega \right. \\
&+ \int_{A_{25}}^{\infty} \left[D_{12}(\omega,0) - (e_{10} + f_{10}) - \frac{e_{12} + f_{12}}{\omega^2} \right] \cos(\omega(x-t)) d\omega \\
&\left. + \int_{A_{25}}^{\infty} \frac{e_{12} + f_{12}}{\omega^2} \cos(\omega(x-t)) d\omega \right\} \quad (C.1m)
\end{aligned}$$

$$\begin{aligned}
H_{26}(x,t) &= \frac{1}{2\pi} \left\{ \int_0^{A_{26}} [D_{12}(-\omega,0) - (g_{10} + h_{10})] \cos(\omega(x-t)) d\omega \right. \\
&+ \int_{A_{26}}^{\infty} \left[D_{12}(-\omega,0) - (g_{10} + h_{10}) - \frac{g_{12} + h_{12}}{\omega^2} \right] \cos(\omega(x-t)) d\omega \\
&\left. + \int_{A_{26}}^{\infty} \frac{g_{12} + h_{12}}{\omega^2} \cos(\omega(x-t)) d\omega \right\} \tag{C.1n}
\end{aligned}$$

$$\begin{aligned}
H_{27}(x,t) &= \frac{1}{2\pi} i \left\{ \int_0^{A_{27}} [D_{12}(\omega,0) - (e_{10} + f_{10})] \sin(\omega(x-t)) d\omega \right. \\
&+ \int_{A_{27}}^{\infty} \left[D_{12}(\omega,0) - (e_{10} + f_{10}) - \frac{e_{12} + f_{12}}{\omega^2} \right] \sin(\omega(x-t)) d\omega \\
&\left. + \int_{A_{27}}^{\infty} \frac{e_{12} + f_{12}}{\omega^2} \sin(\omega(x-t)) d\omega \right\} \tag{C.1p}
\end{aligned}$$

$$\begin{aligned}
H_{28}(x,t) &= \frac{1}{2\pi} i \left\{ \int_0^{A_{28}} [D_{12}(-\omega,0) - (g_{10} + h_{10})] \sin(\omega(x-t)) d\omega \right. \\
&+ \int_{A_{28}}^{\infty} \left[D_{12}(-\omega,0) - (g_{10} + h_{10}) - \frac{g_{12} + h_{12}}{\omega^2} \right] \sin(\omega(x-t)) d\omega \\
&\left. + \int_{A_{28}}^{\infty} \frac{g_{12} + h_{12}}{\omega^2} \sin(\omega(x-t)) d\omega \right\} \tag{C.1r}
\end{aligned}$$

where A_{ij} , ($i=1,2$ and $j=1,2,\dots,8$), integration cut-off points and γ_0 is the Euler's constant.

APPENDIX D

Chebyshev Polynomials

Chebyshev polynomials of the first kind is defined as follows [139]:

$$T_n(x) = \cos(n \arccos(x)) \quad (\text{D.1})$$

Roots of $T_n(x)$ are given as follows [139]:

$$x_j = \cos\left(\frac{2j-1}{n} \frac{\pi}{2}\right), \quad j = 1, \dots, n \quad (\text{D.2})$$

Orthogonality condition of the Chebyshev polynomials is given as follows [139]:

$$\frac{1}{\pi} \int_{-1}^1 T_k(x) T_r(x) \frac{dx}{\sqrt{1-x^2}} = \begin{cases} 0, & k \neq r \\ 1, & k = r = 0 \\ 1/2, & k = r > 0 \end{cases} \quad (\text{D.3})$$

APPENDIX E

INTEGRALS EVALUATED IN CLOSED FORM

The integrals evaluated in closed form to obtain Eq.(2.2.66) are given as follows:

$$\frac{1}{\pi} \int_{-1}^1 \frac{i(a_0 + b_0 - c_0 - d_0)}{2(s-r)} \frac{T_n(r)}{\sqrt{1-r^2}} dr = -\frac{i(a_0 + b_0 - c_0 - d_0)}{2} U_{n-1}(s), \quad |s| < 1 \text{ and } n \geq 1 \quad (\text{E.1})$$

$$-\frac{1}{\pi} \int_{-1}^1 \frac{\hat{e}_1 + \hat{f}_1}{2} \ln(A_{15}^* |s-r|) \frac{T_n(r)}{\sqrt{1-r^2}} dr = \frac{\hat{e}_1 + \hat{f}_1}{2} \frac{T_n(s)}{n}, \quad |s| < 1 \text{ and } n \geq 1 \quad (\text{E.2})$$

$$-\frac{1}{\pi} \int_{-1}^1 \frac{\hat{g}_1 + \hat{h}_1}{2} \ln(A_{16}^* |s-r|) \frac{T_n(r)}{\sqrt{1-r^2}} dr = \frac{\hat{g}_1 + \hat{h}_1}{2} \frac{T_n(s)}{n}, \quad |s| < 1 \text{ and } n \geq 1 \quad (\text{E.3})$$

$$\frac{1}{\pi} \int_{-1}^1 \frac{i(e_{10} + f_{10} - g_{10} - h_{10})}{2(s-r)} \frac{T_n(r)}{\sqrt{1-r^2}} dr = -\frac{i(e_{10} + f_{10} - g_{10} - h_{10})}{2} U_{n-1}(s), \quad |s| < 1 \text{ and } n \geq 1 \quad (\text{E.4})$$

$$-\frac{1}{\pi} \int_{-1}^1 \frac{\hat{a}_{11} + \hat{b}_{11}}{2} \ln(A_{21}^* |s-r|) \frac{T_n(r)}{\sqrt{1-r^2}} dr = \frac{\hat{a}_{11} + \hat{b}_{11}}{2} \frac{T_n(s)}{n}, \quad |s| < 1 \text{ and } n \geq 1 \quad (\text{E.5})$$

$$-\frac{1}{\pi} \int_{-1}^1 \frac{\hat{c}_{11} + \hat{d}_{11}}{2} \ln(A_{22}^* |s-r|) \frac{T_n(r)}{\sqrt{1-r^2}} dr = \frac{\hat{c}_{11} + \hat{d}_{11}}{2} \frac{T_n(s)}{n}, \quad |s| < 1 \text{ and } n \geq 1 \quad (\text{E.6})$$

CURRICULUM VITAE

PERSONAL INFORMATION

Surname, Name: İLHAN, Küçük Ayşe

Nationality: Turkish (TC)

Date and Place of Birth: 14 June 1976, Keskin

Marital Status: Single

Mobile Phone: +90 (532) 250 82 55

E-mail: ayilhan@yahoo.com

EDUCATION

Degree	Institution – Year of Graduation
M.Sc.	METU Department of Mechanical Engineering – 2001
B.Sc.	METU Department of Mechanical Engineering – 1998
High School	Ankara High School – 1993

WORK EXPERIENCE

Year	Place – (Enrollment)
2007- Present	TAI – (Design Specialist / Structural Analysis)
2003-2007	TAI – (Design Engineer / Structural Analysis)
2002-2003	ROKETSAN – (Design Engineer)
1998-2002	METU Department of Mechanical Engineering – (Research Assistant)

PUBLICATIONS

1. DAG, S., ILHAN, K. A. and ERDOGAN, F., 'Mixed-Mode Stress Intensity Factors for an Embedded Crack in an Orthotropic FGM coating', *Proceedings of the Multiscale & Functionally Graded Materials Conference*, Oahu, Hawaii, USA, October 2006. (Keynote lecture, in review)